POLITECNICO DI MILANO

Department of Energy

Doctoral Program in Energy

EXPERIMENTAL STUDY OF POLYBENZIMIDAZOLE BASED HIGH TEMPERATURE POLYMER ELECTROLYTE FUEL CELLS

Doctoral Dissertation of:

Samuele Galbiati

Supervisor:

Prof. Renzo MARCHESI

Tutor:

Prof. Fabio INZOLI

The Chair of the Doctoral Program:

Prof. Carlo E. BOTTANI

Year 2012 - XXIV Cycle

This work is dedicated to S., R. and L.

Acknowledgements

Contents

List of Figures

List of Tables

Abstract

High Temperature Polymer Electrolyte Membrane Fuel Cells (HT-PEMFC) based on acid doped polymers can operate in the temperature range included between 100°C and 200°C with dry reactants. As a consequence, some simplifications are introduced in the operation of the fuel cell: heat recovery is more effective, tolerance to fuel impurities is improved and the reactants humidification system is not necessary. These characteristics ease the use of HT-PEMFC in cogenerative systems where the fuel is produced via a steam reforming process. In the last years research focused on this technology but up to now some unclear points still remain. The present work aims to experimentally study HT-PEMFC fundamental properties contributing to the evaluation of their possible application. The investigation focuses on commercial fuel cells based on a Polybenzimidazole (PBI) electrolyte membrane doped with phosphoric acid. Thanks to the development of innovative and advanced measurement techniques, as in-situ mass transport analysis, Electrochemical Impedance Spectroscopy and Cyclic Voltammetry, a deep analysis of the phenomena that rule both performance and degradation was carried out. The major outcome is represented by the contribution in the understanding of the mechanisms that influence the cathode kinetics, the degradation and the internal water transport.

Keywords: Polymer electrolyte fuel cell, Polybenzimidazole, Phosphoric acid, Water transport, Electrochemical Impedance Spectroscopy, Cyclic Voltammetry.

Introduction

In the last decades Polymer Electrolyte Membrane Fuel Cells (PEMFCs) attracted increasing attention as energy conversion systems mainly due to their high efficiency, high power density, low emissions and modularity. Such features make PEMFCs suitable for both stationary and mobile applications in the perspective of distributed power generation and of internal combustion engines replacement. The currently improved PEMFC technology is based on perfluorosulfonic acid (PFSA) polymer electrolyte membranes, among which the most diffused is Nafion®. PFSA polymers exhibit high proton conductivity only when fully hydrated due to their typical water assisted proton transport mechanism. This requires reactants humidification and limits fuel cell operational temperature below water boiling point (normally 60-80°C) to prevent water evaporation. Consequently some severe constraints are introduced in PEMFC applications:

- A reactants humidification system is necessary

- Reaction kinetics are limited and slower than at higher temperatures

- Cogeneration is not attractive due to low quality heat recovery

- Tolerance to fuel impurities is poor due to easy CO adsorption on the catalyst.

Considering on-site hydrogen production by natural gas reforming, high purity levels (CO concentrations below $20\,ppm$) can be obtained only with a multi

stage fuel processing system provided with water-gas shift and partial oxidation reactors. This feature, together with the necessary presence of gas humidifiers, remarkably contributes to increase plant complexity and costs, representing an obstacle in the proliferation of fuel cell applications. Several attempts have been made to rise fuel cell temperature in order to overcome these limitations [2]. Up to now the best available solution stands in the use of different membrane electrolyte materials in which proton conductivity is not based on the presence of liquid water. This independence can be achieved through the use of basic polymers combined with proton conducting acids. Such systems are also named acid-base complexes and exhibit good proton conductivity in the temperature range between 100°C and 200°C allowing to produce High Temperature Polymer Electrolyte Fuel Cells (HT-PEMFC). Higher working temperature enhances reaction kinetics, extends catalysts tolerance to fuel impurities and eases fuel cell heat recovery. These features, together with the unnecessary reactants humidification, open new possibilities for the use of polymer membrane fuel cells in real applications, especially where gas reforming units are employed to supply fuel. In particular the use of Polybenzimidazole (PBI) polymer membranes imbibed with phosphoric acid (PA) emerges as the best option due to its high thermal stability and proton conductivity[3]. Important steps in understanding the basic principles of HT-PEMFC are necessary due to the early stage of this technology. In this framework the availability of data related to operation in different conditions is extremely important to evaluate HT-PEMFC potential and to find development directions. Aim of the present work is to experimentally investigate the performance, the mass transport phenomena, the effect of humidification and the degradation of HT-PEMFC in order to gain an insight into the basic principles of this technology. The work is organized as follows:

Chapter 1 : State of the Art

Chapter 2 : Performance

Chapter 3 : Internal Gas Crossover Leakage

Chapter 4 : Internal Water Transport

Chapter 5 : Effect of Water on Performance

Chapter 6 : Degradation

Chapter 7 : Evaluation of Gas Diffusion Layer Materials.

Chapter 1

State of the Art

In the following chapter a summary on the main HT-PEMFC properties, issues and applications is provided with the aim to introduce this technology. More specific information about the related chemical and physical aspects can be found in the cited works.

1.1   Polybenzimidazole properties

High temperature PEMFC operation is possible thanks to the development of new polymer electrolytes able to conduct protons without being hydrated, as otherwise needed for low temperature PEMFCs. One of the most widely used materials for membrane fabrication is Polybenzimidazole (PBI) doped with phosphoric acid. Polybenzimidazole (PBI) is a generic name that indicates a wide family of polymers that contain Benzimidazole units (fig.1.1 (a)). Currently, the name PBI is also used to indicate a specific type of polymer used for fuel cell application: $poly(2, 2' - m - (phenylene) - 5, 5' - bibenzimidazole)$ (fig.1.1 (b)). When this polymer is doped with phosphoric acid it exhibits good proton conductivity in the temperature range included between 120°C and 200°C [2, 3]. For this reason it is successfully used in the production of electrolyte membranes for HT-PEMFC [4, 5]. The main PBI properties have been extensively reviewed [6, 2, 1, 7] and are summarized in the following paragraphs.
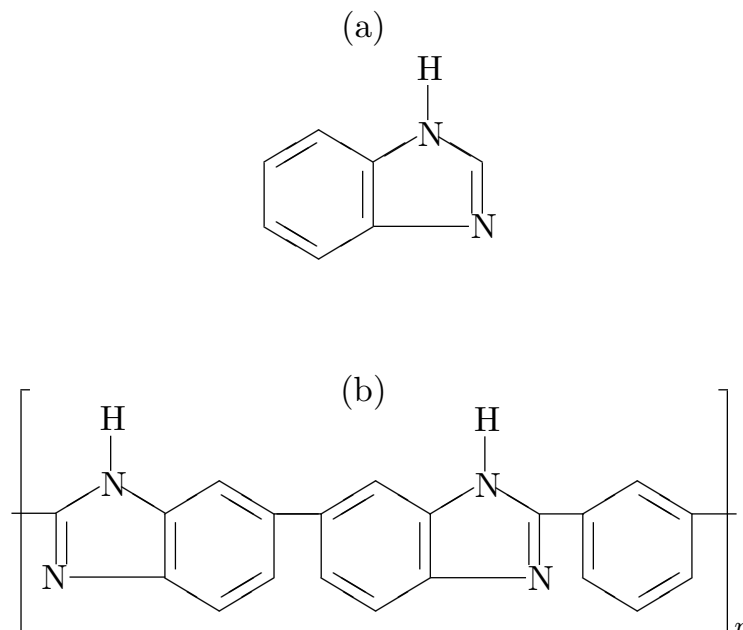
Figure 1.1: (a) Chemical structure of a Benzimidazole unit; (b) Chemical structure of PBI.

1.1.1   Acid doping

The proton conductivity of dry pure PBI is nearly zero [2, 1], higher values can be achieved when this polymer is doped with proton conducting substances. As a basic material, PBI reacts with acids that easily establish chemical bonds with the N sites of the polymer repeating units. Among the acids, amphoteric ones show the best functionality because they can act as both donors and acceptors of protons. In particular, phosphoric acid (PA, H_3PO_4) has the highest value of proton conductivity in comparison with other acids [8] and is therefore used in the PBI doping process. This action is normally carried out by immersing a PBI polymer film in a concentrated phosphoric acid solution. By doing so, the polymer absorbs the acid in amounts that vary depending on the acid solution temperature, concentration and on the doping time [9]. The number of acid molecules per polymer repeating unit is named *doping level* and is normally taken as indicator of the progress in the acid doping process. This number is generally limited below 20 when doping is carried out by immersion of PBI membranes into acid solutions. Higher values can be obtained by directly casting the polymer from a solution of solvents containing phosphoric acid, in this case doping levels up to 70 can be obtained [10]. Considering doped PBI, only 2 molecules of phosphoric acid are chemically bonded to each PBI repeating unit. The majority of the acid is mechanically retained inside of the polymer without being chemically bonded and is therefore defined *free acid* in opposition to the *bonded acid.* The conductivity of PBI increases with the amount of retained acid, while its mechanical strength progressively decreases due to the separation of the polymer chains caused by the swelling [9, 1]. This problem introduces a limit in the doping level that must be optimized taking into account for these two opposite needs.

1.1.2   Water uptake

Pure PBI is hygroscopic, water can actually establish hydrogen bonds with the N and $N-H$ sites of the polymer repeating units [9]. The number of water molecules absorbed per PBI repeating unit is named *water uptake* and is around 3.2 when PBI is in equilibrium with liquid water at ambient temperature. If

PBI is doped with phosphoric acid its ability to absorb water further increases because water directly forms hydrogen bonds with the free acid molecules. For this reason water uptake sensibly depends on phosphoric acid doping level [9].

1.1.3 Mechanical and thermal properties

Pure PBI exhibits good mechanical resistance: the maximum tensile strength is $150\,MPa$ at 125°C and $130\,MPa$ at 180°C with a very limited strain at break value of 2-3% [1, 7]. The good resistance is due to the hydrogen bonds between the N and N-H sites of two adjacent polymer chains. When the polymer is saturated in water its resistance increases and its strain at break value rises up to 7-10%. On the opposite, when the polymer is doped with phosphoric acid, its resistance decreases mainly due to the progressive separation between the polymer chains as acid is absorbed. At doping levels included between 5.5 and 6.7 the maximum tensile strength is $12\,MPa$ which is almost 10 times lower than for pure PBI. Different variations in polymer structure have been invented to allow high doping levels and preserve mechanical resistance. The most popular development direction is based on the creation of links between the polymer chains (*cross-linking process*) and on the achievement of high densities. Pure PBI also shows good thermal properties with a glass transition temperature included between 420°C and 436°C [2, 8]. This makes the polymer suitable for high temperature use without permanent structural damages. As temperature is increased up to 150°C, PBI exhibits a weight loss of 10-15% due to the evaporation of the water retained in its structure [6]. Between 150°C and 500°C no further weight loss is measured, while over 500°C its weight decreases again because part of the carbon included in the polymer oxidizes turning into CO_2. Phosphoric acid doped PBI exhibits lower thermal stability than pure PBI, actually at around 200°C, a weight loss due to phosphoric acid dehydration starts, limiting HT-PEMFC operating range.

1.1.4 Proton Conductivity

Proton conductivity in phosphoric acid doped PBI (PA-PBI) is due to a proton hopping mechanism that involves hydrogen bonding sites of the polymer

and of the acid [11, 8, 2, 12]. Protons jump from one bonding site to another without a net carrier transfer across the membrane. This mechanism is named *Grotthus mechanism* and totally differs from what happens in perfluorosulfonic (PFSA) membranes used in low temperature PEMFCs. In such systems the proton transfer happens through the physical movement of hydronium ions (H_3O^+) that cross the polymer membrane. Water is thus involved with proton transport: up to 3 molecules of water can move together with a proton generating what is named *water electro-osmotic drag* [13, 14]. Proton conductivity in PA-PBI membranes depends on three parameters: acid doping level, humidification and temperature [5, 8, 2]. The presence of phosphoric acid molecules increases the availability of anion sites involved in the proton transfer mechanism, for this reason high doping levels cause high conductivity. Water also plays an important effect on conductivity due to its role in phosphoric acid equilibrium [5, 15, 16, 17, 18]. At HT-PEMFC working temperature, acid tends to dehydrate shifting from the ortophosphoric form to the pyrophosphoric form as shown in the next reaction: $2H_3PO_4 \rightarrow H_4P_2O_7 + H_2O$. During this process two acid molecules merge into one losing a molecule of water that normally leaves the polymer. This causes a decrease in the number of acid molecules with a negative effect on conductivity. The presence of water shifts the acid equilibrium towards the ortophosphoric form keeping the conductivity high. The conductivity loss related to the acid dehydration is anyway limited and does not cover the huge advantage of PBI-based HT-PEMFC operation with non-humidified reactants. Temperature represents the most important factor for conductivity that follows an Arrhenius type dependence [7, 8, 3, 12] according to the following equation:

$$\sigma = \sigma_0 \, exp\left(\frac{-E_{act,\sigma}}{RT}\right) = \frac{A_\sigma}{T} \, exp\left(\frac{-E_{act,\sigma}}{RT}\right) \tag{1.1}$$

Where σ_0 and A_σ are the pre-exponential factors, while $E_{act,\sigma}$ is the activation energy. This relation indicates that, even if the membrane is highly doped, appreciable conductivity is achieved when the temperature is sufficiently high. High temperature causes higher conductivity till convergence to an upper limit. An activation energy is also involved in this process, different values

can be found in the literature [3, 8], anyway they do not exhibit great variations with fuel cell operating parameters and can be retained constant. Proton conductivity of PA-PBI membranes is normally included in between 0.02 and $0.08\,S\,cm^{-1}$ [5] and is competitive with the typical values for conventional PFSA membranes that can rise up to $0.15\,Scm^{-1}$ only when the polymer is fully hydrated [19].

1.1.5 Water transport

Since no water flux is related with proton conductivity, the only available mechanisms for water transport in PBI membranes are diffusion and permeation. Diffusion is due to the water concentration gradient across the membrane. During fuel cell operation water is produced on the cathode electrode and progressively diffuses to the anode following complex dynamics. The diffusivity of PBI plays a key role in this process, ruling water transport. Its value is reported to be approximately 100 times lower than for Nafion (10^{-14} and 10^{-12} $cm^3_{STD}m^{-1}s^{-1}Pa^{-1}$ respectively) [20] but it is still considerable. Water permeation is due to the pressure gradient across the membrane. This is related to the different pressure drops of anode and cathode flows which are normally very limited. For this reason the contribution of permeation to water transport is normally small.

1.1.6 Gas transport

Gas crossover across the membrane represents a critical issue for PEMFCs. The direct passage of fuel or oxidant to the other compartment causes a decrease of voltage and a further consumption of fuel. The direct reaction of fuel and oxidant actually causes mixed potentials and represents a waste of fuel that does not contribute to the production of electricity. Low gas permeation across the membrane electrolyte is thus very important for a correct and efficient fuel cell operation. Pure PBI shows lower gas permeability values in comparison to Nafion due to its dense molecular structure. Nevertheless, when the polymer is doped, gas permeability becomes almost one magnitude order bigger than Nafion one, due to the separation of the polymer chains [1].

Table 1.1: Oxygen and hydrogen permeability values for Nafion, pure PBI and phosphoric acid doped PBI (5 moles per repeating unit). Source:[1]. Permeability is expressed in $10^{17}\,mol\,cm\,cm^{-2}\,s^{-1}\,Pa^{-1}$.

	gas permeability						
	25°C		80°C		120°C		180°C	
	H_2	O_2	H_2	O_2	H_2	O_2	H_2	O_2
Nafion	4.1	2.8	15.7	3.1	-	-	-	-
PBI	-	-	1.6	0.05	3.0	0.06	4.3	0.1
PA-PBI	-	-	120	30	250	70	380	90

1.2 Main PA-PBI fuel cell issues

PA-PBI fuel cells present some issues that still have to be fully understood in order to further improve this technology and make its application more reliable. Three main subjects can be addressed as relevant under a scientific point of view: phosphoric acid leaching, cathode kinetics and three phase contact in the electrodes. On all of these aspects, water is indicated to play a relevant influence which is discussed next.

1.2.1 Phosphoric acid leaching

Phosphoric acid leaching consists in a loss of acid molecules that leave the membrane-electrode assembly during fuel cell operation. This phenomenon causes a decrease in the number of proton transferring units during time, and negatively affects the proton conductivity. PA loss is influenced by humidification, reactants flow rates and temperature [21, 22]. Humidification can dilute the phosphoric acid facilitating its migration and distribution into the electrodes [23, 24]. This positively increases the three phase contact between catalyst particles, acid and carbon, but at the same time allows easier removal of acid molecules in the flow field. When flowrates are high, part of the acid is stripped away from the electrodes together with water and is delivered out of the fuel cell. Acid loss becomes particularly important when liquid water is

present. In this condition acid is literally washed out of the electrodes, due to its miscibility with water, and conductivity immediately drops. For this reason the fuel cell must be operated only when temperature is over the boiling point of water to assure for the absence of liquid phase. This represents a practical constrain that forbids fast startups due to the necessary fuel cell preheating before operation.

1.2.2   Cathode kinetics

In PEM fuel cells the majority of internal losses happens on cathode electrode where the situation is more complex because of water production, mass transport issues and oxygen reduction kinetics [3]. While at the anode electrode the highly reactive hydrogen is easily oxidized, at the cathode electrode the oxygen reduction reaction is slower. This is due to low oxygen concentration, when air is used as oxidant, and to kinetic aspects. In PA-PBI fuel cells phosphoric acid plays a negative influence on oxygen reduction reaction due to its interaction with the catalyst. Acid can form a layer over the catalyst particles hindering the diffusion of oxygen [17]. This phenomenon still needs to be fully clarified and characterized. For this reason, even though the temperature is higher, HT-PEMFCs show slower cathode kinetics than conventional PEMFCs.

1.2.3   Three phase contact

Reaction between protons, electrons and oxygen on cathode electrode can happen only if electrolyte, carbon and catalyst are in direct contact in the so called *three phase contact* [25]. In this way protons and electrons can be delivered to the catalyst particles and can combine together with oxygen that diffuses from the flow field. A good three phase contact within the electrode allows for a better exploitation of the catalyst in the perspective of a growth in the reaction rate and of a reduction in the catalyst load. In HT-PEMFCs the proton conducting phase is represented by phosphoric acid that must be present in the electrode to allow proton transport to and from the catalyst sites. Phosphoric acid diffuses from the doped polymer into the electrodes as a fuel cell is assembled, but variations in its distribution occur during fuel cell operation.

In particular the acid penetration can change, especially according to acid hydration level, with a consequent change in the extension of the region where the three phase contact i present [23, 24], also named *three phase zone*. On the other hand, an excessive presence of phosphoric acid in the electrode may flood the catalyst particles hindering the diffusion of oxygen to the catalyst sites [26]. For this reason the acid presence in the electrodes must be controlled and optimized and its distribution according to the fuel cell operating condition must be studied [27].

1.2.4   Influence of water

As illustrated above in paragraph 1.1.4, water influences the equilibrium of phosphoric acid. A good hydration of the fuel cell increases the number of acid molecules and enhances its penetration in the electrodes. This factor strongly affects all of the three above mentioned phenomena: acid leaching, cathode kinetics and three phase contact. The deeper acid penetration in the electrodes extends the triple contact zone increasing the catalyst active area and improving the kinetics, but at the same time it may clog the electrodes hindering the oxygen diffusion. Furthermore, the excessive acid dilution may facilitate its stripping from the electrodes increasing the acid loss rate. Therefore the humidification of the reactants is useful to enhance the effects of water, moreover this would represent a realistic condition in a real application where the fuel cell is fed with syngas rich of water. A study of the fuel cell behavior under humidified conditions has not been performed yet and is of great importance to clarify these points.

1.3   Main degradation mechanisms

Different operating conditions diversely affect voltage degradation rate due to their influence on fuel cell components. The understanding of degradation mechanisms should provide a useful tool to optimize the operating conditions in order to minimize the voltage decay and extend fuel cell durability. Among the known degradation mechanisms, membrane thinning, catalyst agglomeration and car-

bon corrosion seem to play a major role. Many aspects of degradation are still unclear and their investigation is fundamental to achieve deeper knowledge in the physical mechanisms and develop operational strategies.

1.3.1 Membrane thinning

Polymer electrolyte membrane is attacked by aggressive chemical species mainly represented by reaction intermediates like OH- and OOH- groups [28]. These radicals have a corrosive effect on the polymer that can progressively loose parts of its chains decreasing its thickness. An excessive decrease in this parameter can cause the formation of pinholes and cracks in the electrolyte. In this case reactants crossover and electrical shorts could easily take place.

1.3.2 Catalyst agglomeration

The dispersion of small catalyst particles in the electrodes is very important in order to have big active surfaces per unit of catalyst weight. Anyway such particles tend to agglomerate during fuel cell operation decreasing the active surface with negative consequences on reaction velocity and catalyst use [29]. Platinum agglomeration is particularly enhanced by high voltage (OCV periods) and temperatures. The physical mechanisms that rule this degradation mode are under investigation together with accelerated degradation procedures and fuel cell operation strategies.

1.3.3 Carbon corrosion

Carbon corrosion consists in the loss of carbon from the electrodes and the gas diffusion layers. Carbon can be actually oxidized and lost as CO_2 or it can agglomerate [30, 10]. In both cases it alters the structure of the electrodes and the diffusion layers by changing their porosity. Carbon corrosion is particularly accelerated by voltage reversion related to fuel starvation and by high temperature [31].

1.4   Aim of this work

This work represents an experimental investigation on HT-PEMFC fundamental properties with the aim to provide insight in some of the unclear points that still concern this technology (paragraphs 1.2,1.3). Particular efforts are dedicated to the study of internal mass transport phenomena, to the clarification of the interaction of water with the phosphoric acid doped PBI system and to the analysis of degradation. The investigation is performed using a specially designed and built experimental apparatus which can be easily modified to take different measurements thanks to its modular concept. Different instruments can actually be connected and the test station can be adapted to several types of tests. The uncertainty of the measurements is controlled and minimized with the use of calibrated instruments and with the evaluation of their combined uncertainty. During the whole experimental activity the single fuel cell components are monitored thanks to specifically implemented electrochemical techniques such as Electrochemical Impedance Spectroscopy (EIS), Cyclic Voltammetry (CV) and Linear Sweep Voltammetry (LSV). The present dissertation is organized as follows:

Chapter 2 : Performance

Chapter 3 : Internal Gas Crossover Leakage

Chapter 4 : Internal Water Transport

Chapter 5 : Effect of Water on Performance

Chapter 6 : Degradation

Chapter 7 : Evaluation of Gas Diffusion Layer Materials.

Chapter 2

Performance

A complete characterization of fuel cell performance is reported in this chapter. The investigation is based on the analysis of polarization curves under a wide range of operating conditions. The effect of different operating parameters on the behavior of a PBI-based HT-PEMFC operated with pure hydrogen and air is described.

2.1   Aim

The present investigation aims to evaluate the effect of the operating temperature, cathode stoichiometry and anode stoichiometry on the performance of a PBI-based HT-PEMFC. The investigation was performed by recording polarization curves under different operating conditions. The effect of the operating parameters on the performance of the fuel cell has been widely reported in literature where data are largely available [32, 3, 33, 34]. The published values have been used to make comparisons.

2.2   Experimental

2.2.1   MEA

The object of this investigation is a commercial HT-PEMFC (Celtec-P2100® by BASF Fuel Cells®) based on a phosphoric acid doped PBI membrane. This fuel cell has an active area of $20\,cm^2$ and consists in a package of MEA and gas diffusion layers provided with PTFE gaskets (thickness: $345\,\mu m$ anode, $370\,\mu m$ cathode). Electrode catalyst is Platinum on anode side (loading: $1\,mg\,cm^{-2}$) and Platinum alloy on cathode side (loading: $0.7\,mg\,cm^{-2}$). The membrane doping level is reported to be up to 70 phosphoric acid molecules per PBI repeating unit [10]. The same type of fuel cell described here was used throughout all of the experimental investigations reported in this thesis.

2.2.2   Fuel cell assembly

The MEA was placed between two graphite distributors with carved serpentine flow fields (single serpentine on anode side and triple serpentine on cathode side, both with the same square section: depth and width $0.8\,mm$, length $700\,mm$; ribs width: $0.8\,mm$). The graphite distributors are held together between two stainless steel plates connected with 8 screws tightened with a controlled torque of $12\,(\pm0.5)\,Nm$. The temperature of the plates is measured by a calibrated thermocouple (uncertainty: 1°C, distance from active area: $20\,mm$) and is controlled by a temperature controller connected with two cartridge heaters located

inside of the steel plates. Since the heat capacity of the plates is much higher than that of the graphite distributors and of the MEA, high temperature stability is attained. Furthermore, due to the high thermal conductivity of the graphite distributors and to the small thickness of the MEA, temperature uniformity in the entire fuel cell assembly is assumed.

2.2.3 Test station

The fuel cell was tested in a modular in-house projected and assembled experimental apparatus. Dry air supplied to the cathode is provided by the laboratory compressed air grid, while pure dry hydrogen supplied to the anode is generated by an electrolyzer. Reactants flow rates are controlled and measured by two calibrated flow controllers (BROOKS 5850S, uncertainty: 0.7% of rate $+0.004\,Nl/min$ for air flow controller and 0.7% of rate $+0.0004\,Nl/min$ for hydrogen flow controller). Reactants pressures at cell inlets and outlets are measured by pressure transducers (pressure range: 0-4 bar gauge, uncertainty: $10\,mbar$). The power produced by the fuel cell during operation is dissipated by an electronic load (TDI RBL 488) working in constant current (uncertainty: 0.25%). Fuel cell Ohmic resistance is measured by an AC/milliohmeter (TSURUGA 3566, estimated uncertainty: $1\,mOhm\,cm^2$) that measures cell's impedance at $1\,kHz$ single frequency. All of the instruments are connected to a personal computer through acquisition boards and all of the measured parameters (pressures, temperatures, relative humidities, flow rates, cell voltage and current) are automatically recorded and stored. A simplified scheme of the experimental apparatus is reported in fig.2.1.

2.2.4 Methodology

The PBI-based HT-PEMFC was activated during $70\,h$ at T=160°C, i=0.2 $A\,cm^2$, λ_{H_2}=1.3 and λ_{Air}=2 as suggested by the manufacturer [35]. The fuel cell was then operated performing successive polarization curves by imposing current density values, while voltage was recorded as a response. Every polarization curve was made up by 11 points ranging from $0.025\,A\,cm^{-1}$ to $0.9\,A\,cm^{-1}$ with a constant step of $0.0875\,A\,cm^{-1}$. At current density higher
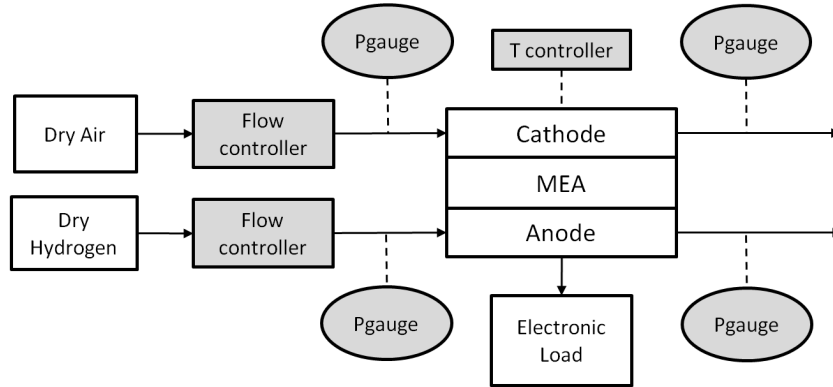
Figure 2.1: Experimental setup scheme: gray squares represent the controlled parameters, while gray circles represent the measured parameters.

than $0.2\,A\,cm^2$ reactants flow rates were automatically regulated to keep constant stoichiometry. Conversely, at current density lower than $0.2\,A\,cm^2$, flow rates were maintained constant due to greater uncertainty in the control of small fluxes. The investigated operating conditions are reported in 2.1. Temperature

Table 2.1: Investigated operating conditions. The reference condition is highlighted in bold letters.

$Temperature$ [°C]	λ_{H_2}	λ_{Air}
140	1.3	1.5 - 2 - 4
140	1.75	1.5 - 2 - 4
160	**1.3**	1.5 - **2** - 4
160	1.75	1.5 - 2 - 4
180	1.3	1.5 - 2 - 4
180	1.75	1.5 - 2 - 4

and stoichiometry values were changed within the typical range suggested for this type of fuel cell [36]. The only value of $\lambda_{Air} = 1.5$ is lower than suggested by the manufacturer and was chosen to investigate possible limitations in the mass transport process. Before measuring a polarization curve, the fuel cell

was maintained in OCV for $60\,s$ in order to measure the open circuit potential. While measuring polarization curves, every current density value was imposed for $600\,s$ to assure for a steady state condition. During this time all of the measured parameters were recorded with a frequency of $1\,Hz$. Only 300 values out of the 600 recorded ones were selected after outliers elimination and were saved as representative of the experimental measure. Every polarization curve was repeated for three times on three different days to assure for repeatability. More information on the experimental setup and methodology is reported in [37].

2.3   Polarization curves

2.3.1   Effect of temperature

The polarization curve obtained under reference conditions (T=160°C, λ_{H_2}=1.3, λ_{Air}=2) is graphed in fig. 2.2 together with the polarization curve provided by the manufacturer in [36] for a similar type of fuel cell under the same experimental conditions. The polarization curve provided by the manufacturer refers to a Celtec-P 1000® PBI-based HT-PEMFC, which is very similar to the Celtec-P 2100® PBI-based HT-PEMFC investigated in this study. Nevertheless, small differences may exist between these two types of fuel cells and also between other characteristics such as active area, flow fields design and reactants mean pressure. Such differences may justify the higher performance declared by the producer, especially at high current density.

Following, the effect of fuel cell temperature on performance is evaluated. In fig. 2.3 polarization curves of the investigated fuel cell at three different temperatures are reported. The increase of temperature causes a consequent increase in fuel cell voltage. At current density of $0.2\,A\,cm^{-2}$, the voltage increase is $1.3\,mV$ °C^{-1} between 140°C and 160°C, while it is $0.5\,mV$ °C^{-1} between 160°C and 180°C. At current density of $0.9\,A\,cm^{-2}$, the voltage increase is $2.5\,mV$ °C^{-1} between 140°C e 160°C and $1\,mV$ °C^{-1} between 160°C e 180°C. The importance of fuel cell temperature on performance is discussed in detail in [33]. In this paper the authors observed that high temperature both increases membrane
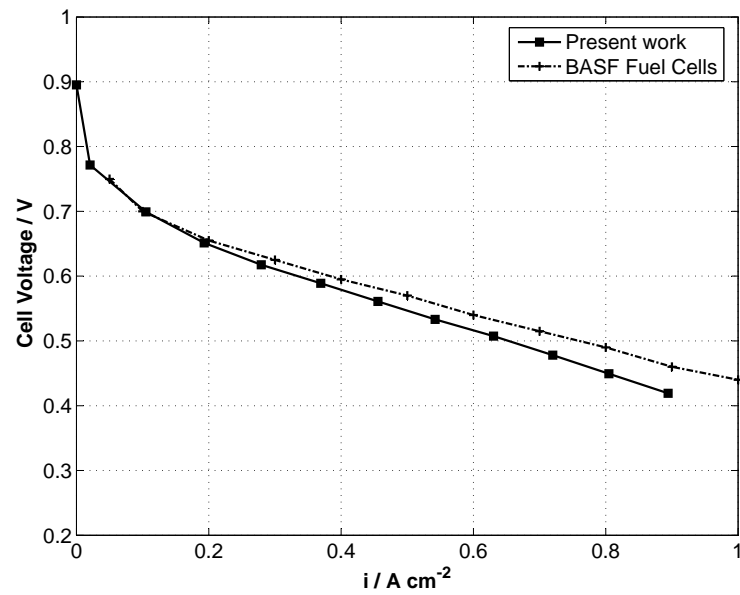
Figure 2.2: Comparison between the polarization curve obtained in this study and the one declared by the manufacturer for a similar type of fuel cell. Reference operating conditions: $T=160°C$, $\lambda_{H_2}=1.3$, $\lambda_{Air}=2$.
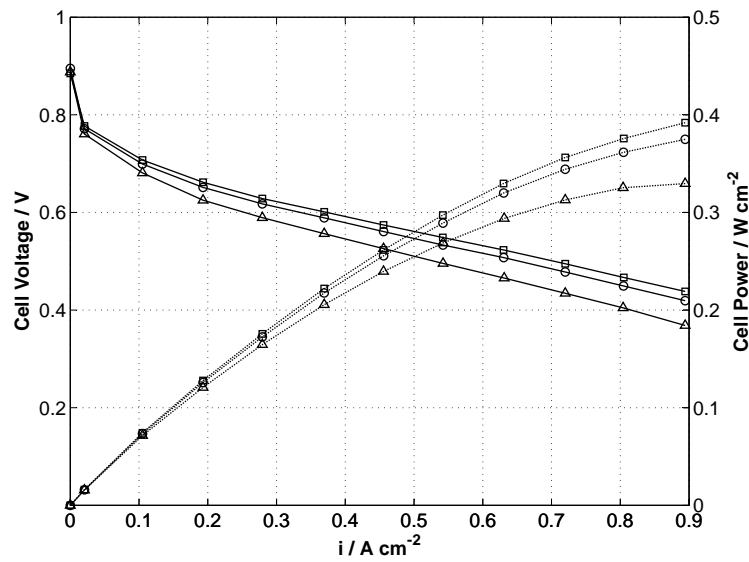
Figure 2.3: Polarization and power curves at different temperature values. Conditions: $\lambda_{H_2}=1.3$ e $\lambda_{Air}=2$. Temperature: 140°C ($\triangle$), 160°C ($\bigcirc$), 180°C ($\square$).

proton conductivity and improves cathode catalyst activity. Thus, the positive effect of temperature can be related to lower ohmic and activation losses. Data shown in fig. 2.3, indicate that the benefit of higher temperature progressively decreases. In tab. 2.2 different values of voltage increase due to temperature are

Table 2.2: Voltage improvement due to the temperature increase: comparison between values available form this work and from literature.

Source	ΔT [°C]	$\Delta V/\Delta T$ [mV/°C]
This work	140 - 160	1.3
	160 - 180	0.5
M.Hori et al. [33]	120 - 140	5
	140 - 200	1
J.Zhang et al. [3]	120 - 140	2.45
	140 - 160	1.25
	160 - 180	1.25
	180 - 200	1
J.Lobato et al. [32]	100 - 125	3
	125 - 150	0.5
	150 - 175	-3

reported. Aim of this table is to compare the values measured in this study with the values available in literature obtained by other research teams. The imperfect agreement between the reported values is mainly due to the different experimental conditions and especially to possible differences in the tested MEAs (membrane thickness, catalyst loading, acid doping). As a general conclusion, voltage improvement is more consistent below 160°C, while it progressively decreases at higher temperature. This behavior can find an explanation referring to phosphoric acid equilibrium. Over 160°C phosphoric acid starts to dehydrate causing a reduction in the number of proton exchanging units(1.1.4) both in the membrane and in the electrodes [23]. This partially compensates the positive effect of high temperature on the kinetics, and leads to a reduction

in the voltage increase rate. Furthermore, phosphoric acid is also present in the electrodes where it acts as proton conductor.

2.3.2   Effect of cathode stoichiometry

Here the effect of the cathode stoichiometry on HT-PEMFC perfromance is discussed. Three different cathode stoichiometry values have been experimentally investigated: λ_{Air}=1.5, 2 and 4; the three related polarization curves are reported in fig. 2.4. The increase in air stoichiometry from 2 to 4 causes an evident improvement of voltage ($13\,mV$ at $0.2\,A\,cm^{-2}$, $49\,mV$ at $0.9\,A\,cm^{-2}$), while the decrease of air stoichiometry from 2 to 1.5 causes a remarkable decrease of voltage ($-20\,mV$ at $0.2\,A\,cm^{-2}$, $-75\,mV$ at $0.9\,A\,cm^{-2}$). This effect is more important at high current density. In particular, with λ_{Air}=1.5, a voltage drop is evident at high current density, which indicates lack of oxygen and consequent mass transport limitations. The effect of air stoichiometry is extensively dis-
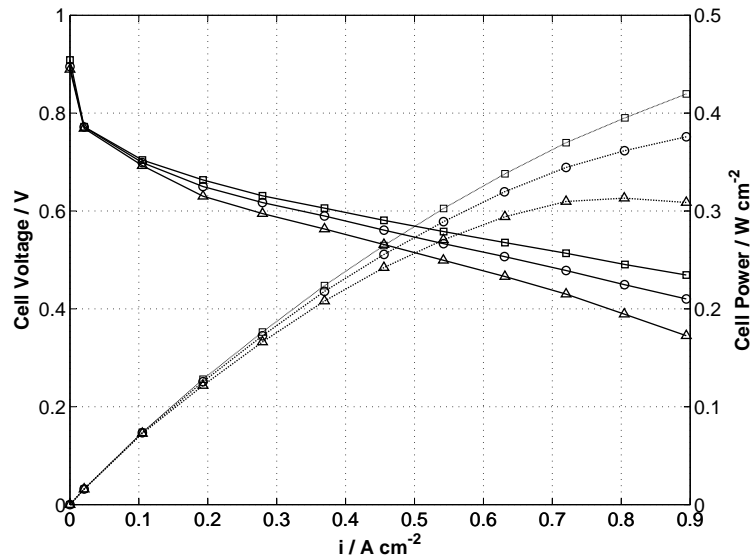
Figure 2.4: Polarization and power curves for three air stoichiometry values; T=160°C, λ_{H_2}=1.3, λ_{Air}=1.5 (△), 2 (○), 4 (□).

cussed in [3]. Increasing air flow at cathode side increases oxygen mean partial pressure. This is due to two simultaneous effects: an increase in total pressure because of higher pressure drops, and larger oxygen availability. As a conse-

quence of the mentioned effects, the ideal equilibrium potential of the fuel cell is higher and oxygen mass transport to the cathode electrode improves. This is the main reason of the important contribution of air stoichiometry to the fuel cell voltage especially at high current density, where mass transport issues are more weighty.

In fig. 2.5 and 2.6 polarization curves at the three investigated air stoichiometries are graphed at cell temperature of 140°C and 180°C respectively. As clearly visible, the trends are similar to what reported and discussed at a temperature of 160°C. Shown values are very similar: at $0.9\,A\,cm^{-2}$, where the effect of
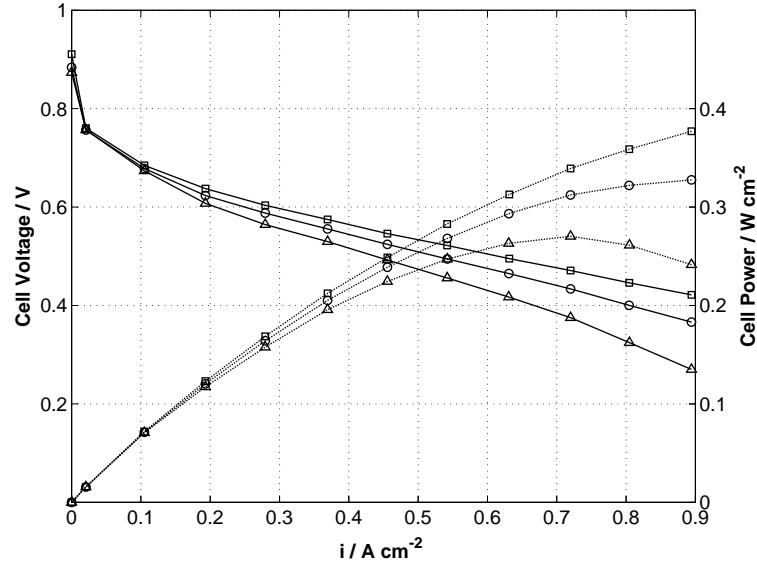
Figure 2.5: Polarization and power curves for three air stoichiometry values; T=140°C, λ_{H_2}=1.3, λ_{Air}=1.5 ($\triangle$), 2 ($\bigcirc$), 4 ($\square$).

stoichiometry has the biggest relevance, an increase of λ_{Air} from 2 to 4 causes a voltage improvement of $50\,mV$ for all of the investigated temperature values: 140°C, 160°C, 180°C. Still considering a current density of $0.9\,A\,cm^{-2}$, a decrease of λ_{Air} from 2 to 1.5, causes a voltage decrease of approximately $-100\,mV$ at 140°C, $-75\,mV$ at 160°C and $-60\,mV$ at 180°C. This finding underlines that the lack of oxygen has greater impact when temperature is low. Since involved phenomena are complex, a linear combination of temperature and stoichiometry effects is not expected. It is therefore possible that the effect of low stoichiom-
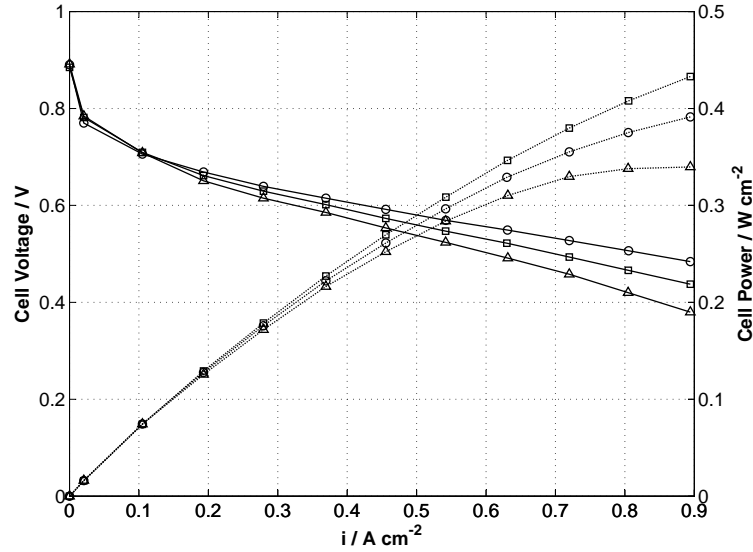
Figure 2.6: Polarization and power curves for three air stoichiometry values; T=180°C, λ_{H_2}=1.3, λ_{Air}=1.5 ($\triangle$), 2 ($\bigcirc$), 4 ($\square$).

etry is different at different temperature.

2.3.3   Anode stoichiometry

As last, the effect of anode stoichiometry was investigated. In order to do this, hydrogen stoichiometry was increased from 1.3 to 1.75 while fuel cell temperature and air stoichiometry have been maintained constant at reference values. As a result, hydrogen stoichiometry demonstrated to be totally unimportant for fuel cell voltage: polarization curves obtained with λ_{H_2}=1.75 and λ_{H_2}=1.3 resulted identical and therefore have not been reported. This indicates that a large hydrogen excess does not bring benefits in the fuel cell operation and anodic losses are small in comparison with cathodic ones. Anodic losses may become noticeable at high current density and considerably low hydrogen stoichiometry [38]. In this condition the phosphoric acid retained in the anode electrode may hinder the diffusion of hydrogen to the catalyst particles. Such issue is anyway minor in comparison with cathode and is not relevant in this work.

2.3.4 Proton resistivity

Proton resistivity was measured with an AC milliohmeter working at $1\,kHz$ constant frequency, as also done in [10] on a similar type of fuel cell. Proton resistivity was measured during all of the performed tests, obtained results show that its value is included in the interval between 75 and $85\,mOhm\,cm^2$ coherently with [10]. In fig. 2.7 and fig. 2.8 the proton resistivity values measured for all of the investigated temperatures and air stoichiometries are shown. Proton
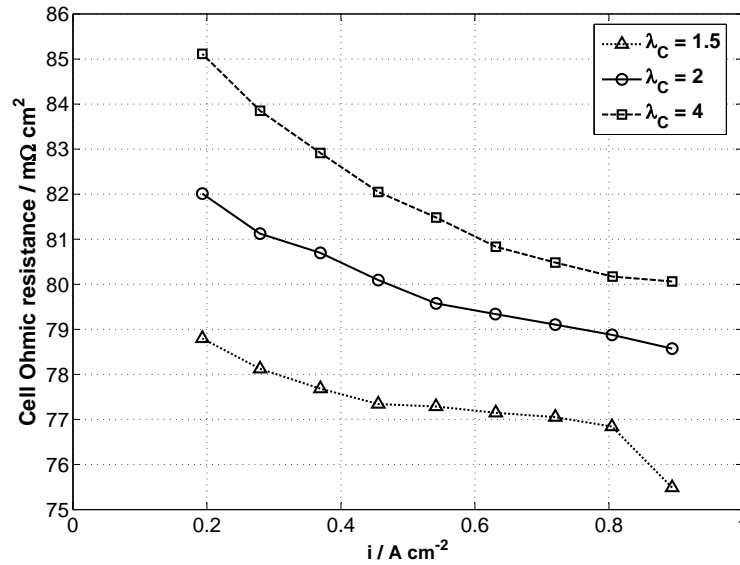
Figure 2.7: Proton resistivity at different air stoichiometry; T=160°C, λ_{H_2}=1.3, λ_{Air}=1.5 ($\triangle$), 2 ($\bigcirc$), 4 ($\square$).

resistivity increases at high air stoichiometry and low temperature [3]. High air flow rates contribute in drying the MEA because they carry water away (1.1.4). Low temperature affects the Arrhenius-like proton transport mechanism which is strongly related to the temperature as also explained in 1.1.4. These variations are anyway small and close to the measurements uncertainty ($1\,mOhm\,cm^2$). The same behavior is again observed for hydrogen stoichiometry variations and is displayed in fig. 2.9. By increasing λ_{H_2} from 1.3 to 1.75, the electrolyte dries out and proton resistivity increases. As a conclusion, the parameters that can influence proton resistivity are temperature and membrane hydration state. This finding is coherent with the literature [3, 2, 18, 5]. Nevertheless, no huge
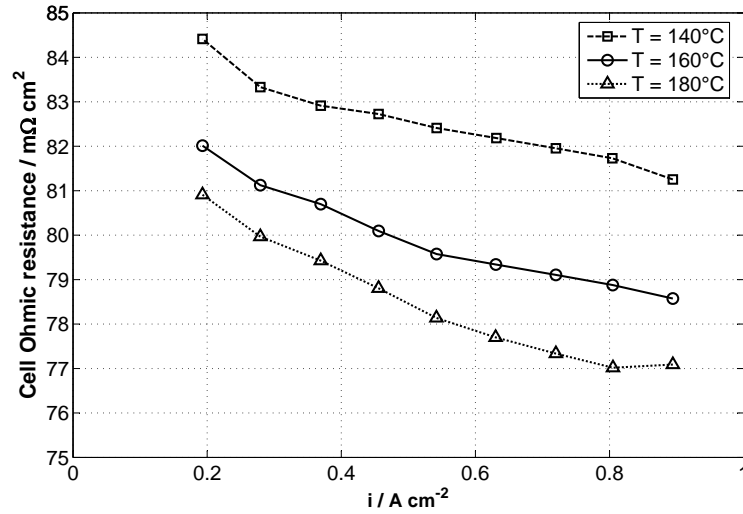
Figure 2.8: Proton resistivity at different temperature; λ_{H_2}=1.3, λ_{Air}=2, T=140°C ($\square$), T=160°C ($\bigcirc$), T=180°C ($\triangle$).

proton resistivity variations have been observed in this study throughout the investigated range of operating conditions. Performed measurements confirm that PBI proton conductivity (about $0.1\,S\,cm^{-1}$) is slightly lower than the one of fully hydrated Nafion® (about $0.2\,S\,cm^{-1}$) as reported by other groups [39, 40].

2.4   Remarks

The performance of BASF Celtec-P2100® high temperature PEMFC was characterized on an extensive range of operating conditions. Attention was dedicated to measurements reliability through the use of calibrated instruments and through the evaluation of the combined measurements uncertainty. The measured polarization curves demonstrated to be in agreement with the literature and showed good repeatability. The effect of temperature and reactants stoichiometry was quantified: voltage is remarkably influenced by cell temperature and air stoichiometry but is independent on hydrogen stoichiometry which plays no effect. The Ohmic resistance of the polymer membrane was also monitored throughout the investigation thanks to an AC milliOhmeter operating at $1\,kHz$ constant frequency. The measured values are supported by the data
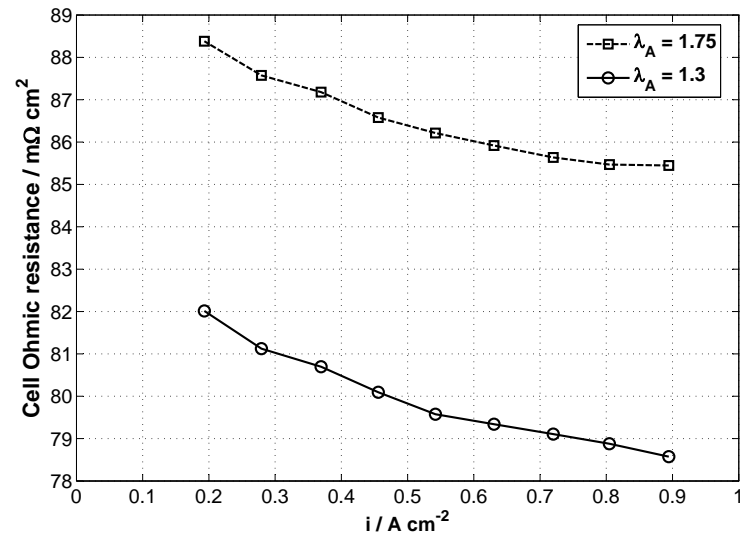
Figure 2.9: Proton resistivity at different anode stoichiometry; T=160°C, λ_{Air}=2, λ_{H_2}=1.3 (◯), 1.75 (□).

published in the literature and slightly change according to the hydration level of the membrane.

Chapter 3

Internal Gas Crossover Leakage

Here an experimental in-situ analysis of internal gas crossover leakage in a single high-temperature polymer electrolyte membrane fuel cell is reported. The study is based on the analysis of the exhausts from the anode and the cathode of the fuel cell during operation. The effects on fuel cell performance are evaluated.

3.1 Aim

Polymer electrolyte membrane fuel cells (PEMFC) are particularly attractive due to their modularity, low environmental pollution and high energy conversion efficiency. Improved reliability is essential for the wide-spread use of fuel cells, especially for automotive applications. Failure modes, which have recently been reviewed [28, 41, 30], are several and are generally classified according to the component involved. Among the many failure modes, great importance is covered by gas transfer leaks which are divided into two categories: external or *overboard* transfer leaks and internal leaks. External leaks occur when gas leaks from reactant streams to the external environment. Internal leaks occur when gas leaks from one reactant stream to the other one, as defined in [42, 43]. Internal leaks, also known as *crossover leakage*, can occur when separation of reactants is not maintained, due to the presence of defects in the electrolyte membrane or in the gaskets. If fuel and oxidant mix, they can directly react on the electrodes to generate hot spots and aggressive radicals, which can compromise fuel cell integrity and reduce durability [28, 41, 30, 43, 44, 45]. For these reasons, there are many studies that evaluate crossover detection and analysis methods [42, 43, 46, 47, 48, 49, 50, 51, 52, 53]. The majority of these works focus on low temperature polymer electrolyte membrane fuel cell stacks and report leakage detection techniques that cannot be performed when the fuel cell is normally operating. A work that describes a continuous in-line monitoring method is [47], but such technique is based on the analysis of the gas composition in the oxidant stream and requires complex and sometimes very expensive gas analysis systems. In the case of high temperature polymer electrolyte membrane fuel cells (HT-PEMFC), crossover leakage could be enhanced due to the harsher operating conditions, which may reduce the integrity of the components [30, 33]. Throughout the experimental activities using HT-PEMFC reported in this thesis, this problem was detected on some single cells. The present work describes the experimental characterization of such internal crossover leakage and proposes a new in-situ method to detect and quantify the leaks. The reported investigation of fuel cell exhausts is based on the analysis of water molar flow rate and dry molar flow rate using simple instruments. This method can be

continuously applied during fuel cell operation; therefore, it is also suitable for long-time degradation testing.

3.2 Experimental

3.2.1 Methodology

A single phosphoric acid-doped PBI-based HT-PEMFC of the same type described in paragraph 2.2.1 was operated with dry hydrogen as a fuel and dry air as an oxidant, fed in co-flow configuration at ambient temperature. Polarization measurements were consecutively performed by applying a current across the fuel cell, and flow rates were automatically regulated to keep constant stoichiometry. The conditions that were investigated are reported in table 3.1. The voltage was recorded in response to imposed currents, and the mass balance was investigated by measuring water molar flux and dry gas molar flux at anode and cathode outlets. Every polarization curve was randomly repeated three times on three different days to assure for measurements repeatability. Representative values of each experimental condition are reported as an average of three tests. More details on the experimental methods can be found in [54].

Table 3.1: Investigated experimental conditions.

$Temperature$ [°C]	λ_{H_2}	λ_{Air}
140	1.3	2 - 4 - 6
160	1.3	2 - 4 - 6
180	1.3	2 - 4 - 6

3.2.2 Experimental setup

A 20 cm² PBI-based MEA (2.2.1) was placed between two graphite distributors where serpentine flow fields are machined (single and triple serpentine on anode and cathode side, respectively, both with the same square section: depth

$0.8\,mm$, width $0.8\,mm$, length $700\,mm$). Graphite distributors are held together between two stainless steel plates by 8 screws and tightened with a controlled torque of $12(\pm 0.5)\,Nm$. The temperature of the plates was measured by a calibrated thermocouple ($\pm$1°C) and was set by a temperature controller (2.2.2). Air and hydrogen flow rates were controlled and measured by two calibrated flow controllers (uncertainty: 0.7% of setpoint $+\,0.004\,Nl\,min^{-1}$ for air flow controller and 0.7% of setpoint $+\,0.0004\,Nl\,min^{-1}$ for hydrogen flow controller). Pressure at the fuel cell inlets and outlets was measured by four transducers (pressure range: $4\,bar$ relative, uncertainty: $10\,mbar$). Relative humidity at both anode and cathode outlets was measured by temperature and relative humidity transmitters based on a capacitive sensor (temperature range: 0-120°C, uncertainty: 0.3°C; relative humidity range: 0-100%, uncertainty: 1.5% RH + 1.5% of reading). The sensors were housed in two heated metal cases in which temperature is adjusted to prevent vapor condensation. Water was then separated by two condensers operating at 20°C so that dry volumetric fluxes could be measured using two graded cylinders (estimated uncertainty: 2%), taking into account for the presence of residual water. The power produced by the fuel cell during operation was dissipated by an electronic load working in constant current mode (uncertainty: 0.25%). Such experimental setup represents a development of the one described in par. 2.2.3, its simplified scheme is reported in fig.3.1. More details about the hardware are reported in [54]. The combined uncertainty of the analyzed parameters is evaluated according to [55] and is reported in table 3.2.

Table 3.2: Uncertainty of measured parameters.

Parameter	Estimated uncertainty
Fuel cell voltage	7 mV
Cathode exhaust dry flow	2%
Anode exhaust dry flow	5%
Cathode exhaust water flow	6%
Anode exhaust water flow	10%
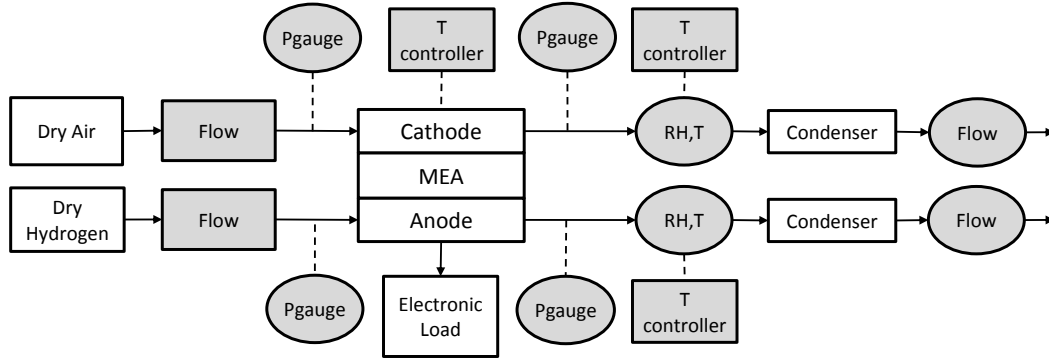
Figure 3.1: Experimental setup scheme: gray squares represent the controlled parameters, while gray circles represent the measured parameters.

3.3 Results and discussion

3.3.1 Crossover leakage analysis

The overall mass balance in a PEMFC must take into account for the consumption of the reactants and for the production of the water due to the electrochemical reaction. A distinction is made here between water flows and dry flows, with the latter including any species different from water. Throughout the experimental activities on HT-PEMFCs reported in this thesis, the global mass balance was closed within measurement uncertainty, and consistency between expected and measured exhaust flows could be verified [54]. However, in this work, measured dry molar flow is less than expected at the cathode outlet and dramatically higher at the anode outlet (fig.3.2). This difference increases at high current density and cathode stoichiometry. An anomalous behavior is also observed for the water mass balance. Because dry reactants are fed to the fuel cell and the current production is controlled, the total fuel cell water output is normally expected to be equal to the internal electrochemical water generation. In the reported case, considering total water molar flow in anode and cathode exhausts, the measured water output is considerably higher than would be generated from the electrochemical reaction. The water excess is represented in fig.3.3 as a ratio between the total water exiting the fuel cell and electrochemical water production. As can be observed, the extra water
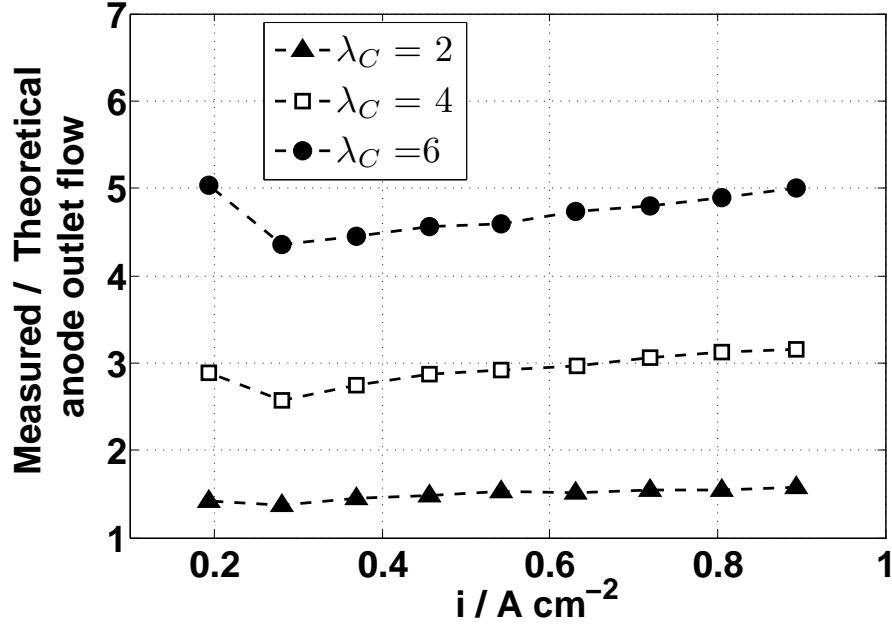
Figure 3.2: Measured to theoretical dry flow ratio in anode exhaust versus current density at different air stoichiometry; T_{cell}=160°C, λ_{H_2}=1.3.

production increases with cathode stoichiometry and can be up to 30% of the electrochemical water at low current densities. The previous findings indicate the presence of an internal gas leak from the cathode to the anode. Such a leak is responsible for the high dry molar flow at the anode exhaust and for the excess water production. Assuming that the additional water production is due to a direct reaction of hydrogen with oxygen coming from the cathode compartment, this reacting component of crossover $\dot{n}^{cross}_{reacting}$ can be estimated with the following relation:

$$\dot{n}^{cross}_{reacting} = \frac{\dot{n}^{c,out}_{H_2O} + \dot{n}^{a,out}_{H_2O} + I/2F}{2} \qquad (3.1)$$

where $\dot{n}^{c,out}_{H_2O}$ is the water flow measured at the cathode outlet, $\dot{n}^{a,out}_{H_2O}$ is the water flow measured at the anode outlet and $I/2F$ is the electrochemical water production. High dry flow rates exiting the anode exhaust indicate the presence of a nonreacting component of crossover. This component can be evaluated as the difference between the total dry flow $\dot{n}^{a,out}_{dry}$ and dry hydrogen flow in the
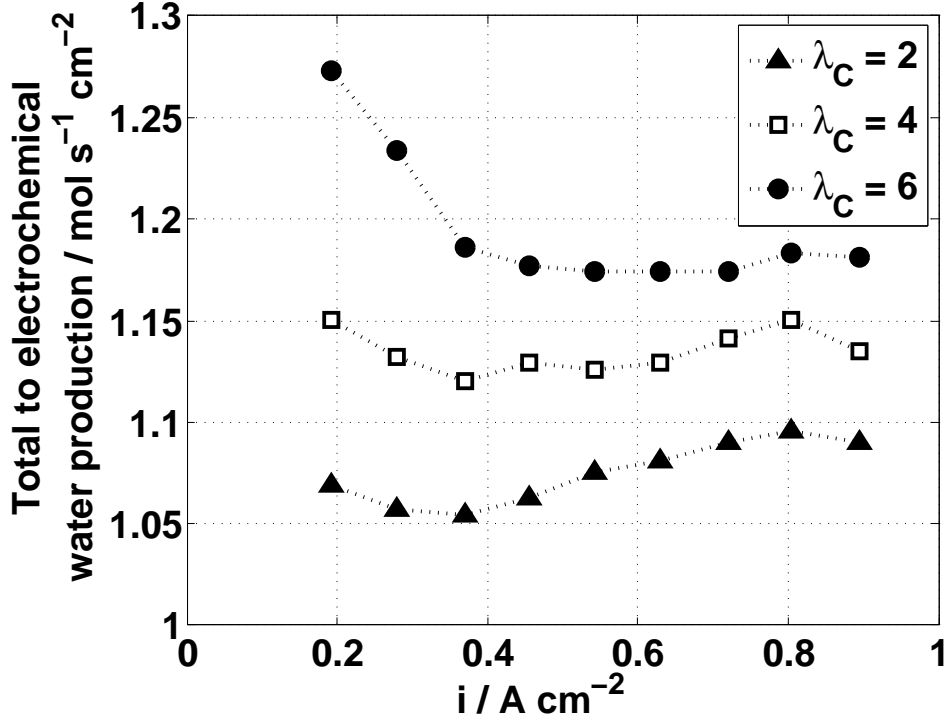
Figure 3.3: Ratio of total water production over electrochemical water production versus current density at different air stoichiometry; T_{cell}=160°C, λ_{H_2}=1.3.

anode exhaust, according to the following relation:

$$\dot{n}^{cross}_{nonreacting} = \dot{n}^{a,out}_{dry} - \left[\dot{n}^{a,in}_{H_2} \frac{\lambda_{H_2} - 1}{\lambda_{H_2}} - 2\dot{n}^{cross}_{reacting} \right] \tag{3.2}$$

where $\dot{n}^{a,in}_{H_2}$ is the hydrogen molar flow at the anode inlet, λ_{H_2} is the hydrogen stoichiometry and $2\dot{n}^{cross}_{reacting}$ is the hydrogen consumption related to reacting oxygen crossover. In fig.3.4, the total crossover flux $\dot{n}^{cross}_{reacting} + \dot{n}^{cross}_{non-reacting}$ is graphed as a function of the pressure difference between the cathode and anode inlets. The pressure difference between the reactants has been reported to play a role on crossover leakage rates [30, 52], but no characterization of such relation is available yet. The calculated crossover flux shows a linear trend, indicating that air crossover is due to gas permeation with linear proportionality to the pressure difference between the fuel cell inlets. This value grows with cathode flow rate, due to pressure drops, as the current density and stoichiometry are
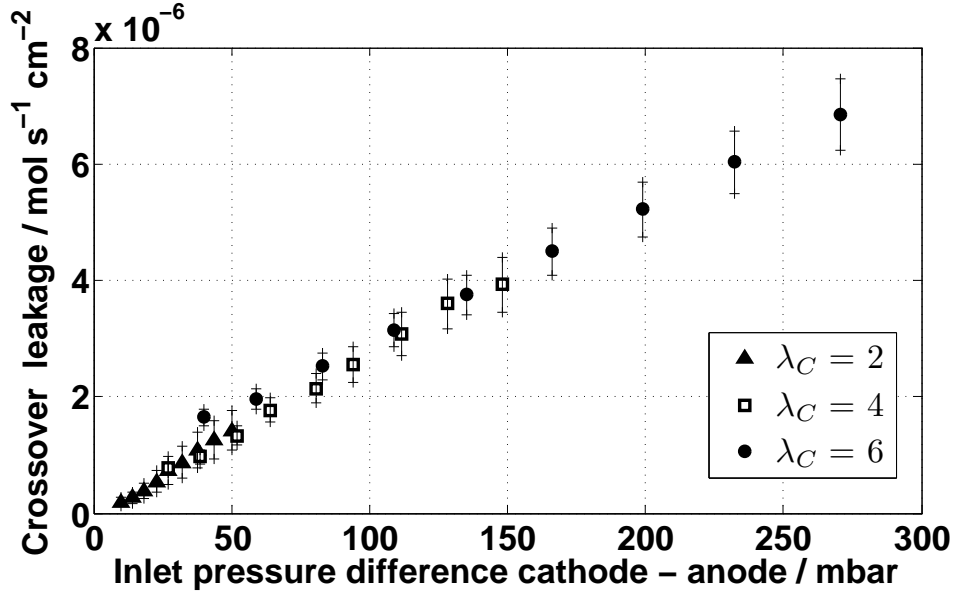
Figure 3.4: Total molar crossover flux versus the pressure difference between the cathode and anode inlets; T_{cell}=160°C, λ_{H_2}=1.3.

increased. Crossover leakage can increase to as much as 10% of the air feed stream, which is more than that reported in literature, in the case of hydrogen crossover in non-defected HT-PEMFC [56, 26, 57, 1, 58]. Crossover leakage rates measured at fuel cell temperatures of 140°C and 180°C (data not shown) are consistent with those shown here. This finding indicates that temperature has no significant influence on the measured leakage rates, thus the crossover occurs as a result of a pressure difference only. A possible reduction in air crossover was investigated by manually setting the reactant flow rates (values not reported in table 3.1). During this test, the fuel cell temperature and current were set at 160°C and $0.2\,A\,cm^{-2}$, respectively, and the automatic regulation of reactants flow rates was interrupted to achieve independent control of the air and hydrogen streams. Hydrogen stoichiometry was gradually increased from λ_{H_2}=1.3 (equivalent to $0.036\,Nl\,min^{-1}$) to λH_2=7.6 (equivalent to $0.2\,Nl\,min^{-1}$), while air stoichiometry was kept constant at λ_{Air}=2 (equivalent to $0.133\,Nl\,min^{-1}$). Under these conditions, the anode compartment mean pressure rose above that of the cathode. This finding was due to different pressure drops at the anode and

cathode sides related to different fluid properties and flow field geometry. As a result, the dry flux at the anode outlet was always lower than expected. This mismatch increased with an increasing pressure difference between the anode and cathode. These observations highlight the presence of hydrogen crossover leakage due to higher anode pressure. This finding further upholds the proposed interpretation that pressure difference is the driving force of crossover leakage. By reversing the pressure difference between fuel cell compartments, the crossover flux direction is also reversed.

3.3.2   Fuel cell performance

Performance of the previously mentioned fuel cell and of a similar non-defected fuel cell was compared. Lower voltages were expected in the first case due to the presence of mixed potentials as reported in [30] for a leaking cell within a stack. Conversely, the polarization curve of the damaged cell did not show a lower voltage, as can be observed by fig.3.5. This finding indicates that, in the
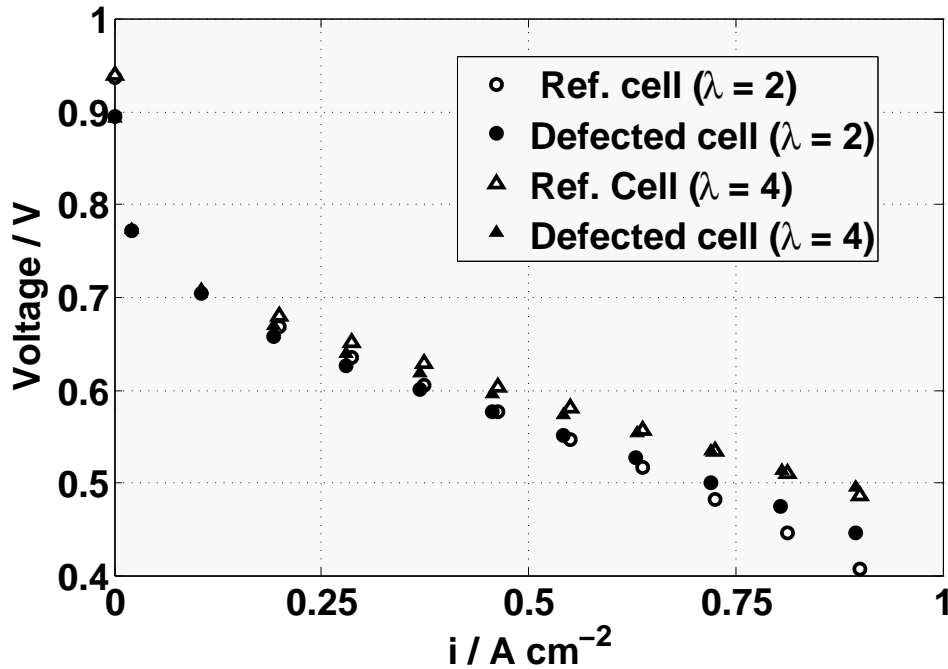
Figure 3.5: Polarization curves of the defected cell compared to a similar non-defected cell at different air stoichiometry; T_{cell}=160°C, λ_{H_2}=1.3.

investigated case, crossover leakage does not affect performance considerably. Thus, such a defect cannot be detected by simply evaluating the fuel cell voltage but only through performing a mass balance analysis. A definitive explanation for this behavior is not available. A post mortem analysis, using an optical microscope, did not reveal any evidence of holes or defects in the membrane. Micro-cracking, pinholes and gasket detachment could all be possible origins of the leakage [28, 41]. Unaltered voltage could be motivated if crossover leakage occurs at the end of the fuel cell active area. In this case, the variation in air and hydrogen partial pressure and the effect of their mixing do not greatly affect the fuel cell voltage. Even though no significant decrease is observed in fuel cell voltage and performance, the hydrogen content in the anode exhaust remarkably decreases. The presence of crossover actually leads to further hydrogen consumption, which becomes no longer available for recovery, which strongly affects the overall energy efficiency. The extra consumption of hydrogen due to the crossover leakage is reported in fig.3.6 as a percentage of the expected hydrogen content of the anode exhaust when no leakage is present. This figure shows that the hydrogen loss in the anode exhaust significantly increases with growing cathode stoichiometry and consequently with crossover. As air stoichiometry increases from λ_{Air}=2 to λ_{Air}=6, the additional depletion of hydrogen increases from approximately 30% to as much as 60% at $0.9\,A\,cm^{-2}$. The energy loss becomes even greater at $0.2\,A\,cm^{-2}$, ranging from 20% to 90% of the total amount. This finding represents a significant problem when considering energy recovery from fuel cell anode exhaust, as done in cogenerative systems where a fuel cell stack is coupled with a fuel reforming unit [59, 60, 61, 5].

3.4   Remarks

The experimental analysis was effective in detecting and characterizing the crossover leakage in a defected single HT-PEMFC. The investigation was based on the analysis of fuel cell exhausts and was carried out using simple instruments without interrupting fuel cell operation. Observed trends indicate that crossover leakage depends with linear proportionality on the pressure difference between the fuel cell compartments and is not influenced by the fuel cell tem-
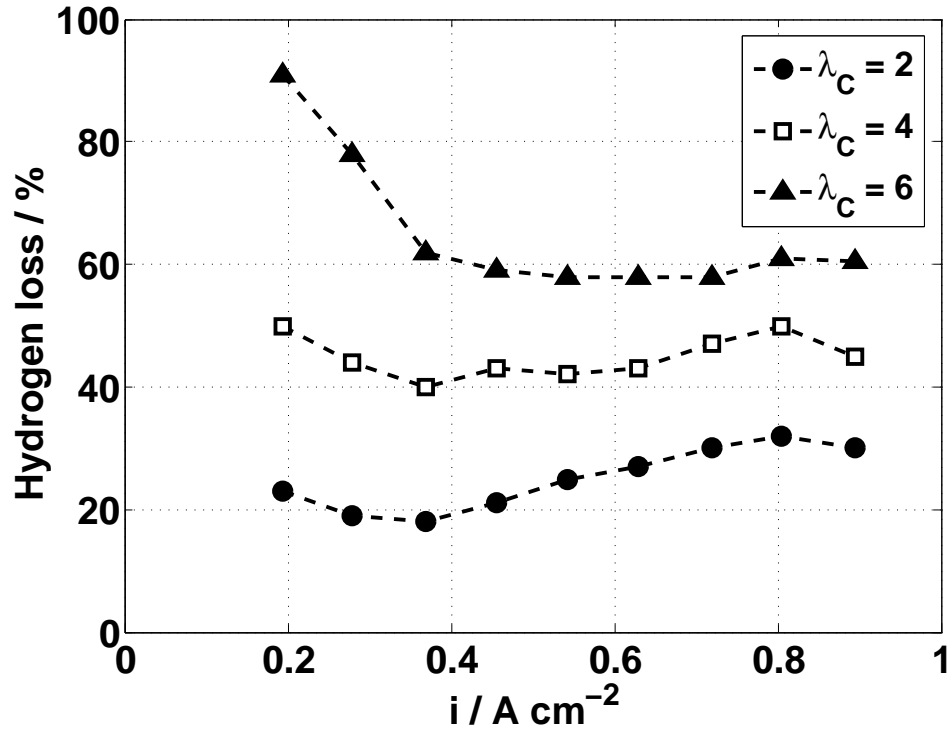
Figure 3.6: Loss of hydrogen in the anode exhaust as a percentage of the expected amount at different air stoichiometry; T_{cell}=160°C, λ_{H_2}=1.3.

perature. During normal working conditions, the cathode inlet pressure always exceeded the anode pressure, thus generating considerable air crossover. Hydrogen crossover is otherwise obtained by reverting the pressure difference through a remarkable increase in hydrogen stoichiometry. This finding confirms that crossover is driven by permeation, which is the cause of a dramatic gas transport when internal damage to the fuel cell is present. In this specific case, the crossover leakage does not affect voltage, which is comparable with the voltage of a non-defected fuel cell. Nevertheless, hydrogen consumption is remarkably increased, thus reducing the hydrogen availability in the anode exhaust and considerably compromising fuel cell energy recovery. The methodology and experimental setup employed in this study allowed for the analysis of fuel cell outlet streams using simple instruments and without interrupting fuel cell operation, thus making this a useful tool for crossover leakage detection during long-time degradation testing.

Chapter 4

Internal Water Transport

In this chapter an experimental analysis of internal water transport in a phosphoric acid doped PBI-based HT-PEMFC is presented. Effect of cell temperature, reactants stoichiometry and current density is analyzed when dry and humidified reactants are fed. Measurements uncertainty, repeatability and mass balance are analyzed to assure for reliable results interpretation.

4.1   Aim

The effect of water transport on HT-PEMFC behavior is particularly important. Actually, even though HT-PEMFCs can operate in dry conditions, it does not occur in real applications where a high water content is always present in the syngas produced by fuel processors. The eventual necessity of fuel drying would imply an expensive water removal system, thus HT-PEMFCs tolerance to humidified conditions needs further investigation to clarify some concurrent effects. Water is reported to improve proton conductivity both in the membrane and in the electrodes due to its effect on acid equilibrium [5, 15, 16, 17, 18, 23]. Furthermore water on anode side can contribute to water-gas shift reaction to oxidize CO when reformed gas is used [62]. On the other side supplying water through the humidification of feed streams decreases reactants partial pressure [24, 38] and can increase the acid leaching from the electrodes with negative effects on the performance due to a reduction in the three phase zone [23]. Therefore quantifying water transport within the MEA in dry and humidified conditions is of relevant interest. Reactants humidification is a useful instrument to enhance the effects of water presence even if running an HT-PEMFC with humidified reactants appears questionable. The present chapter reports a systematic experimental analysis on water transport in a phosphoric acid doped PBI-based high temperature PEM fuel cell.

4.2   Experimental

4.2.1   Methodology

A single PBI based HT-PEMFC is operated with pure hydrogen and air in co-flow configuration. After an activation period of 70 hours at reference conditions (T_{cell}= 160°C, i=0.2 $A\,cm^{-2}$, λ_{H_2}=1.2, λ_{Air}=2) as recommended by the manufacturer [35], two consecutive sets of polarization curves were performed during which an extensive range of cell temperatures and reactants stoichiometries is covered. During the first set of polarization curves (tab.4.1) both reactants are fed as dry, while during the second set (tab.4.2) humidification of anode (A) or

cathode (C) stream is alternatively performed.

Table 4.1: Investigated conditions with dry reactants.

Temperature [°C]	λ_{H_2}	λ_{Air}
140	1.3	2 - 4
160	1.2-1.3	1.5- 2 - 4
160	1.5-1.75	2
180	1.3	2 - 4

Table 4.2: Investigated conditions with humidified reactants.

Temperature [°C]	λ_{H_2}	λ_{Air}	Humidified side	Saturation temperature [°C]
160	1.2	2	A	30 - 40 - 50
160	1.2	2	C	30 - 40 - 50
160	1.2	4	A	30 - 40
160	1.2	4	C	30 - 40
160	1.5	2	A	30 - 40 - 50
160	1.5	2	C	30 - 40 - 50

Polarization curves were run imposing fuel cell current, while reactants flow rates were automatically regulated in order to keep stoichiometry constant. All curves are made up by nine current density values ranging from 0.2 to 0.9 $A\,cm^{-2}$ with constant step; during each test OCV is kept for 100 s and voltage is checked. Current density values lower than 0.2 $A\,cm^{-2}$ are not considered due to poor accuracy in analyzing mass balance. Each current density value is kept for 1200 s to make sure that cell's internal transport phenomena reach steady state. Data are recorded at 1 Hz frequency and are processed with a robust method for outliers elimination. The method eliminates values not included in the interval: median ±3 times standard deviation, estimated through median absolute

deviation (MAD). Representative values for every working point are obtained as average of 600 elements among the remaining ones. In both sets every polarization curve is randomly repeated for three times in three different days to assure for reproducibility, considering measurements uncertainty (tab. 4.3). The Representative value for each measured parameter is obtained as average of the three measures.

Table 4.3: Uncertainty of measured parameters.

Parameter	Estimated Uncertainty
Fuel cell voltage	$7\,mV$
Water concentration	5%
Cathode exhaust water flow	$4.7\% + 2.5\,10^{-8}\,mol\,s^{-1}\,cm^{-2}$
Anode exhaust water flow	$7.1\% + 7\,10^{-9}\,mol\,s^{-1}\,cm^{-2}$

4.3   Experimental setup

4.3.1   MEA and Fuel cell assembly

The HT-PEMFC used for this experimental investigation is a Celtec-P2100® by BASF Fuel Cells based on a phosphoric acid doped PBI membrane. This is the same type of fuel cell used in the previously described experimental activities. Its characteristics have already been reported in paragraph 2.2.1 and 2.2.2.

4.3.2   Test station

Fuel cell was tested in a further evolution of the experimental setup described in paragraph 3.2.2. Dry air supplied to the cathode is provided by laboratory compressed air grid, while pure dry hydrogen supplied to the anode is generated by an electrolyzer. Reactants flow rates are controlled and measured by two calibrated flow controllers (BROOKS 5850S, uncertainty: 0.7% of rate $+0.004Nl\,min^{-1}$ for air flow controller and 0.7% of rate $+0.0004Nl\,min^{-1}$ for hydrogen flow controller). Reactants are alternatively saturated at 30,40 and

50°C using a temperature controlled bubble humidifier. Reactants pressures at cell inlets and outlets are measured by pressure transducers (pressure range: 0-4 bar gauge, uncertainty: 10 $mbar$). Relative humidity at anode and cathode outlets is measured using temperature and relative humidity transmitters based on a capacitive sensor (VAISALA HMT 333, temperature range: 0-120°C, uncertainty: 0.3°C; humidity range: 0 − 100%, uncertainty: 1.5%RH + 1.5% of reading). The same measurement is introduced on anode or cathode inlet only when humidification is performed. Temperature and relative humidity sensors are lodged in heated metal blocks in order to prevent vapor condensation. Water content in cathode exhaust is then separated in a condenser operating at 20°C in order to measure dry volumetric flow (BROOKS 5850S flowmeter, uncertainty: 0.7% of rate +0.004$Nl\,min^{-1}$) taking into account for the presence of residual water vapor. The power produced by the fuel cell during operation is dissipated by an electronic load (TDI RBL 488) working in constant current (uncertainty: 0.25%). Fuel cell Ohmic resistance is measured by an AC/milliohmeter (TSURUGA 3566, estimated uncertainty: 1$mOhm\,cm^2$) that measures cell impedance at 1 kHz single frequency. All instruments are connected to a personal computer through acquisition boards and all measured parameters (pressures, temperatures, relative humidities, flow rates, cell voltage and current) are automatically recorded and stored. A simplified scheme of described experimental apparatus is reported in fig.4.1. The overall combined measurement uncertainty of the investigated quantities is evaluated according to [55] and is reported in table 4.3.

4.4   Results

4.4.1   Dry reactants: anode exhaust water flow

When dry reactants are fed, water within the fuel cell is present due to the electrochemical reaction in the cathode electrode. If water transport occurs across the polymer electrolyte, migrated water is found in anode exhaust. Relative humidity measurement at anode outlet is thus used to detect and quantify water transport from cathode electrode to anode channel across the MEA. Water mo-
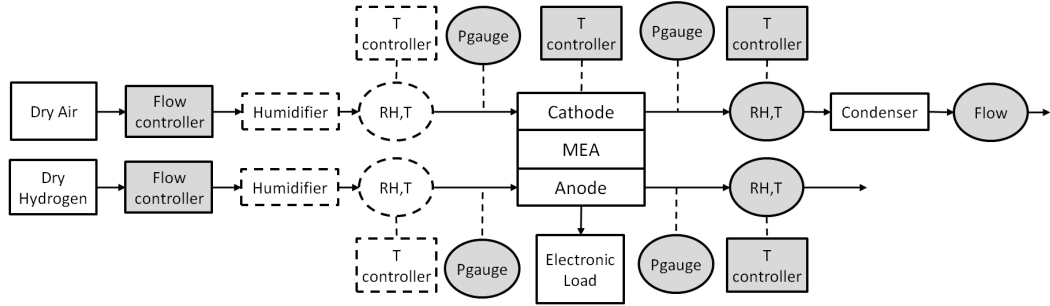
Figure 4.1: Experimental setup scheme: gray squares represent controlled parameters, while gray rounds represent measured parameters. Components in dashed line are connected only when humidification is performed.

lar flow is obtained by multiplying water concentration and dry volumetric flow as explained by Eq. (7,8,9) in [63]. For every tested condition, water flow in anode exhaust is far higher than measurements uncertainty, proving the presence of water transport from cathode to anode across the membrane. Experimental results are reported in fig. 4.2 where water molar flux to anode is plotted versus current density for different reactants stoichiometries. It is possible to observe that reactants stoichiometries play a decisive role in determining water redistribution between cathode and anode. Increasing air stoichiometry sensibly reduces water transport from cathode resulting in lower anode exhaust water flow. On the opposite, higher hydrogen stoichiometry increases water transport from cathode leading to higher water flux in anode exhaust. Such trends find explanation in the fact that higher flow rates reduce local water concentration, thus enhancing water removal. Differently, temperature has negligible influence on water transport: values recorded under the same stoichiometry are always coincident, even when fuel cell temperature is changed from 160°C to 140°C and 180°C. Fig. 4.2 shows that water molar flux in anode exhaust increases almost linearly with current density, suggesting that water back diffusion across the membrane is directly proportional to water production at cathode electrode. This behavior is justified considering the negligible electro osmotic drag coefficient of PBI [20, 7]. The data of fig. 4.2 are reported also as fraction of the

electrochemical water production in fig. 4.3 to evaluate their proportionality with the current density. A strong deviation from a constant value is evident. When λ_{H_2} is equal to 1.3 the data are included between 5% and 12% and show an increasing trend with current density. Differently, when λ_{H_2} is equal to 1.75, values rise up till 18% and seem to be just slightly decreasing. These results underline the critical influence of hydrogen stoichiometry and depletion on water transport through the membrane. Further information can be obtained by analyzing water concentration at anode and cathode outlets.
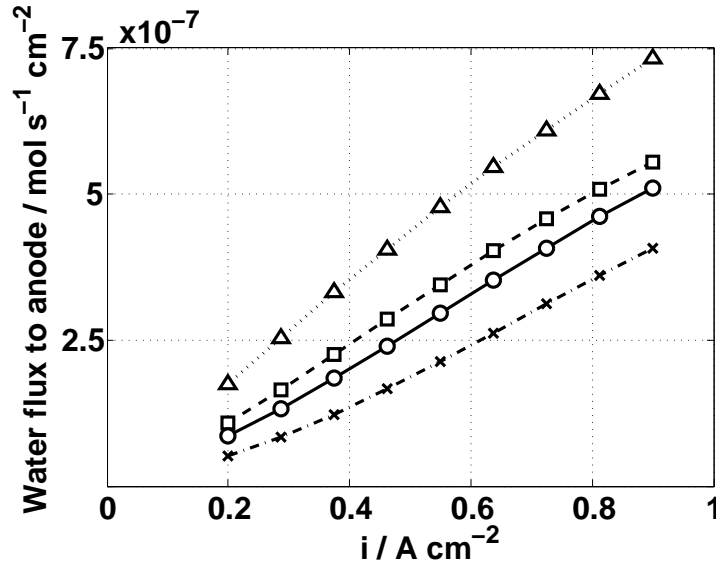
Figure 4.2: Water flux to anode vs current density in dry conditions at 160°C for all investigated reactants stoichiometries. (□) λ_{H_2}=1.3, λ_{Air}=1.5; (○) λ_{H_2}=1.3, λ_{Air}=2; (X) λ_A=1.3, λ_C=4; (△) λ_A=1.75, λ_C=2.

4.4.2   Exhausts water concentrations

Water concentration in anode and cathode exhausts is reported in fig. 4.4 as a function of current density at different stoichiometries. In all tests performed with dry reactants, anode outlet water concentration is higher than cathode one and coherently reproduces the trends reported in fig. 4.3. On the other side cathode outlet water concentration is seen to be always almost constant, indeed
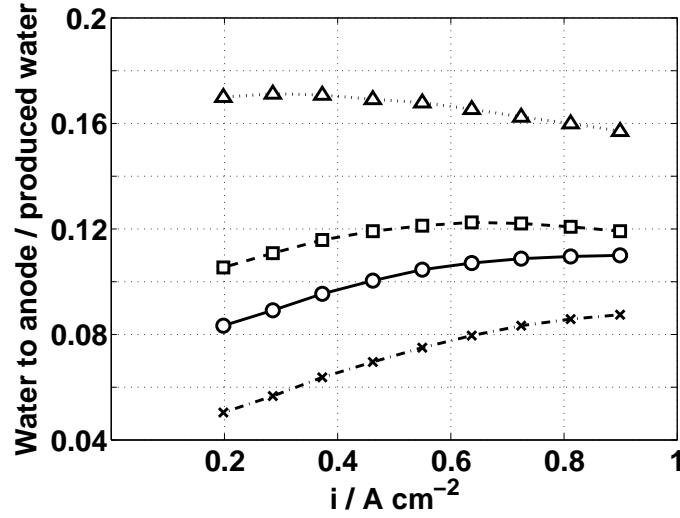
Figure 4.3: Water flux to anode over electrochemical water production vs current density in dry conditions at 160°C for all investigated reactants stoichiometries. ($\square$) λ_{H_2}=1.3, λ_{Air}=1.5; ($\bigcirc$) λ_{H_2}=1.3, λ_{Air}=2; (X) λ_A=1.3, λ_C=4; ($\triangle$) λ_A=1.75, λ_C=2.

a slight decrease is necessary for mass balance closure. Even though the net water transport through the membrane is from cathode to anode, as reported in fig. 4.2, a local reverse water flow, from anode to cathode, is expected near the fuel cell outlet. The rising trend of anode water concentration is also due to hydrogen depletion along the flow field causing non linear profiles that can explain the trends shown in fig. 4.3 and fig. 4.4. In fact, when hydrogen stoichiometry is high (fig. 4.4D), anode water concentration diminishes and flattens due to dilution in a higher flowrate. Analogously, when cathode stoichiometry is increased, both outlet cathode water concentration (fig. 4.4C,A,B) and water flux through the membrane (fig. 4.2) decrease, causing also lower anode water concentrations. A further possible reason of water transport non linearity can be the dependence of membrane diffusivity on water content. Therefore, internal transport phenomena exhibit great complexity and the performed global measurements do not allow to draw further conclusions.
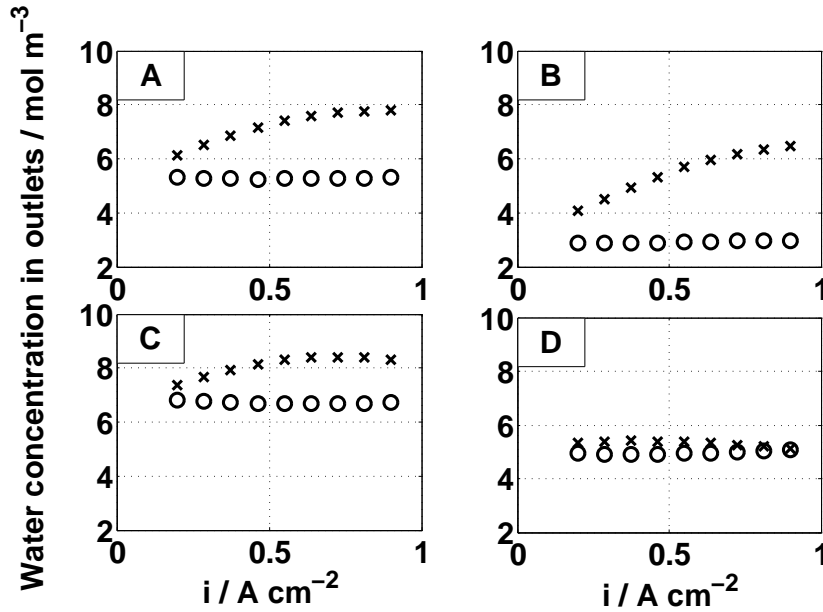
Figure 4.4: Water concentration values in anode and cathode exhausts. (X) anode water concentration; (◯) cathode water concentration. λ_{H_2}=1.3(A,B,C),1.75(D); λ_{Air}=2(A,D),4(B),1.5(C).

4.5 Humidified reactants

4.5.1 Exhausts water flow

Trends described in this section are observed for all experimental conditions reported in table 4.2, the effect of reactants stoichiometries on water transport confirms what already explained in section 4.4.1 for dry reactants. In this section reactants are alternatively humidified to evaluate changes in water redistribution. Humidification level is controlled by saturating reactants at 30, 40 and 50°C with a bubble humidifier. Higher saturation temperatures were not achieved because in such conditions water concentration measurements at fuel cell outlets have high uncertainty and poor reliability. Anyway this limit does not restrict the validity of the analysis, actually in [38], where also higher saturation temperatures are investigated, the major humidity effects are already evident at 50°C. In humidified conditions water content at fuel cell inlets is no more null and the global water transport from cathode to anode can be

quantified with the following equation:

$$\dot{n}_{water}^{c->a} = \dot{n}_{water}^{out,a} - \dot{n}_{water}^{in,a} \tag{4.1}$$

where $\dot{n}_{water}^{c->a}$ is water molar transport from cathode to anode, $\dot{n}_{water}^{out,a}$ is water molar flow in anode exhaust and $\dot{n}_{water}^{in,a}$ is water molar flow in anode feed stream. Water transport is graphed versus current density in fig. 4.5. When cathode is humidified, water transport to anode is higher than in dry conditions and increases with increasing cathode saturation temperature. Conversely when anode is humidified, water transport from cathode to anode is lower than in dry conditions and decreases with increasing anode saturation temperature. Rising this temperature progressively hinders water transport from cathode to anode till, at anode saturation temperature of 50°C, water transport becomes negative indicating that net water flow is from anode to cathode. These trends confirm that water transport is influenced by water concentration in reactants streams and underline the possibility of a reverse water transport with intensive anode humidification, as can occur in real CHP applications. Water transport from cathode to anode is also graphed as fraction of electrochemical water production in fig. 4.6. When no humidification is performed (white circles), water flow to anode is included between 5% and 10% of electrochemical production. By performing cathode humidification (white markers), this value progressively increases till around 14% of electrochemical water production at high current density and saturation temperature. Conversely, by rising anode saturation temperature (black markers), water transport values decrease until they become negative at 50°C. This means that water migration changes direction and net water flow now occurs from anode to cathode. In such condition water content in cathode exhaust exceeds electrochemical production due to a water flux coming from anode.

4.6   Remarks

Water transport in a PBI based HT-PEMFC is experimentally investigated on a wide range of fuel cell operating temperatures and stoichiometries. The effect
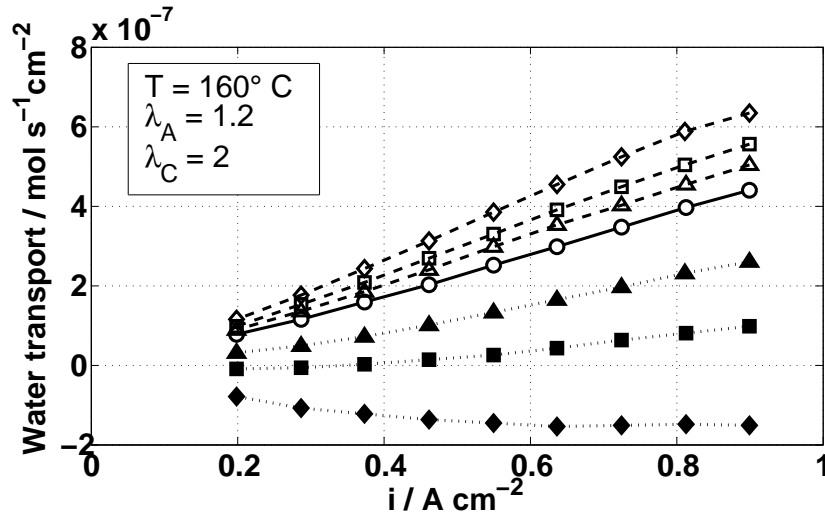
Figure 4.5: Water transport vs current density with dry and saturated reactants. ($\bigcirc$)dry reactants; cathode saturation: ($\triangle$)T_{sat}=30°C, ($\square$)T_{sat}=40°C, ($\diamond$)T_{sat}=50°C; anode saturation: ($\blacktriangle$)T_{sat}=30°C, ($\blacksquare$)T_{sat}=40°C, ($\blacklozenge$)T_{sat}=50°C.

of separate reactants humidification on water redistribution is quantified and evaluated by means of global mass conservation measurements. Calibrated instruments and reliable methodology are employed to assure for uncertainty and repeatability. With dry feed streams, up to 18% of electrochemically produced water is found on anode side confirming the presence of water transport from cathode electrode. Water transport appears independent of fuel cell temperature but demonstrates important dependence on reactants flow rates and humidification. Water moves in direction of increasing molar flow and decreasing humidification rate. This trend is explained by enhanced water removal mainly due to lower mean water concentrations occurring in such conditions. With intensive anode humidification, water transport direction can change obtaining net water flow from anode to cathode. In all investigated conditions, anode exhaust water concentration is higher than cathode one and shows increasing trends that underline water transport non linearity.
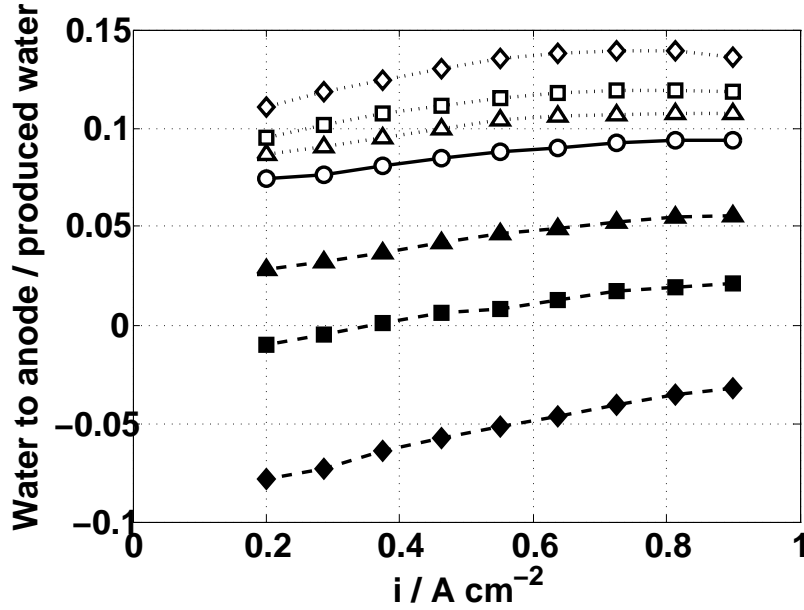
Figure 4.6: Water flux to anode over electrochemical water production. (◯) dry reac-
        tants; cathode saturation: (△)T_{sat}=30°C, (□)T_{sat}=40°C, (◇)T_{sat}=50°C;
        anode saturation: (▲)T_{sat}=30°C, (■)T_{sat}=40°C, (◆)T_{sat}=50°C.

4.7   Appendix

4.7.1   Dry molar balance verification

During all tests dry molar flux balance is verified on cathode side by means of
the following mass conservation equation:

$$\dot{n}_{air}^{in} - I/4F - \dot{n}_{air}^{out} = 0 \tag{4.2}$$

where $\dot{n}_{air}^{in}$ is dry air molar flux at cathode inlet, $I/4F$ is oxygen molar con-
sumption due to electrochemical reaction and $\dot{n}_{air}^{out}$ is dry air molar flow measured
at cathode outlet. The error in closure of this balance is always smaller than
measurements uncertainty. This means that error is not statistically meaning-
ful, consequently mass conservation can be assumed attesting that measuring
system is reliable and internal leakages are negligible.

4.7.2   Water molar balance verification

Water balance during all tests is checked by considering water entering the fuel cell with the feed streams, water production due to reaction and water output within exhausts, as reported in the following equation:

$$\dot{n}_{water}^{in,c} + \dot{n}_{water}^{in,a} + I/2F = \dot{n}_{water}^{out,a} + \dot{n}_{water}^{out,c} \tag{4.3}$$

where $\dot{n}_{water}^{in,c}$ and $\dot{n}_{water}^{in,a}$ are water molar flow within cathode and anode feed streams, $\dot{n}_{water}^{out,a}$ and $\dot{n}_{water}^{out,c}$ are water molar flow within cathode and anode exhausts and $I/2F$ is fuel cell electrochemical water production. The error in closure of this balance is always smaller than water flow measurements uncertainty (tab.4.3). This indicates that also water conservation can be assumed, giving further confirmation to measurements reliability.

Chapter 5

Effect of Water on Performance

This chapter discusses the impact of humidification on the performance of the HT-PEMFC. The effect of water on the single fuel cell internal components is separated by means of Electrochemical Impedance Spectroscopy and Cyclic Voltammetry.

5.1 Aim

The effect of water transport on the behavior of an HT-PEMFC has been extensively reported in the previous Chapter 4. Such analysis provides information on the water balance of the fuel cell, while no information is given on the performance under humidification. Such topic is the object of the present chapter, where the voltage variation due to humidification of the reactants is discussed. Humidification is actually inevitable when feeding reformed gas to a fuel cell, and the eventual gain or loss in its power output and efficiency needs to be quantified. In the present study the reason of voltage variation is investigated by separating the contribution of the single fuel cell components. Aim of this investigation is to individuate the cause of voltage variation and achieve deeper knowledge in fuel cell internal phenomena. This was made possible by means of Electrochemical Impedance Spectroscopy (EIS) and Cyclic Voltammetry (CV).

5.2 Experimental

The effect of humidification on the performance of the fuel cell was evaluated by analyzing the polarization curves described in Chapter 4. The experimental setup and the methodology are described in paragraphs 4.2.1 and 4.3.2 of the above referred Chapter, where the reader can find all of the necessary information. New measurements are represented by Electrochemical Impedance Spectroscopy (EIS) and Cyclic Voltammetry (CV), which are described next. Both the EIS and the CV were performed using a potentiostat (Autolab PGSTAT 30® by Ecochemie B.V.) provided with a frequency-response analysis module. When measuring EIS, this instrument was operated in connection with the electronic load which worked as controlled device. The Ohmic resistance of the fuel cell was continuously monitored by an AC milliOhmeter connected to the fuel cell.

5.2.1 Electrochemical Impedance Spectroscopy

Electrochemical Impedance Spectroscopy (EIS) is a measurement technique which is used to study a variety of electrochemical processes and systems [64]. In

the case of fuel cells, such technique is used to obtain information on the fuel cell internal losses under real operating conditions [65]. The development of correct EIS measurements and the interpretation of its result is complex and still under discussion within the scientific community. This measurement technique was learnt during a period of research at *Research Center Julich* (Julich, Germany) and was then reproduced in the *M.R.T. Fuel Cell Laboratory* at *Politecnico di Milano*. In this specific work the EIS was performed in galvanostatic mode [66], which consists in sending to the fuel cell a small sinusoidal current perturbation (in the order of $100\,mA$) over a wide range of frequencies (from $20\,kHz$ to a few $100\,mHz$), and in observing its voltage response. The module and the phase shift between the voltage response and the current perturbation is due to the electrical impedance of the fuel cell [67, 68]. According to the frequency of the AC current signal, different fuel cell physical phenomena will be excited, depending on their typical time scale. Fast electrochemical reactions will respond at high frequency, while slower mass transport phenomena will respond at low frequency. This will originate changes in the impedance module and phase giving useful insight on the entity of the internal fuel cell losses [67]. The most debated outcome of the EIS measurement is called *impedance spectrum* and consists in a plot that reports the real and the imaginary values of the fuel cell impedance, recorded at different frequency [68]. An example of impedance spectrum recorded on a BASF Celtec-P2100® HT-PEMFC is reported in fig. 5.1. In this figure the following elements can be recognized reading from left to right: a linear branch departing from the real axis, a first big circle and a second smaller circle. These elements are typical for HT-PEMFC and can be attributed to the equivalent impedance of well known physical processes occurring inside of the fuel cell [67, 69, 70], respectively to:

 1) proton conduction in the electrodes,

 2) oxygen reduction reaction,

 3) oxygen diffusion to the cathode catalyst layer.

Widespread agreement is conferred to this qualitative interpretation of EIS. Contrarily, the quantitative interpretation of the EIS spectra can be achieved
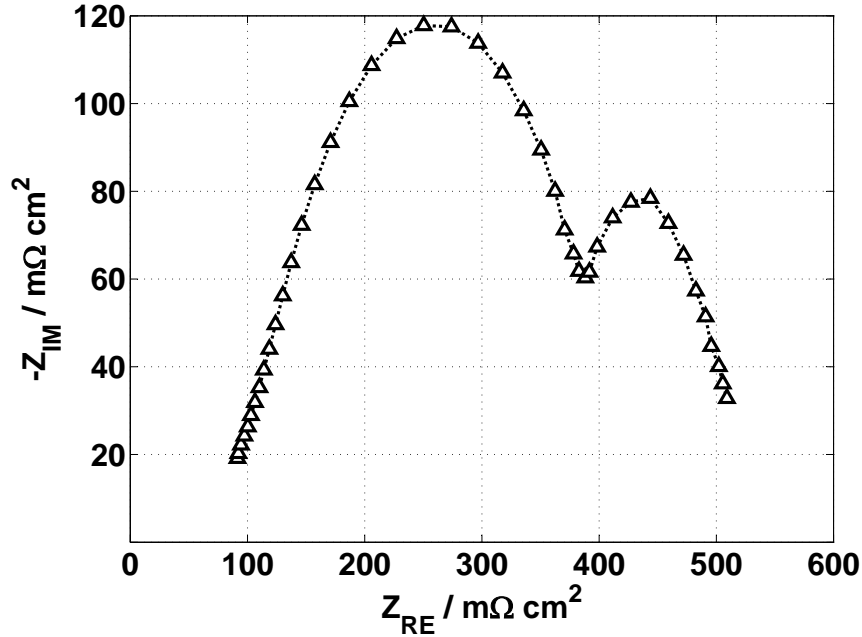
Figure 5.1: Example of impedance spectrum for a BASF Celtec-P2100® HT-PEMFC. T_{cell}=160°C, λ_{H_2}=1.2, λ_{Air}=2.

only by fitting the experimental data through equivalent circuits [68, 66, 71, 72, 73] or by developing complex physical models [74, 75]. In both cases, the connection between the observed impedance trends and the single physical mechanisms is not completely clear and is still under investigation. Only some trends are nowadays confirmed and widely accepted, and the hereon reported considerations will only concern these arguments. Therefore, an in depth modeling analysis of the EIS spectra will not be treated in this work, since it goes beyond its target.

5.2.2 Cyclic Voltammetry

Cyclic Voltammetry (CV) is a measurement technique which is normally applied in the study of catalyst systems and electrochemical reactions. In the fuel cell field, CV is widely used to evaluate the catalyst active area of the electrodes [65]. In this experimental activity, it was used to measure the catalyst active area of the cathode electrode, where most of the fuel cell losses take place.

During this measurement the fuel cell was fed with hydrogen on the anode side and nitrogen on the cathode side. In this condition the cathode is covered by hydrogen coming from the anode side which cannot be consumed, due to the absence of oxygen. The CV was performed by cyclically scanning the potential of the cathode between $0\,V$ and $0.6\,V$ with a speed rate of $100\,mV\,s^{-1}$. As a consequence of this continuous voltage variation, a non stationary current was generated inside of the fuel cell because of the successive hydrogen desorption and adsorption on the cathode catalyst. By plotting the measured non stationary current as a function of the imposed voltage a *voltammogram* is obtained. This plot represents the outcome of CV and shows a positive current peak which is related to the hydrogen desorption from the cathode catalyst particles. By integrating this non stationary current peak over time, an estimation of the charge adsorbed on the cathode catalyst can be obtained. The catalyst active area can therefore be calculated assuming that the catalyst is covered by a monolayer of hydrogen with a charge density of $210\,\mu\,C\,cm^{-2}$ [65]. During the measurement, the potential was intentionally limited below $0.6\,V$ to observe only hydrogen adsorption-desorption without entering the oxygen adsorption-desorption region [76]. As explained above, the CV cannot be performed under real operative conditions. For this reason it was essential to reproduce measurement conditions which are as similar as possible to the real operative ones. The proper choice of flow rates and humidification was therefore critical and was done with particular care.

5.3   Results

5.3.1   Polarization curves

The impact of humidification on fuel cell performance was evaluated by comparing polarization curves recorded when feeding dry and humidified reactants. Humidification always caused a very small decrease in fuel cell performance (fig.5.2). The reason for this voltage decrease is not clear and needs further investigation. Actually, concurrent effects take place inside of the fuel cell when humidification is performed. Therefore the effect of water on the
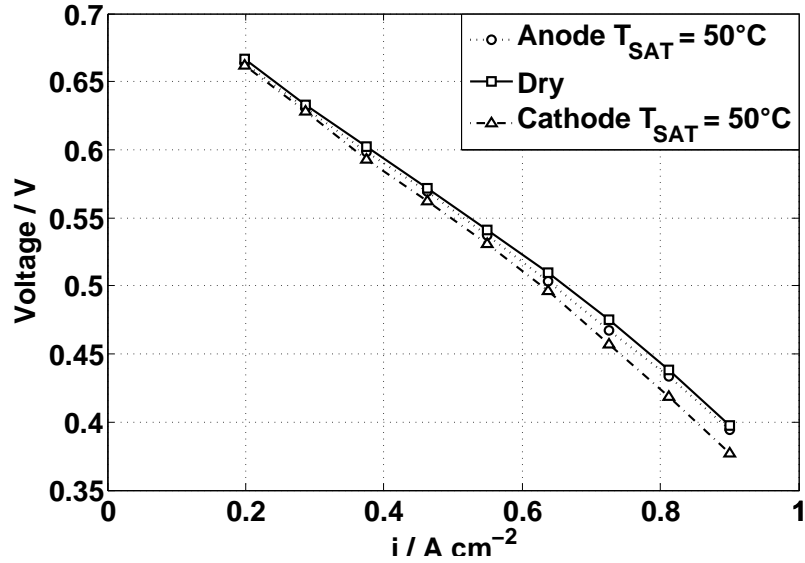
Figure 5.2: Fuel cell polarization curves with dry and saturated reactants; T_{cell}=160°C, λ_{H_2}=1.2, λ_{Air}=2.

single fuel cell components was investigated in order to quantify the single contributions to the voltage drop.

5.3.2 Ohmic cell resistance

Ohmic cell resistance measurements were done at 1kHz constant frequency by using an AC/milliohmeter described in paragraph 4.3.2, as also done in [10]. Measures are shown in fig. 5.3 and fig. 5.4 for different current density and reactants humidification rate. Reported values are always included between 70 and 80 $mOhm\,cm^2$ in agreement with the range indicated by BASF in [36] and with other publications on the same type of MEA [24, 10]. In both cases of hydrogen and air humidification, resistance progressively decreases from around 76 $mOhm\,cm^2$ in dry conditions to around 70 $mOhm\,cm^2$ with reactants saturated at 50°C. This expected phenomenon is due to hydration of phosphoric acid which shifts its equilibrium to the more conductive orthophosphoric form 1.1.4. For every investigated condition, Ohmic resistance decreases as current density increases. This trend is more pronounced in the low current density region,

where water content within the polymer increases. In the high current density region, resistance trend is almost constant due to the establishment of an equilibrium in polymer hydration level as explained in [3]. This variation is comparable to measurement uncertainty ($1\,mOhm\,cm^2$) indicating that water production due to electricity generation has a negligible impact in the investigated range. In spite of the important variations in water transport through the membrane (Chapter 4), very limited effects are evident on fuel cell resistance.
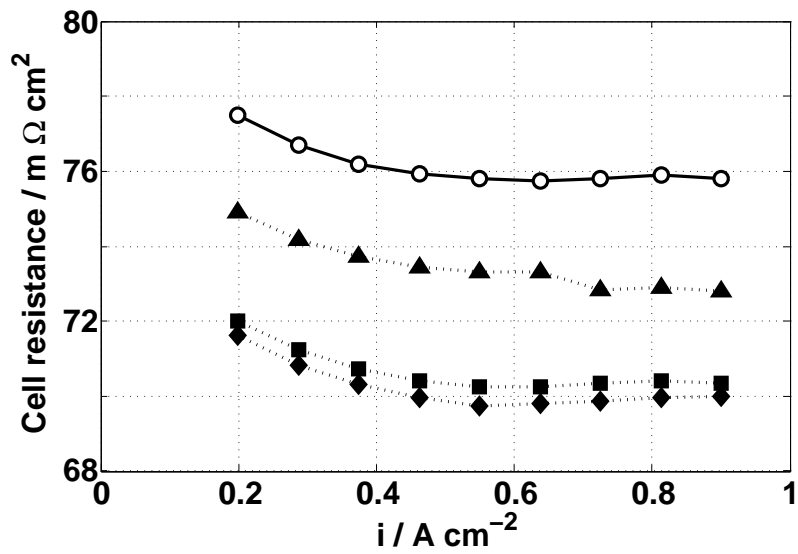
Figure 5.3: Ohmic cell resistance in presence of anode humidification. ($\bigcirc$)Dry reactants; anode saturation: ($\blacktriangle$)T_{sat}=30°C, ($\blacksquare$)T_{sat}=40°C, ($\blacklozenge$)T_{sat}=50°C.

5.3.3 Impact on voltage variation

According to the results discussed in paragraph 5.3.2, the variation in the ohmic resistance of the fuel cell would play a limited, but anyway positive influence on its voltage. Nevertheless, a global voltage loss is observed. This outcome is the result of other negative effects which are stressed by the important presence of water. Effect of these phenomena in terms of fuel cell voltage variation was quantified and reported in fig.5.5 and fig.5.6 where voltage gain due to resistance reduction and voltage loss are separately graphed versus current density
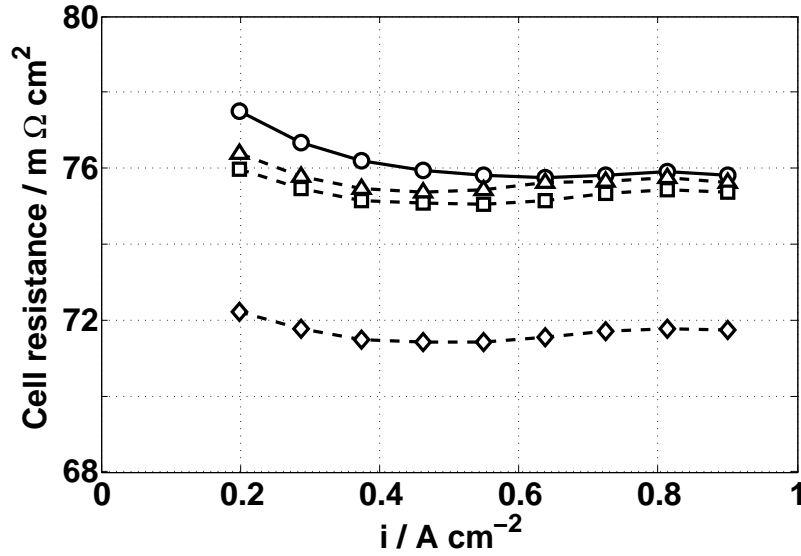
Figure 5.4: Ohmic cell resistance in presence of cathode humidification. (○)dry reactants; cathode saturation: (△)T_{sat}=30°C, (□)T_{sat}=40°C, (◇)T_{sat}=50°C.

when reactants are saturated at 50°C. In both cases Ohmic resistance decreases giving a voltage gain between 0 and 5 mV. On the other side voltage loss is always higher and reaches -10 mV and -25 mV when anode and cathode are respectively humidified. The sum of the discussed contributions is also reported in fig.5.5 and fig.5.6 and is always negative underlining the negative outcome of humidification in the investigated conditions. This behavior is in agreement with the findings reported in [24], where similar MEA and operating conditions are tested. Instead in [38] a positive effect of humidification is observed. Such difference is due to different MEA and operating conditions, in particular to the high oxygen partial pressure. In the next paragraphs further measurements are described, with the aim to clarify the negative voltage variation that offsets the positive effect of the Ohmic resistance reduction. Two main opposite effects due to water vapour presence are addressed: a variation in the catalyst active area related to the acid dilution [23, 24] and a negative decrease of the reactants partial pressure [38].
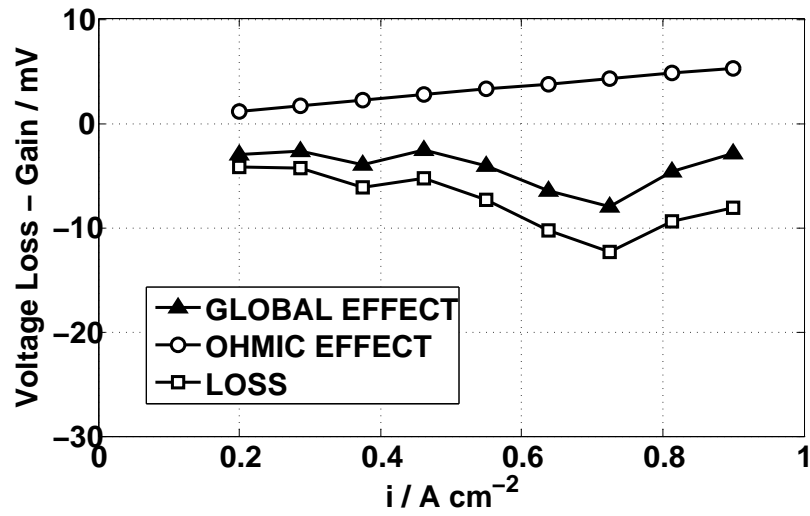
Figure 5.5: Contributions to fuel cell voltage variation with anode saturation at 50°C.
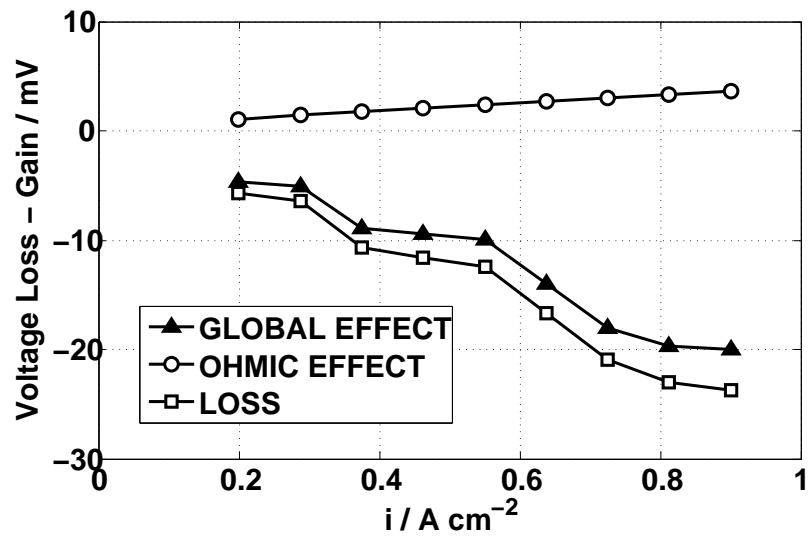
Figure 5.6: Contributions to fuel cell voltage variation with cathode saturation at 50°C.

5.4   Catalyst active area

5.4.1   Cyclic Voltammograms

The active area of the catalyst deposited in the cathode electrode was estimated by measuring Cyclic Voltammetry on the fuel cell used to investigate water transport 4 after its operation (approximately $4000\,h$ of life). The fuel cell was fed with hydrogen and nitrogen at anode and cathode side respectively. In order to reproduce the real fuel cell operative conditions, the flow rates of the reactants were set at the same values used during operation. The effect of humidification was evaluated by saturating the nitrogen at 70°C and 90°C and comparing the recorded catalyst area with the one recorded under dry conditions. The hydrogen desorption peaks measured under these conditions are reported in fig. 5.7. When nitrogen is saturated at 70°C and 90°C, the reported peaks
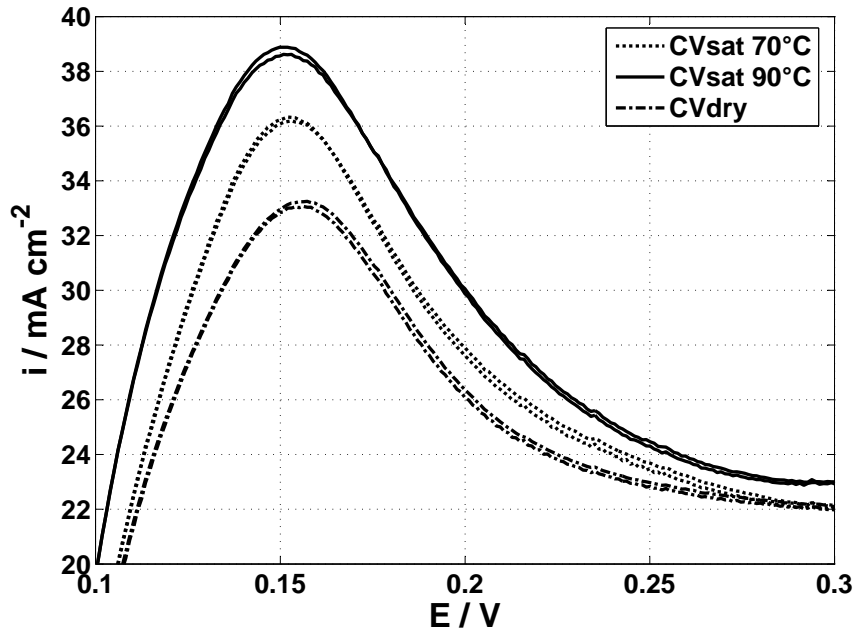
Figure 5.7: Hydrogen desorption peaks measured under different nitrogen saturation
levels.

increase due to a higher hydrogen desorption current. Considering that the size of the peaks is proportional to the catalyst active area, a positive effect of humidification can be observed. By integrating the current density profiles over

time, the catalyst active area was estimated as described in paragraph 5.2.2, the obtained values are reported in table 5.1. The reported values point out a

Table 5.1: Cathode catalyst active area measured by CV at different nitrogen humidification levels. Assumptions: catalyst loading: $0.7\,mg_{Pt}/cm^2$, Initial specific surface: $64\,m^2/g_{Pt}$, H_2 monolayer charge density: $210\,\mu C/cm^2$.

Cell lifetime [h]	T_{cell} [°C]	$T_{sat.}$ of N_2 [°C]	catalyst area $[cm^2/cm^2_{cell}]$	catalyst area $[m^2/g_{Pt}]$	catalyst use [%]
4000	160	0	38.6	5.5	8.6
4000	160	70	51.6	7.3	11.5
4000	180	90	60.5	8.6	13.5

sensible increase of the catalyst active surface with humidification. This trend is reasonable and in agreement with other published data [27]. The hydration of the fuel cell due to the humidification of the reactants dilutes the phosphoric acid and allows for its deeper penetration in the electrodes [23, 24]. In this way, the so called *three phase zone* progressively extends in the electrodes and includes an increasing number of catalyst particles. This explains the increased catalyst active surface which leads to its better use. The values of catalyst active area discussed here are smaller than reported in the cited works. This fact is due to the advanced lifetime of the investigated cell that underwent catalyst agglomeration. Degradation issues are explained in depth in Chapter 6.

5.4.2   Electrochemical Impedance Spectra

Electrochemical Impedance spectroscopy was also used to investigate the changes in the catalyst active area. As widely accepted in the literature, a more extended catalyst active area allows faster reactions and consequently decreases the kinetic resistance associated to the ORR [77]. This kinetic resistance is represented by the high frequency circle in the impedance spectrum. Therefore the variations in the kinetic resistance are followed by variations in the size of the high frequency circle of the impedance. In order to focus on this element, dedicated EIS were measured at low current density (i=0.05, 0.1

and $0.2\,A\,cm^{-2}$), with λ_{H_2}=5 and λ_{Air}=20. Being the stoichiometry so high, losses due to mass transport limitations are minimized. In this condition the impedance spectrum is made up by only one circle, due to the kinetic losses, and its analysis becomes simpler and more accurate. The humidification of air was performed by saturation at 50°C and 70°C. Recorded EIS spectra are shown in figures 5.8,5.9,5.10.
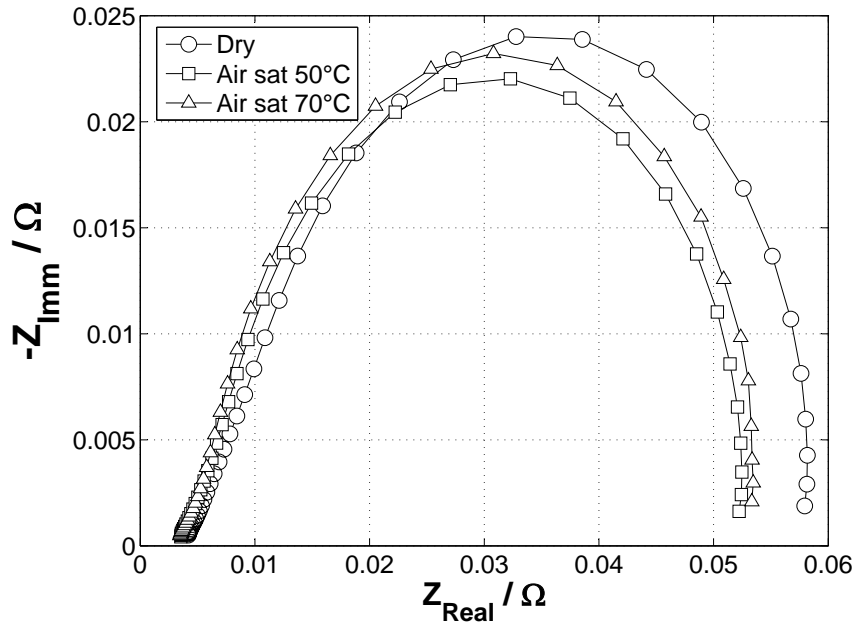
Figure 5.8: EIS spectra at i=0.05 $A\,cm^{-2}$, λ_{H_2}=5 and λ_{Air}=20.

These pictures show the same trend: the dry spectrum is the biggest one and it decreases when the air is saturated at 50°C. Conversely, further humidification by air saturation at 70°C causes an increase in the circle diameter. This means that humidification by air saturation at 50°C is positive, and causes a reduction in the kinetic losses, confirming for the outcome of the CV measurements. On the other side, when air is saturated at 70°C, oxygen suffers from dilution and this causes an increase in the kinetic losses which is explained by lower concentration. Under both of the humidification rates, the kinetic loss is smaller than under dry conditions, pointing out a positive effect of humidification on the catalyst active area. All of the recorded spectra show a linear branch at high frequency, this branch represents the proton transport in the catalyst
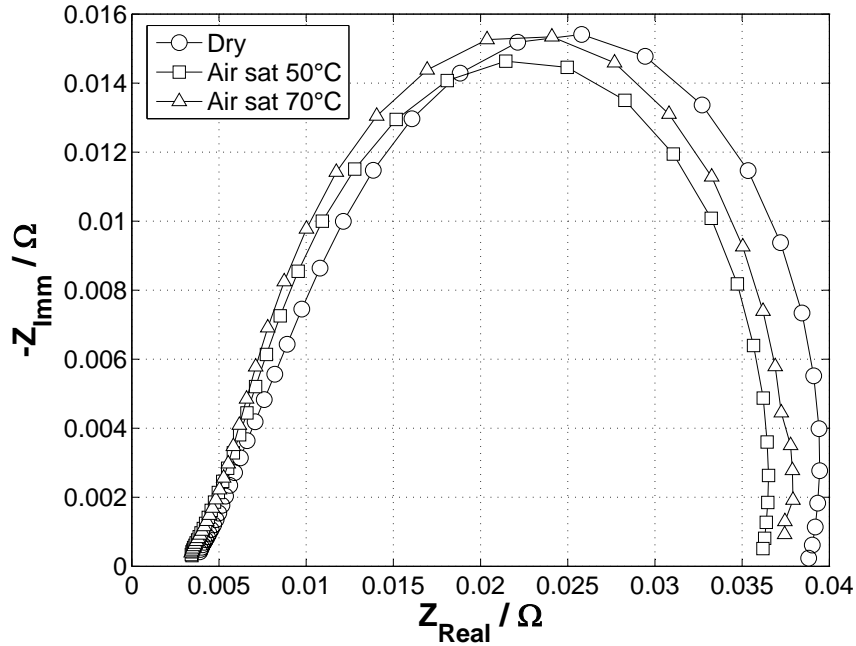
Figure 5.9: EIS spectra at $i=0.1\,A\,cm^{-2}$, $\lambda_{H_2}=5$ and $\lambda_{Air}=20$.

layer [67] and changes with the humidification rate. When the cell is dry, this branch is longer while, when the cell is humidified, the branch becomes shorter indicating a lower proton transport resistance. This behavior is explained by the increased proton conductivity of the phosphoric acid located inside of the electrodes [24], which occurs when the cell is well hydrated.

5.5   Mass Transport Limitations

As discussed in the previous paragraph 5.4.2, the increase in the losses under air saturation at 70°C, suggests the rise of mass transport problems, which are mitigated by the high stoichiometry. Under usual stoichiometry values, the dilution of oxygen may become important and could justify the voltage drop of the fuel cell. The effect of humidification on mass transport was investigated by means of EIS. Kinetic losses were minimized in order to focus on the mass transport problems, this was possible by increasing the current density. Actually as current density increases, the kinetic circle becomes smaller as demon-
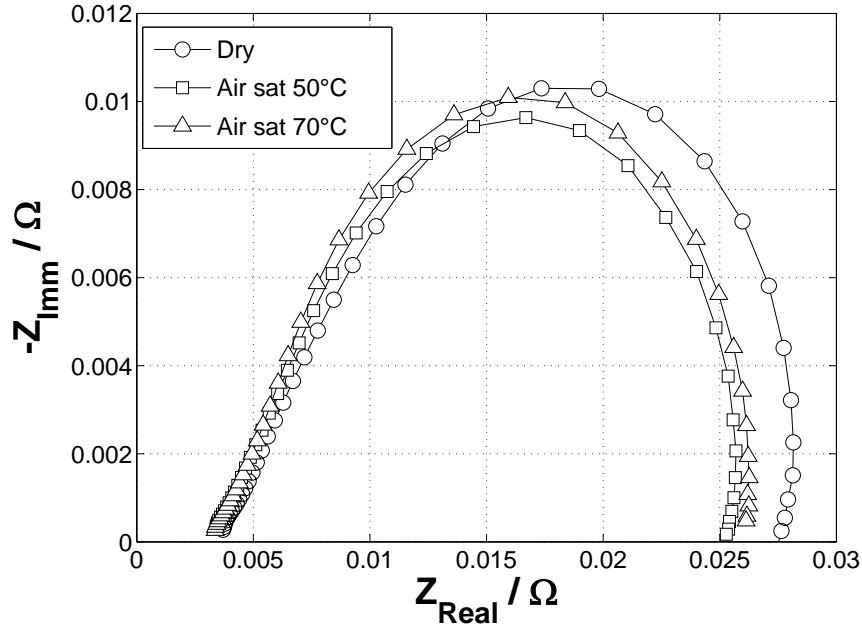
Figure 5.10: EIS spectra at i=0.2 $A\,cm^{-2}$, λ_{H_2}=5 and λ_{Air}=20.

strated by other works [73, 78] and as visible by comparing the figures 5.8, 5.9 and 5.10. Therefore the current density was set at $0.9\,A\,cm^{-2}$, and EIS spectra were recorded at reference conditions: T_{cell}=160°C, λ_{H_2}=1.2 and λ_{Air}=2. In this condition, the EIS spectrum was made up mainly by the low frequency circle, which is related to mass transport limitations. The first circle, related to kinetic losses was not visible due to the limited value of the related impedance. The effect of humidification on mass transport issues was studied by saturating the air at 50°C and 70°C. The obtained spectra are shown in figure 5.11. The shown trends underline the importance of humidification on the oxygen mass transport process. When air is saturated, the size of the low frequency circle in the impedance spectrum increases consistently. Such effect is due to the dilution of oxygen that decreases its partial pressure. The increase in the mass transport resistance is sufficient to justify the worse fuel cell performance with humidified air. In spite of the improvement in the kinetic and in the Ohmic resistance, the mass transport issues increase and easily overcome the positive described improvements.
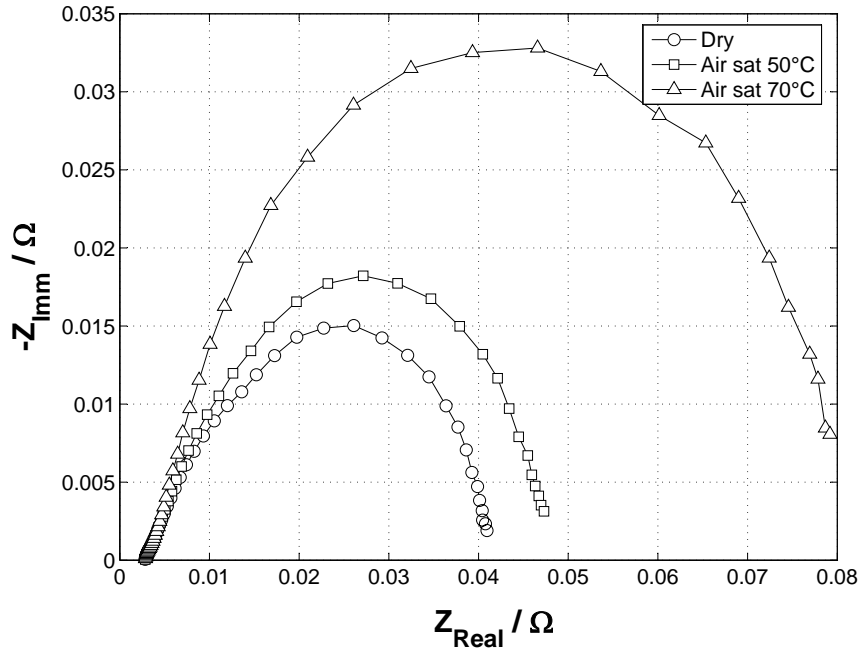
Figure 5.11: EIS spectra at i=0.9 $A\,cm^{-2}$, λ_{H_2}=1.2 and λ_{Air}=2.

5.6   Remarks

The reason of lesser fuel cell performance under humidification has been investigated and clarified thanks to polarization curves, EIS and CV measurements. Voltage drop takes place in both the cases of anode and cathode humidification but becomes more evident when cathode is directly humidified indicating a more critical situation on this side. When humid hydrogen is used, water transport increases the water concentration at cathode side also, contributing to the fuel cell voltage loss. Cell Ohmic resistance presents a limited reduction when the reactants are humidified. Catalyst active surface positively increases causing a positive drop in the kinetic resistance of the fuel cell. These improvements are anyway compensated by the rise of mass transport limitations due to the dilution of oxygen on the cathode side. This issue is the reason of the fuel cell performance worsening. Keeping reactants saturation below 50°C, the voltage undergoes no significant change, confirming the sturdiness of HT-PEMFC to water management.

Chapter 6

Degradation

In this chapter a study of degradation is presented. The study is based on the continuous monitoring of the fuel cell voltage during long time tests. The effect of the operating parameters on the voltage decay rate is considered. Insight in the internal fuel cell degradation mechanisms is obtained by means of Cyclic Voltammetry and Electrochemical Impedance Spectroscopy.

6.1   Aim

The widespread application of fuel cells in the stationary and automotive market is limited by cost and durability. A longer lifetime would positively decrease the cost of this technology making it more attractive. The durability of a PEMFC is object of discussion in many publications that investigate the main degradation mechanisms [28, 30, 79, 80, 81]. Considering an HT-PEMFC, the degradation may be accelerated because of the higher operating temperature [30, 33]. The possibility of a life extension is related to better materials and to optimized operational strategies [79]. The first topic is carried out mainly by chemists, who develop new material structures that exhibit lower degradation rates. The second topic is mainly pursued by engineers, who aim to individuate management strategies with low impact on the components of the fuel cell. A deep knowledge of the effect of each operating parameter on the components of the fuel cell is fundamental to achieve this target [28]. For this reason testing the fuel cell in a steady state condition for long times is necessary. Aim of this work is to evaluate the voltage decay rate of the tested HT-PEMFC under the most common operating conditions. Insight in the degradation of the single components is obtained by means of Electrochemical Impedance Spectroscopy(EIS) and Cyclic Voltammetry(CV).

6.2   Experimental

6.2.1   Methodology

The degradation of the fuel cell was evaluated by estimating its voltage drop over time during long time tests in steady state operation. The HT-PEMFC was operated in constant current and only one single operating parameter was changed from test to test. This method provided information on the impact of the single operating parameters on the decay of the HT-PEMFC performance. This time-consuming experimental activity is still in progress and up to now a limited number of parameters have been evaluated. As first, the voltage decay rate under reference operating conditions (i=0.2 $A\,cm^{-2}$, λ_{Air}=2, λ_{H_2}=1.2) was

evaluated on a new fuel cell for $700\,h$ after activation. This fuel cell was then substituted with another new one of the same type. This new cell was again operated under the same reference conditions for $700\,h$ after activation. This procedure was done to confirm the voltage decay rate under reference conditions on two different samples in order to get a reliable value. Afterwards the temperature of the fuel cell was risen at 180°C for $400\,h$ to verify the expected increase in the voltage decay rate. After this period the temperature was again set at the reference value of 160°C to detect permanent changes on the degradation rate after going back at reference temperature. The investigated experimental conditions are summarized in table 6.1.

Table 6.1: Investigated conditions in degradation tests, 1st cell was replaced with the 2nd cell after 700h. Test durations only refer to degradation after activation.

Tested Cell	T_{cell} [°C]	λ_{H_2}	λ_{Air}	Load $[A\,cm^{-2}]$	Test duration $[h]$
1st	160	1.2	2	0.2	700
2nd	160	1.2	2	0.2	700
2nd	180	1.2	2	0.2	400
2nd	160	1.2	2	0.2	600

6.2.2   Fuel cell and test station

The fuel cells used to carry on these experimental tests belong to the same type (Celtec-P2100® by BASF Fuel Cells) described in paragraph 2.2.1. The single fuel cell was tested in a self projected and assembled test station that represents a modification of the setup reported in paragraph 3.2.2. A simplified scheme of this apparatus is shown in fig.6.1. In this test station the water flow measurement was performed only at the outlet of the anode of the fuel cell. This measure was used to monitor the water output over time assuming for the coherence between the fuel cell internal water production and the fuel cell water output as expected when no leakage phenomenon takes place [82]. Furthermore,

the reading of the fuel cell voltage was performed also through an high precision acquisition board (uncertainty : $1\,mV$) in order to promptly detect even small variations. The acquisition of all of the measured parameters was done with a frequency of $0.5\,Hz$. Information about the single hardware components and about measurements uncertainty can be found in chapter 4. EIS and CV measurements were periodically performed connecting a potentiostat (Autolab PGSTAT 30® by Ecochemie B.V.) to the test station. In this configuration the load was controlled by the potentiostat.
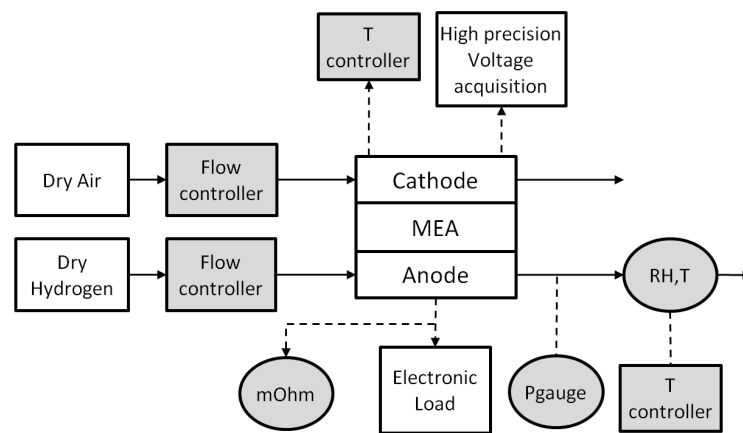
Figure 6.1: Experimental setup scheme: gray squares represent the controlled parameters, while gray circles represent the measured parameters.

6.2.3   Data elaboration

The recorded voltage values were stored and processed to obtain a reliable value of the voltage decrease over time. A dedicated procedure was developed implementing statistical methods in Matlab® environment. This procedure divides the different voltage decay periods into 400 intervals which are individually analyzed for outliers elimination as described in paragraph 4.2.1. The remaining values are then averaged to obtain a single representative value for each interval. The voltage slope is calculated by linear regression over the obtained 400 representative voltage values. In this way every degradation period is divided in the same number of intervals, therefore similar values for the variance of the

different data sets are obtained. This allows for a direct comparison between the data collected under different tests with different duration. The number of 400 intervals is the outcome of an optimization process: a larger number of shorter intervals is influenced by temporary voltage fluctuations, while a smaller number of longer intervals shows poor sensitivity to voltage changes. A supplementary verification on the stability of the voltage slope during the degradation test was performed by calculating the voltage drop rate on subsequent data intervals. This process allowed to verify for the absence of important variations in the voltage decay rate which can be considered constant within all of the investigated test periods. More information on this data analysis method is available in [83].

6.3   Results

6.3.1   Voltage decay rates

The voltage decay rates measured on the 1st and 2nd tested cells under the previously reported conditions (table 6.1) are listed in table 6.2.   The voltage trend

Table 6.2: Voltage decay values measured under the investigated operating conditions.

Tested Cell	T_{cell} [°C]	λ_{H_2}	λ_{Air}	Load $[A\,cm^{-2}]$	Voltage decay $[\mu V\,h^{-1}]$
1st	160	1.2	2	0.2	5.6
2nd	160	1.2	2	0.2	8.3
2nd	180	1.2	2	0.2	4.35$\Rightarrow$19.6
2nd	160	1.2	2	0.2	16.2$\Rightarrow$4.8

of the 2nd cell during the previously listed test periods (table 6.1) is also shown in fig. 6.2 for sake of completeness. The voltage decay rate of the investigated type of fuel cell under reference conditions was determined and confirmed on two different samples (1st and 2nd cell, table 6.1). The obtained values are $5.6\,\mu V\,h^{-1}$ and $8.3\,\mu V\,h^{-1}$, these values show good agreement and are coherent with the
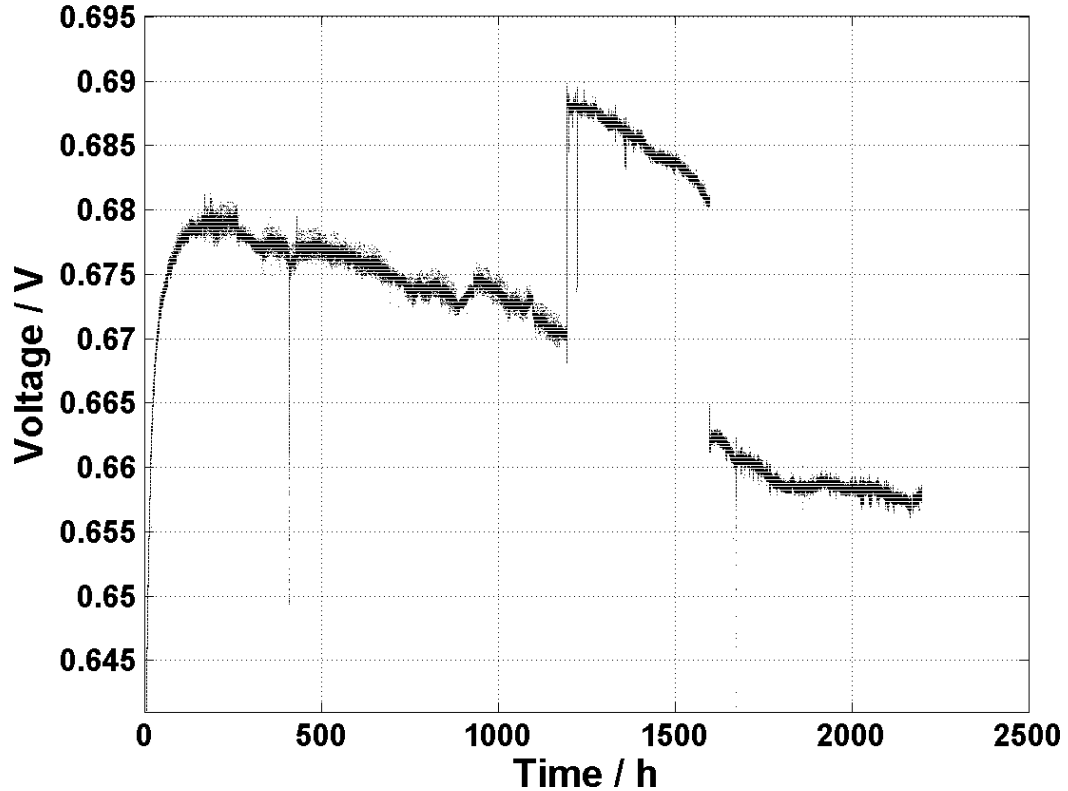
Figure 6.2: Voltage trends over time for the 2nd tested cell.

information provided by the manufacturer [36] and with other publications on HT-PEMFC [10, 22]. The test duration for each condition was chosen to fulfill the need for a sufficient number of experimental values to be analyzed. When the temperature is increased to 180°C the voltage decay rate undergoes some variations: in the first $100\,h$ it is similar to the reference value: $4.35\,\mu V\,h^{-1}$, while in the following $300\,h$ it increases becoming $19.6\,\mu V\,h^{-1}$. Higher temperature causes higher voltage decay rates [22, 33], but the change is not immediate and includes a transitional period in which the system exhibits hysteresis. Such slow change indicates the establishment of an equilibrium which requires quite a long time and could be related with the hydration state of the MEA. When the temperature is again decreased to 160°C, a similar voltage behavior is observed. During the first $200\,h$ the voltage decay rate is $16.2\,\mu V\,h^{-1}$ which is similar to the value previously measured at 180°C. During the following $400\,h$ this value

decreases and goes down to $4.8\,\mu V\,h^{-1}$ which is the typical degradation rate under reference conditions. Again these findings point out the presence of a slow equilibrium that must be re-established after changing the temperature of the fuel cell. The measured decay rates must be carefully taken into account when operating an HT-PEMFC. Even though at 180°C performances are considerably higher than at 160°C, as reported in Chapter 2, the degradation rate becomes more than double. Therefore, the operating condition of a fuel cell or of a stack has to be optimized as trade off between these two opposite tendencies.

6.3.2   Permanent degradation

The voltage decay rates measured during operation and discussed in paragraph 6.3.1 may include recoverable effects. Nevertheless, the correct evaluation of the permanent fuel cell voltage loss is fundamental for the study of degradation and of its mechanisms. In order to evaluate the permanent degradation rates, three polarization curves were measured on the 2nd cell at the end of each one of the three test periods listed in table 6.1. During polarization measurements the current density was imposed at five different values: i=0.05, 0.1, 0.2, 0.3 and $0.4\,A\,cm^{-2}$ with λ_{Air}=2 and λ_{H_2}=1.2 and T_{cell}=160°C. The measured polarization curves are reported in fig.6.3. The permanent voltage decay rates were obtained dividing the voltage gap between the measured polarization curves by the elapsed fuel cell test time. This procedure allowed to evaluate the permanent effect of both the test period at 180°C and the following test period at 160°C on the fuel cell voltage. The obtained values are reported in table 6.3. The reported values are in good agreement with the corresponding ones shown in table 6.1. This agreement indicates that the voltage slope measured during operation is entirely due to permanent degradation phenomena. The continuous voltage monitoring resulted anyway fundamental for the detection of the hysteresis that occurred when the fuel cell temperature was changed. The permanent voltage decay rates confirm for a faster degradation at 180°C, actually values are greater in this case. The difference between the permanent voltage loss rate measured at 180°C and 160°C progressively increases with current density. At $0.05\,A\,cm^{-2}$ the ratio between them (last row of table 6.3) is about 2,
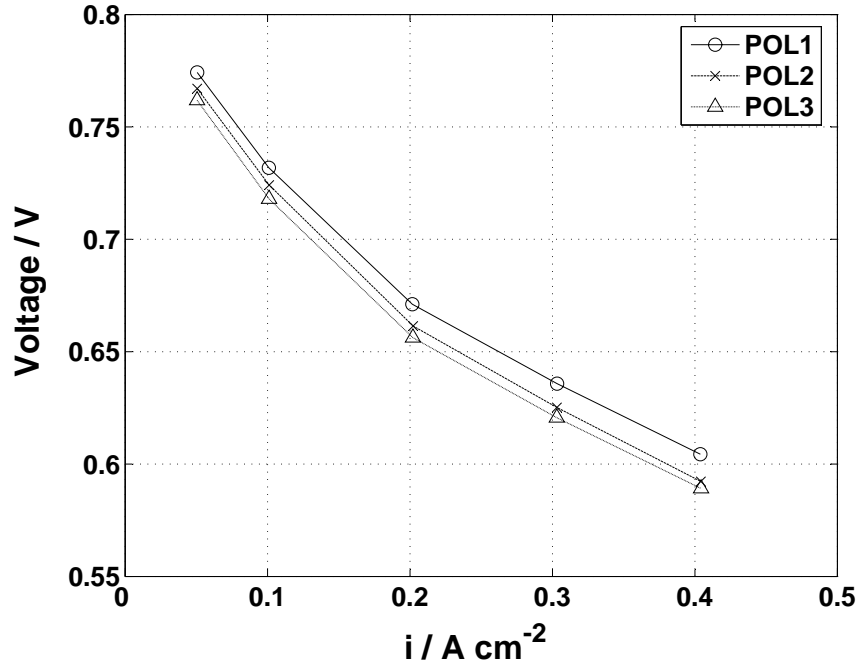
Figure 6.3: Polarization curves measured on the 2nd cell after the first period at 160°C (POL1), after the period at 180°C (POL2) and after the second period at 160°C (POL3).

Table 6.3: Permanent voltage decay rates at 180°C and 160°C

	Current density $\left[A\,cm^{-2}\right]$				
	0.05	0.1	0.2	0.3	0.4
$\Delta V_1/\Delta t\,@\,180°C$ $[\mu V\,h^{-1}]$	17.8	19.3	24.3	27	30
$\Delta V_2/\Delta t\,@\,160°C$ $[\mu V\,h^{-1}]$	8.8	10	8.7	7.7	5.3
ratio $\Delta V_1/\Delta V_2$	2	1.9	2.8	3.5	5.7

while it becomes 5.7 at $0.4\,A\,cm^{-2}$. Fuel cell degradation is more evident at high current density. This finding suggests that the permanent changes due to operation at 180°C affect the electrodes and in particular the catalyst active area and the structure of the carbon support [10, 29].

6.3.3   Catalyst active area

The catalyst active area was estimated through Cyclic Voltammetry (CV) [65, 76]. The aim of this measurement was to estimate the catalyst active area at two different times during the experimental activity. A reduction of this area during the fuel cell operation is actually expected due to catalyst agglomeration and carbon corrosion phenomena [29]. The active area was measured on the 2nd cell after recording the polarization curves at the end of the test period at 180°C and at the end of the following test period at 160°C (6.1). This measurement was performed feeding the fuel cell with dry hydrogen at the anode and dry nitrogen at the cathode, where the catalyst active area was estimated. In this condition the cathode catalyst surface is easily covered by hydrogen coming from the anode side. The Cyclic Voltammetry consists in scanning the potential of the fuel cell between $0.05\,V$ and $0.5\,V$ with a speed rate of $100\,mV\,s^{-1}$. In this way a positive current density peak related to the hydrogen desorption from the cathode catalyst can be observed [65]. The two measured peaks are graphed in fig. 6.4. The integration of such peaks was used to estimate the catalyst surface available for the reaction at the cathode electrode. The estimation was done assuming that the catalyst is covered by a monolayer of hydrogen with a charge density of $210\,\mu C\,cm^{-2}$ [65]. Such measurements represent a preliminary stage in the development of this technique and need to be further improved. Nevertheless the obtained results are in the same range of some of the values available in the literature [27, 56] and describe the reduction that the catalyst active area undergoes during fuel cell operation. The obtained results indicate a catalyst active area around $145\,cm^2/cm^2_{cell}$ (or $20,7\,m^2/g_{Pt}$) after the test period at 180°C and around $120\,cm^2/cm^2_{cell}$ (or $17,1\,m^2/g_{Pt}$) after the subsequent test period at 160°C. These results indicate a reduction of 17% in the catalyst active surface during the $600\,h$ under reference operating conditions. Unfortunately, due to hardware unavailability, the catalyst active area could not be measured before the test period at 180°C. Therefore the reduction of the catalyst active area due to the test time at 180°C could not be estimated. The catalyst active area was also evaluated on the cell used to study the internal water trasnport (chapter 4), after its operation. This cell was run for a time of approximately $4000\,h$ which
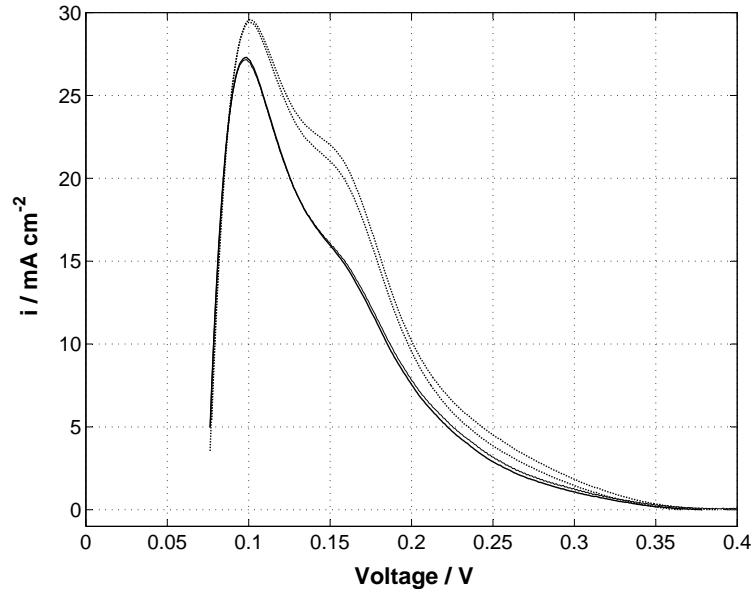
Figure 6.4: Hydrogen desorption peaks. Dashed line: CV after the test period at
180°C, continuous line: CV after the test period at 160°C.

is considerably longer than the $1700\,h$ of operation of the cell investigated here. Its catalyst active surface is around $39\,cm^2/cm^2_{cell}$ (or $5,6\,m^2/g_{Pt}$) which is much lower than the previously reported ones. This indicates that the reduction of the catalyst active area continues along the life of the fuel cell and represents one of the main reasons of its degradation [29, 81].

6.3.4   EIS analysis

Further information on HT-PEMFCs internal degradation was obtained by analyzing the electrochemical impedance spectra recorded on the 2nd cell before and after each one of the tested conditions reported in table 6.1. These spectra were recorded under the same reference conditions (i=0.2 $A\,cm^{-2}$, λ_{Air}=2, λ_{H_2}=1.2, T_{cell}=160°C) and are shown in fig. 6.5. As can be observed in all of the reported spectra, the first circle on the left side progressively grows. This part of the fuel cell impedance represents the resistance related to the Oxygen Reduction Reaction (ORR). Its growth is coherent with the outcome of the CV measurements (6.3.3) and points out the reduction of the catalyst active area.
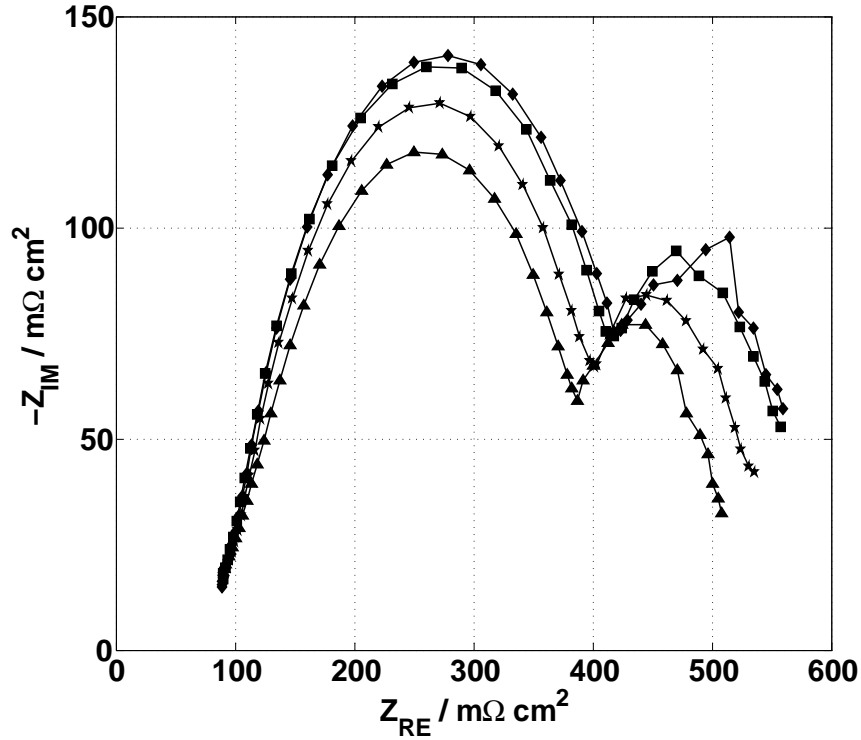
Figure 6.5: EIS spectra recorded on the 2nd cell: (▲) after activation; (⋆) after the first period at 160°C; (■) after the period at 180°C; (♦) after the second period at 160°C.

A reduction in the catalyst active area actually slows the reaction rate with a consequent increase of its kinetic resistance. Conversely, the size of the second circle located on the right side in the spectra remains almost constant. This part of the spectra is progressively translated to the right due to the increasing size of the first circle, but no change can be observed in its diameter. Such part of the spectra represents the mass transport resistance and its behavior indicates that no detectable variation takes place. The Ohmic resistance of the fuel cell is also indicated by these measurements. This value is represented by the high frequency intercept of the EIS spectra with the real axis on the left side of the plot. In fig. 6.5 the reported spectra do not reach the real axis. Therefore the intercept value was obtained by extending the plots to the real axis after their interpolation. All of the measured spectra are coincident in the high frequency region and indicate a cell resistance value of around $80\,mOhm\,cm^2$ coherently

with [10, 23, 54]. This means that the measure of the Ohmic resistance is repeatable and that its value remains constant during this part of the fuel cell life. Therefore the Ohmic resistance is not responsible for the degradation of the fuel cell.

6.3.5   Hydrogen crossover

Hydrogen crossover across the polymer membrane was measured by means of Linear Sweep Voltammetry (LSV) [65]. During this measurement, hydrogen was supplied to the anode of the fuel cell and nitrogen was supplied to the cathode, as done for Cyclic Voltammetry (6.3.3). In this condition hydrogen diffuses from the anode and deposits on the catalyst on the cathode electrode. The LSV consisted in linearly rising the potential of the cathode over the anode from $0\,V$ up to $0.5\,V$ so that the hydrogen adsorbed on the cathode catalyst [65] is progressively oxidized. During this measurement the potential was increased slowly, with a speed rate of $1\,mV\,cm^{-2}$, in order to avoid current peaks and achieve the equilibrium between hydrogen crossover and oxidation. The current related to the hydrogen oxidation was measured as indication of the hydrogen crossover rate. When the voltage is sufficiently high, equilibrium between the hydrogen crossover and its desorption can be achieved allowing for its quantification [56]. LSV was performed on two different cells: the 2nd tested cell at the end of the second test period at 160°C indicated in table 6.1(with nearly $1700\,h$ of operation), and the cell used to investigate water transport in Chapter 4 (with nearly $4000\,h$ of operation). For sake of simplicity, the former cell will be hereon referred to as CELL 1, while the latter cell will be referred to as CELL 2. The LSV current measured in these two cells is reported in figure 6.6 as function of the imposed potential. The current density profile of CELL 1 shows a slightly increasing trend which stabilizes around a value of $8\,mA\,cm^{-2}$. Differently, the current density profile of CELL 2 shows a very steep trend which reaches a value of around $18\,mA\,cm^{-2}$ at $0.5\,V$. The linear increase in current density is due to an internal short circuit across the electrolyte membrane that occurs as the potential is increased. Actually, during operation the membrane progressively thins with the consequent formation of pinholes and micro-cracks [33, 28].
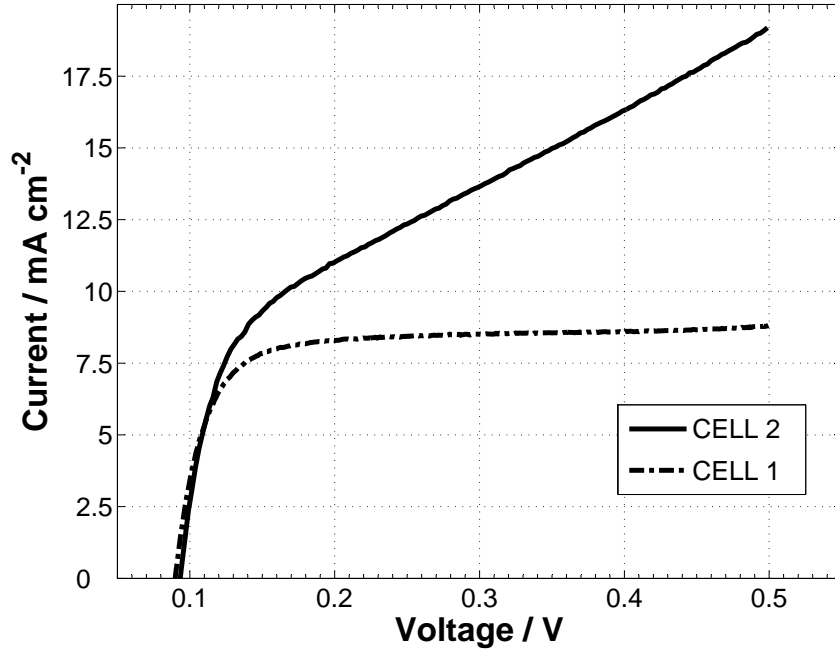
Figure 6.6: Comparison between crossover currents measured by LSV on the cell with nearly $1700\,h$ of operation (CELL 1) and on the cell with nearly $4000\,h$ of operation (CELL 2).

Therefore the electrical separation of the fuel cell electrodes can not be guaranteed, and current is generated when a voltage difference is imposed. In this situation the membrane behaves like a pure resistor obeying Ohm's law and this explains the linearity of current with voltage. The electrical resistance of the membrane can be quantified by calculating the reverse of the slope of the LSV current density profile. CELL 1 exhibits a resistance of $834\,Ohm\,cm^2$, while CELL 2 exhibits a resistance of nearly $2\,Ohm\,cm^2$. These values are in agreement with [65] and their huge difference is due to the longer operational lifetime of CELL 2 which caused further membrane degradation. In figure 6.6 the short circuit current is superimposed to the hydrogen crossover current. The sole crossover component can be obtained by subtracting the short circuit current from the total current [84]. This value can be graphically obtained by extending the linear part of the current profiles to the Y axis. The value indicated by the intercept represents the crossover current density. For both CELL 1 and CELL 2 the crossover current is around 7-$8\,mA\,cm^{-2}$, in agreement with [26, 56, 1]. This

value is huge in comparison with LT-PEMFC which reach a similar magnitude only at the end of their life. In spite of the huge difference in the electrical resistance of the two cells, the crossover current is almost the same. This indicates that the degradation mechanisms affected the membrane electrical properties, but poorly affected the crossover rate.

6.3.6   Fuel cell activation

The fuel cell activation period (also named *conditioning period*) covers relevant interest. During this time considerable variations take place within the fuel cell. The acid-doped PBI system actually needs time to equilibrate mainly due to the acid distribution in the electrodes. This procedure is necessary for the correct operation of the fuel cell and for the achievement of the desired power density. In the present degradation study two different cells were activated (1st and 2nd cell). The activation procedure consisted in running the fuel cell as suggested by the manufacturer in [35] (T_{cell}= 160°C, i=0.2 $A\,cm^{-2}$, λ_{H_2}=1.2, λ_{Air}=2) as long as voltage keeps increasing. The EIS spectra of the two cells before and after activation are shown in fig. 6.7. It is easy to notice that, during activation, the impedance of the cells decreases due to a visible reduction in the size of the first circle. On the other side the second circle and the Ohmic resistance show no variation. This indicates that the ORR kinetic resistance decreases while the mass transport resistance and the Ohmic resistance remain unchanged. The better performance of the activated fuel cell is thus due to the improvement in the kinetics. This fact is explained by the acid redistribution between the membrane and the electrodes that occurs during activation as reported in [23, 27]. A better acid distribution may increase the triple phase zone in the electrodes contacting a larger number of catalyst sites. For this reason, the catalyst active area increases and the reaction is enhanced. Figure 6.7 points out a considerable difference between the EIS spectra of the two cells. This difference may be due to the different tested item that gives origin to a behavior that cannot be perfectly reproduced. The difference in the two EIS spectra is reflected in the voltage profiles during activation which are shown in Fig. 6.8. A lower voltage profile is evident for the 1st cell which presents the highest internal losses. A def-
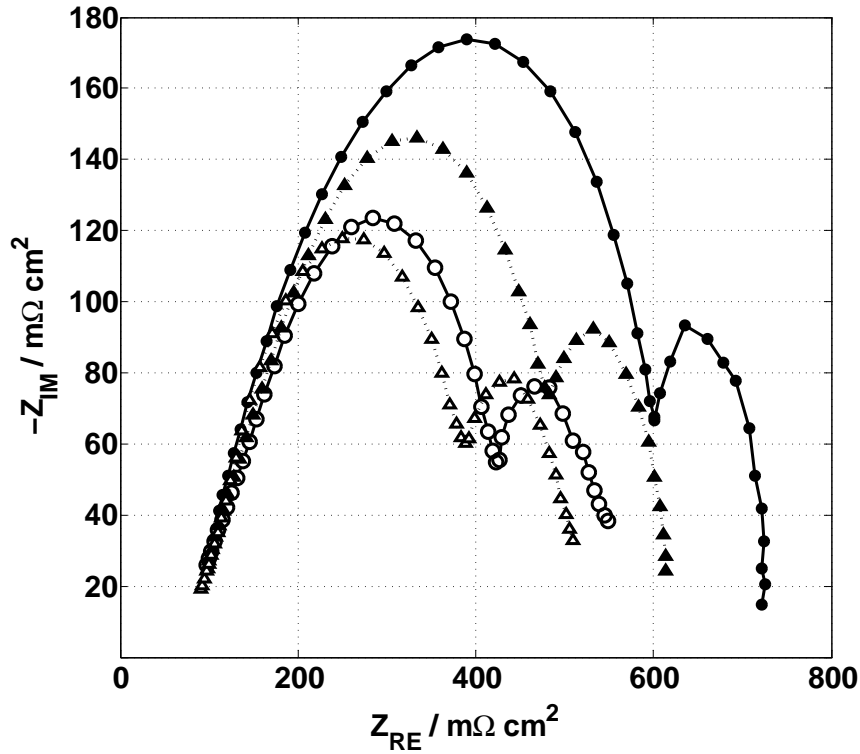
Figure 6.7: EIS spectra during fuel cell activation. ($\bullet$) 1st cell before activation; ($\bigcirc$) 1st cell after activation; ($\blacktriangle$) 2nd cell before activation; ($\triangle$) 2nd cell after activation.

inite explanation for this behavior is not available. A higher kinetic resistance, related to a non sufficient or improper acid distribution is a possible reason.

6.4   Remarks

This chapter represents a preliminary study on the degradation phenomena that involve an HT-PEMFC. The reported analysis is still in progress and up to now a limited number of conditions have been investigated due to time constrains. The voltage decay rate under reference operating conditions was measured and confirmed on two different fuel cells. This value is included between 5 and $9 \, \mu V \, h^{-1}$ and is supported by the values published in the literature. When the temperature was increased up to 180°C, the voltage decay rate became more than double because of permanent changes in the electrodes. Hysteresis was
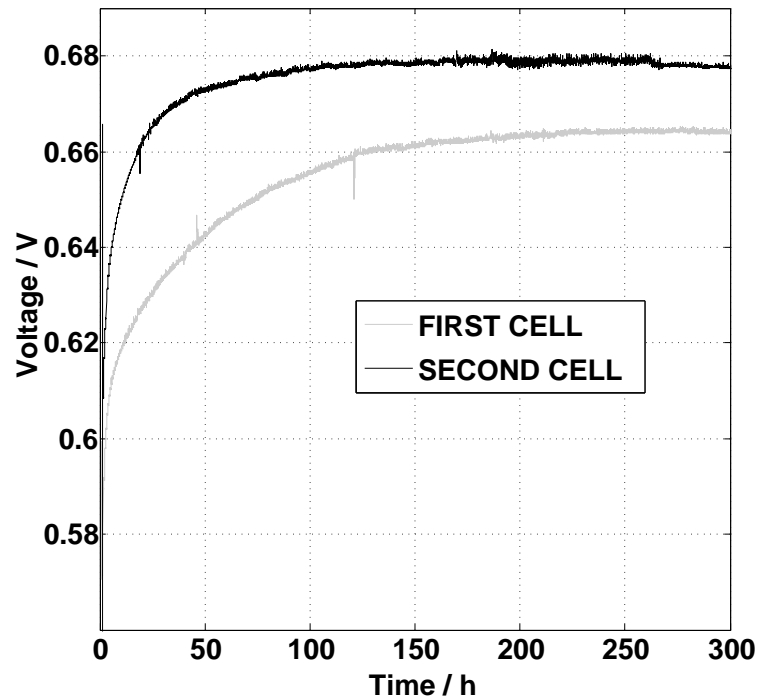
Figure 6.8: Voltage profiles of the two tested cells during activation.

detected when changing the temperature of the fuel cell and was attributed to slow hydration-dehydration mechanisms that influence the acid equilibrium. Information on the fuel cell internal components was obtained by means of Cyclic Voltammetry (CV) and Electrochemical Impedance Spectroscopy (EIS). During activation the kinetic resistance of the fuel cell decreased due to an increase in the catalyst active area related to acid distribution in the electrodes. During degradation an important reduction of the catalyst active surface was observed, this represents the main reason of degradation.

Chapter 7

Evaluation of Gas Diffusion Layer Materials

In the present chapter the influence of cathode Gas Diffusion Layer materials on HT-PEMFC operation is documented. This activity was developed during a research period at the *Institute of Energy and Climate Research (IEK-3)* of *Research center Juelich Gmbh* (Juelich, Germany). The further diffusion or use of the here displayed data is subject to the permission of such institute.

7.1   Foreword

Before starting this chapter the autor would like to acknowledge the scientific
and technical personnel of *Forschungszentrum Juelich*. Without their help and
assistance this experimental investigation could not have been realized. Grati-
tude is addressed to all of the people who directly or indirectly contributed to
realize this project. A specific thank goes to: Dr. Werner Lehnert for the or-
ganization of this research project, Dr. Roswitha Zeis for her guide throughout
the whole experimental activity, Dr. Wiebke Maier for her patience in teaching
the laboratory and testing procedures, Dr. Klaus Wippermann for the indis-
pensable help in analyzing and in understanding the Electrochemical Impedance
Spectra.

7.2   Aim

High temperature polymer electrolyte fuel cells (HT-PEMFC) represent a rel-
atively young technology. Materials and components such as catalysts, gas
diffusion media and flow fields are often taken from low temperature fuel cells
(LT-PEMFCs) and direct methanol fuel cells (DMFCs) and still need to be op-
timized. Considering the absence of liquid water in an HT-PEMFCI, the Gas
Diffusion Layer (GDL) may assume very different features. Actually the need
for a Microporous Layer (MPL) and for the hydrophobic treatment, which is
necessary in the traditional LT-PEMFCs due to the presence of liquid water,
may cease in HT-PEMFCs where only vapor is present. In this perspective, the
use of the currently available materials must be evaluated in order to find limita-
tions and possible development directions. Some investigations on GDL, MPL
and Catalyst Layer (CL) structures are reported in the literature [85, 86, 87],
but further analysis and measurements are necessary to clarify the role of the
GDL in an HT-PEMFC and assert general conclusions. A test of different com-
mercially available GDL materials on working HT-PEMFCs is thus presented
with the aim to clarify which type of material is more suitable for this recent
technology.

7.3 Experimental

7.3.1 Methodology

In order to evaluate the impact of the GDL material on the behavior of the fuel cell, 6 different HT-PEMFC were assembled and tested. The polymer membrane, the electrodes and the anode GDL material were the same for all of the built cells and were not changed. Conversely, different GDL materials were used on the cathode side, where a more complex mass transport situation takes place due to the local water production and to the oxygen diffusion. The properties of the tested diffusion media are listed in tab.7.1 in order of increasing through plane air permeability. This property is regarded as the most important for mass transport in a gas-phase system such as the cathode of an HT-PEMFC. The GDL material used on the anode side for all of the assembled fuel cells is *Freudenberg H2315-CX165* which has been taken as reference material. The behavior of the assembled fuel cells was evaluated by means of polarization curves, Electrochemical Impedance Spectroscopy (EIS), and exhaust water collection.

7.3.2 Membrane preparation

A cross-linked AB-PBI polymer film with a thickness of $50\mu m$ supplied by *Fumatech Gmbh* was used to prepare the electrolyte membranes. Single polymer squares with an area of $5cm$ x $5cm$ were cut and put into an oven at 150°C for 30 minutes to evaporate residual solvents. Afterwards the membranes were immersed in a 85% weight phosphoric acid solution at 110°C to dope for a time included between 15 and 20 hours. The doping level always resulted between 330% and 370% weight showing no correlation with time. During the doping, the size of the polymer non uniformly increased exceeding $6cm$ x $6cm$ while the membrane thickness almost doubled reaching around $100\mu m$. After their preparation, the membranes were immediately used to assemble the fuel cells in order to reduce the possible acid dilution due to the water uptake from the surrounding environment.

Table 7.1: Properties of the employed Gas Diffusion Layers materials.

Cell number	1	2	3	4	5	6
GDL producer	Freudenberg					Toray
GDL model	H2315 I3 CX190	H2315 CX 165	H2315 IX11 C4	H2315 I6	H2315	TGP H-60
Hydrophobic treatment	yes	yes	yes	yes	no	no
Microporous Layer	yes	yes	yes	no	no	no
GDL Thickness $[\mu m]$	246	247	262	210	210	190
Through plane air permeability $[l/(m^2 s)@200\,Pa]$	0.16	1	5	160	410	566
Electrode Thickness $[\mu m]$	138	116	133	126	141	108

7.3.3 Electrodes preparation

The fuel cell electrodes were obtained by spreading a catalyst ink on the gas diffusion layer substrates through the *doctor blade* technique. The catalyst ink was prepared by adding pure water (*Millipore Milli–Q® system*) and solvents (*1propanol–isopropanol* 1 : 1) to a 20% Pt/C catalyst powder (*BASF Fuel Cells*). The obtained solution was dispersed with an ultrasonic horn for 4 minutes. After, PTFE suspension drops were added as a binder and ultrasonic mixing was then continued for 30 minutes to obtain a homogeneous paste. The prepared catalyst ink was poured into the doctor blade and was spread on the GDL substrate with a coating velocity of $7.5\,mm\,s^{-1}$ to originate a wet film with a thickness of $1\,mm$. The obtained gas diffusion electrode was initially slowly dried in a fume hood for approximately 15 hours and afterwards it was put into an oven for further drying at 60°C for 30 minutes. The dry electrode thickness ranged from 110 to $140\,\mu m$ while the resulting catalyst loading was $1\,mg_{Pt}/cm^2$.

7.3.4   Fuel cell assembly

The prepared membrane and electrodes were sandwiched together to form a membrane electrode assembly (MEA) with an active area of $14,4\,cm^2$. Reactants were fed by means of in house built graphite flow fields provided with a triple serpentine, while an internally designed system of gaskets was used to avoid leakages. The flow fields were held together between two heated stainless steel plates tightened with eight screws to achieve a gas diffusion layer thickness reduction of 25%.

7.3.5   Fuel cell test

The fuel cells were run at 160°C with dry air and hydrogen as reactants both with λ=2. The break in procedure included 1 hour at OCV followed by progressive steps of $0.05\,A\,cm^{-2}$ till reaching a current density value of $0.2\,A\,cm^{-2}$, this condition was then kept constant for $140\,h$. During fuel cell operation the output water was collected; at $70\,h$ and at $140\,h$ (end of the test) the collected water was weighted, polarization curves and EIS measurements were performed and analyzed. In the following sections the polarization curves and the EIS spectra measured at $140\,h$ are not discussed due to their complete similarity with the ones taken at $70\,h$.

7.4   Results

7.4.1   Polarization curves

At $70\,h$ and $140\,h$ three polarization curves were measured respectively with λ_{H_2}=2 and λ_{Air}=1.2-2-6. These curves were performed starting from OCV and increasing the current density with $0.05\,A\,cm^{-2}$ steps till voltage went below $0.35\,V$. The current was then decreased backward to OCV and the representative voltage values were obtained as average between the two ways. The obtained curves for the six tested cells at the three different investigated cathode stoichiometries are reported in fig.7.1,7.2 and 7.3. All of the polarization curves exhibit a very similar behavior on the whole investigated current den-
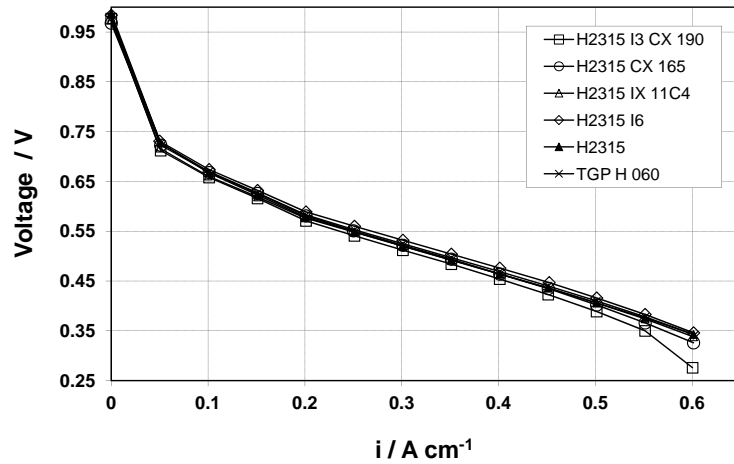
Figure 7.1: Polarization curves of the assembled fuel cells. $\lambda_{H_2}=2$, $\lambda_{Air}=1.2$.
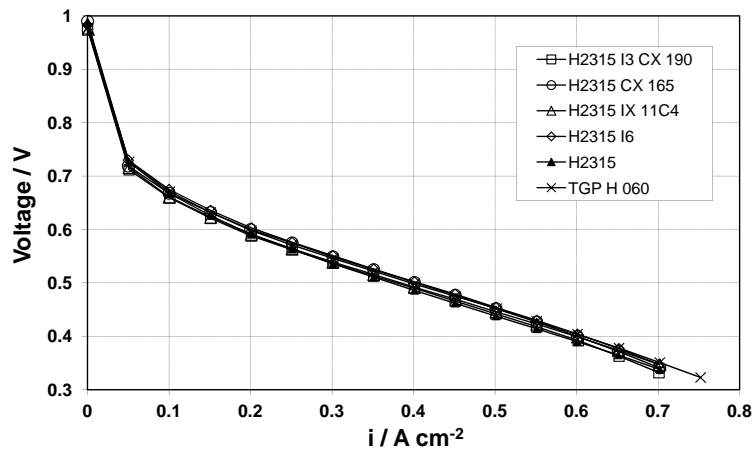
Figure 7.2: Polarization curves of the assembled fuel cells. $\lambda_{H_2}=2$, $\lambda_{Air}=2$.

sity range. A slight difference is visible with $\lambda_{Air}=1.2$ (fig.7.1) only when the cathode material with the lowest permeability (*Freudenberg H2315 CX 190*) is used. In this case the polarization curve exhibits a more pronounced decreasing trend over $0.5\,A\,cm^{-2}$ and starts to part from the rest. Such a trend underlines the rising importance of mass transport issues at cathode side when the gas diffusion media permeability is considerably low. The performance loss is anyway limited and occurs when the voltage is lower than $0.4\,V$. In this condition the electrochemical efficiency of the fuel cell is low and its application is not appeal-
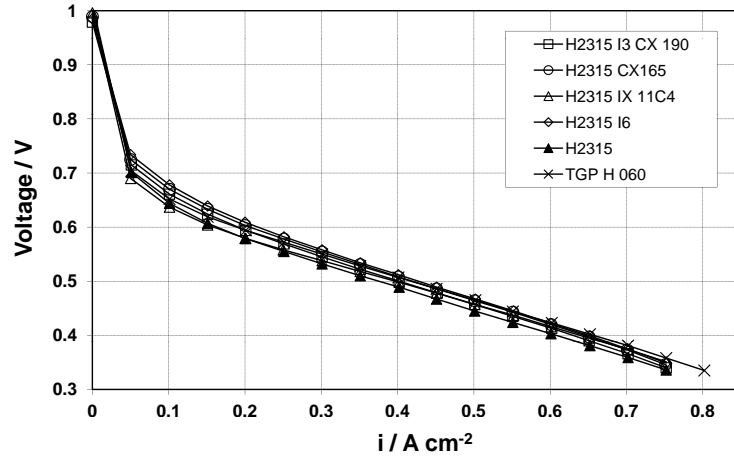
Figure 7.3: Polarization curves of the assembled fuel cells. $\lambda_{H_2}{=}2$, $\lambda_{Air}{=}6$.

ing. For all of the other investigated materials and stoichiometries, no different trend between the polarization curves could be observed. The measured voltages are actually very similar and no distinction can be made. Only the highest permeability material (*TGP H 060*) can reach slightly higher current densities but this is of poor importance considering the low voltage range. This indicates that the cathode gas diffusion layer structure plays a very limited influence that can be neglected when the usual stoichiometries are employed.

7.4.2   Electrochemical Impedance Spectroscopy

The Electrochemical Impedance Spectroscopy (EIS) measurements were performed at the values of current density and stoichiometry reported in table7.2. A sinusoidal voltage perturbation with an amplitude of $5\,mV$ was applied to the fuel cell by means of a potentiostat. The frequency interval covered by such a perturbation ranged from $50\,kHz$ to $0.1\,Hz$ with the aim to investigate electrochemical and mass transport phenomena. All of the measured spectra exhibit a similar shape as can be observed in fig.7.5,7.6,7.7. The spectra are successively made up by:

1) an high frequency inductive part located on the left side of the plot below the real axis

2) an oblique linear branch, located above the real axis, which is immediately subsequent to the previous inductive element

3) a first high frequency arch

4) a second low frequency arch.

These single parts of each spectrum can be attributed to different physical phenomena occurring inside of the fuel cell [3, 67, 69, 70], which are respectively:

1) the inductance of the cables of the potentiostat

2) the diffusion of the protons inside of the cathode catalyst layer

3) the oxygen reduction reaction (ORR) happening at cathode side

4) the diffusion of oxygen from the cathode flow field to the cathode electrode.

The equivalent circuit used for the interpretation of the experimental data was built taking into account for the previously described characteristics of the measured spectra. This circuit is displayed in fig.7.4 together with the description of its single components. The measured spectra are similar for all of the investigated cathode materials and stoichiometries at a current density of 0.2 and $0.4\,A\,cm^{-2}$ (fig.7.5,7.6). Conversely, when the current density is $0.6\,A\,cm^{-2}$ and λ_{Air}=1.2 (fig.7.7), the differences between the spectra become evident underlining the rise of mass transport issues.

Table 7.2: EIS measurements conditions.

Current density $[A\,cm^{-2}]$	λ_{H_2}	λ_{Air}
OCV	2	1.2-2-6
0.2	2	1.2-2-6
0.4	2	1.2-2-6
0.6	2	1.2-2-6
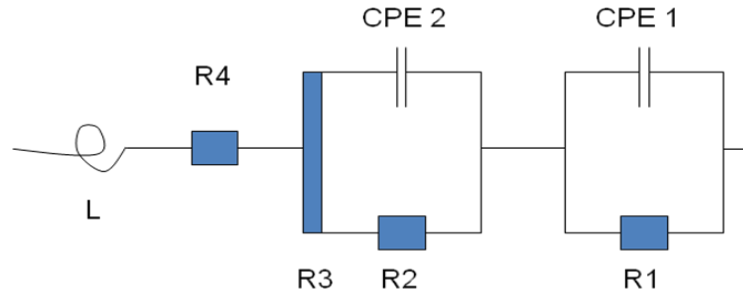
Figure 7.4: Fuel cell equivalent circuit. L=cables inductance; R4=ohmic resistance; R3=catalyst layer proton resisitivity; R1=diffusion resistance; CPE1=constant phase element of diffusion; R2=kinetic resistance of oxygen reduction reaction; CPE2=double layer constant phase element.

Figure 7.5: EIS spectra: comparison between highest (H2315 13 CX190, white markers) and lowest (TGP H60, black markers) permeability materials. T=160°C, i=0.2 $A\,cm^{-2}$, λ_{H_2}=2, λ_{Air}=1.2 (triangles), 2(circles), 6(squares).

The showed EIS spectra indicate that the effect of the GDL material on the mass transport phenomena becomes evident with low stoichiometry (λ_{Air}=1.2) and high current density (0.6 $A\,cm^{-2}$). When air stoichiometry is higher than 1.2, or current density is lower than 0.6 $A\,cm^{-2}$, the mass transport is not in-

Figure 7.6: EIS spectra: comparison between highest (H2315 13 CX190, white markers) and lowest (TGP H60, black markers) permeability materials. T=160°C, i=0.4 $A\,cm^{-2}$, λ_{H_2}=2, λ_{Air}=1.2 (triangles), 2(circles), 6(squares).

fluenced by the cathode GDL material. Actually no difference can be noticed between the spectra recorded on the cell with the lowest and the highest permeability material. This underlines that the influence of the cathode GDL material is not significant under these conditions. In spite of this, a trend in the oxygen diffusion resistance could be observed by the EIS spectra when the current density was 0.6 $A\,cm^{-2}$ and λ_{Air}=1.2. The mass transfer resistance actually behaves as a logarithmic function of the GDL through plane permeability as shown in fig.7.8. The fuel cell Ohmic resistance is also influenced by both the stoichiometry and the current density, confirming for a typical behavior of phosphoric acid doped electrolytes 1.1.4. When the cathode stoichiometry is risen, the Ohmic resistance increases due to membrane drying. Differently, when the current density is risen, the ohmic resistance decreases due to water production and consequent membrane hydration. Such trend is clearly visible in fig.7.9 where the ohmic resistance of the electrolyte at different current density is reported. When current is drawn, the Ohmic resistance is quite small and only slightly increases when the air flow rate increases. Conversely, at
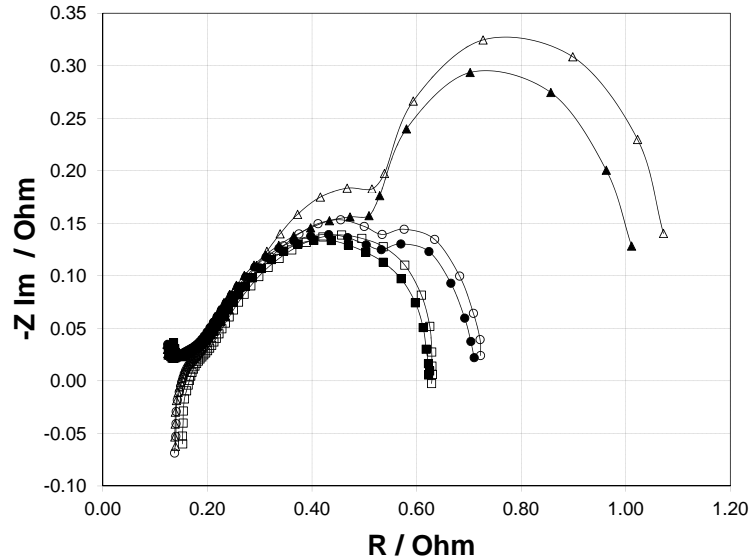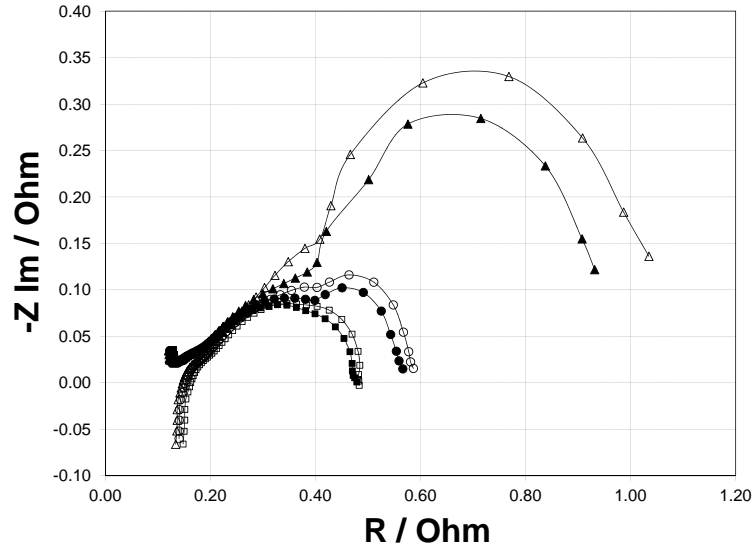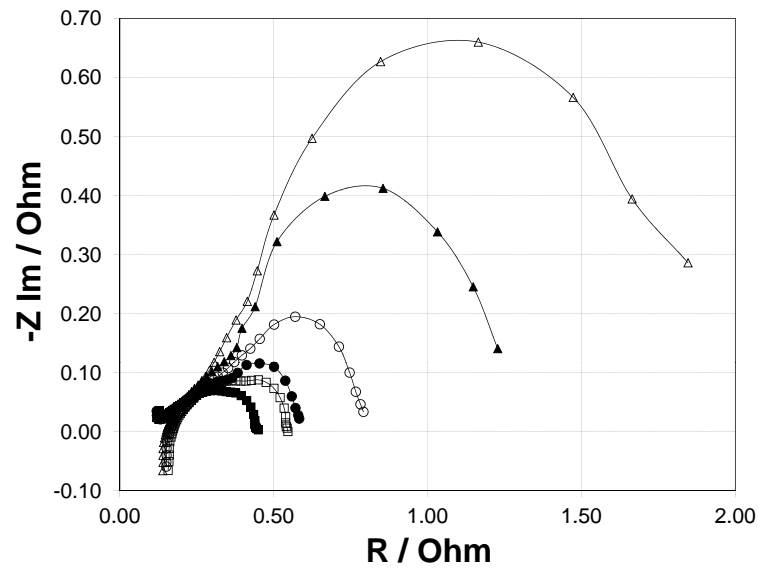
Figure 7.7: EIS spectra: comparison between highest (H2315 13 CX190, white markers) and lowest (TGP H60, black markers) permeability materials. T=160°C, i=0.6 $A\,cm^{-2}$, λ_{H_2}=2, λ_{Air}=1.2 (triangles), 2(circles), 6(squares).
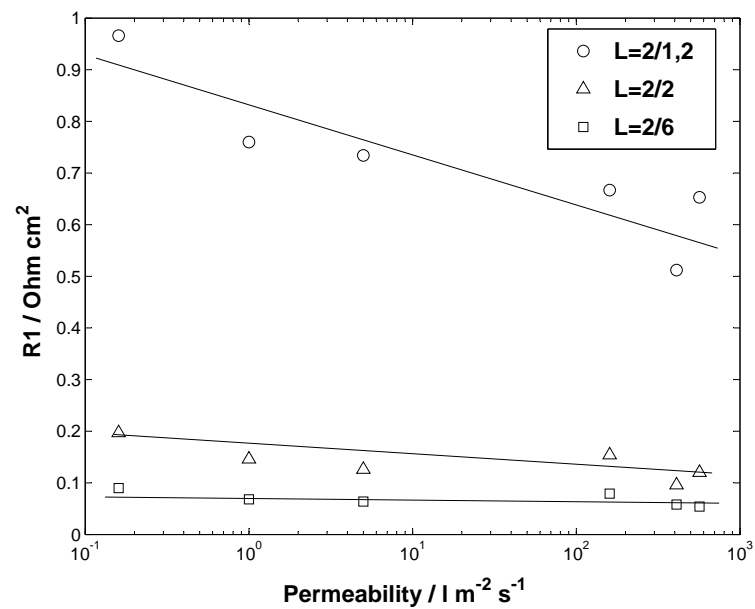
Figure 7.8: Cathode diffusion resistance vs GDL permeability in logarithmic scale.

OCV, the Ohmic resistance value becomes more than double and remarkably increases with cathode stoichiometry. The reported trends underline that the Ohmic resistance of the fuel cell considerably decreases when the water is produced, but does not sensibly depend on the water production rate. The cathode
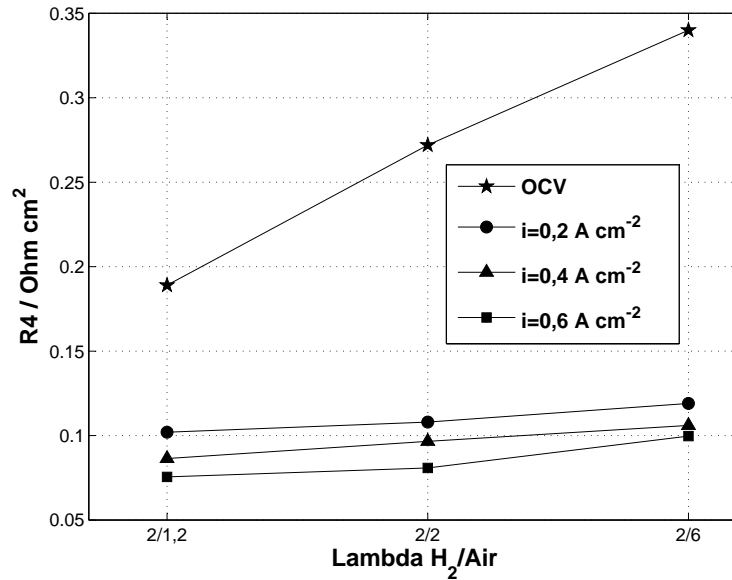
Figure 7.9: Cell Ohmic resistance at different air stoichiometry with Toray TGP-H-60.

stoichiometry plays an important effect also on the proton transfer resistance of the cathode catalyst layer. The proton resistivity of the cathode electrode under OCV is reported in fig.7.10. This resistance increases with increasing air stoichiometry, which contributes to further electrode drying. On the opposite, as a small current is drawn, the proton transfer resistance decreases by nearly ten times due to the sufficient hydration of the catalyst layer. This behavior reproduces what previously observed for the electrolyte ohmic resistance: the presence of even a minimal amount of water sensibly reduces the proton resistivity. This behavior can be explained referring to the influence of water on the phosphoric acid equilibrium which has been discussed in 1.1.4. The presence of water promotes the acid orthophosphoric form increasing the number of proton conducting elements in both the polymer membrane and the electrodes [23].
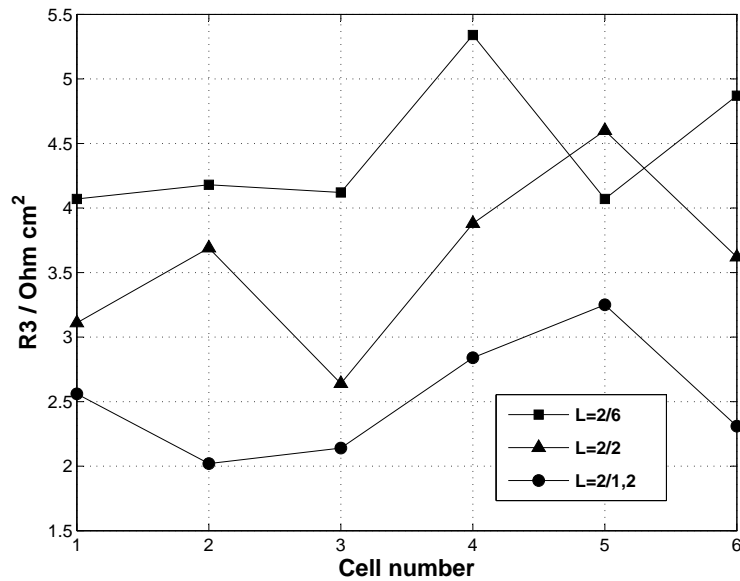
Figure 7.10: Electrode proton resistivity for all of the tested GDL materials at OCV

7.4.3 Water collection

The water contained in the anode and in the cathode exhausts was collected after $70\,h$ and $140\,h$ of fuel cell operation by condensing the water vapor by means of a cooling system working at 7°C. The total collected water was always in good agreement with the electrochemical generation rate (error $< 5\%$) attesting for a reliable collecting procedure. The collected water was weighted to estimate its distribution between the anode and cathode compartments. For every tested material, the cathode water output was almost constant and ranged from 91 to 95% of the total, while the anode water output covered the rest as reported in fig.7.11. The internal water transport resulted very small and independent on cathode diffusion layer material which seems to play no influence on the internal water redistribution.

7.5   Determination of diffusivity

In order to further investigate the effect of the catalyst coating on the mass transport process, the diffusivity of the coated and non coated GDLs were es-
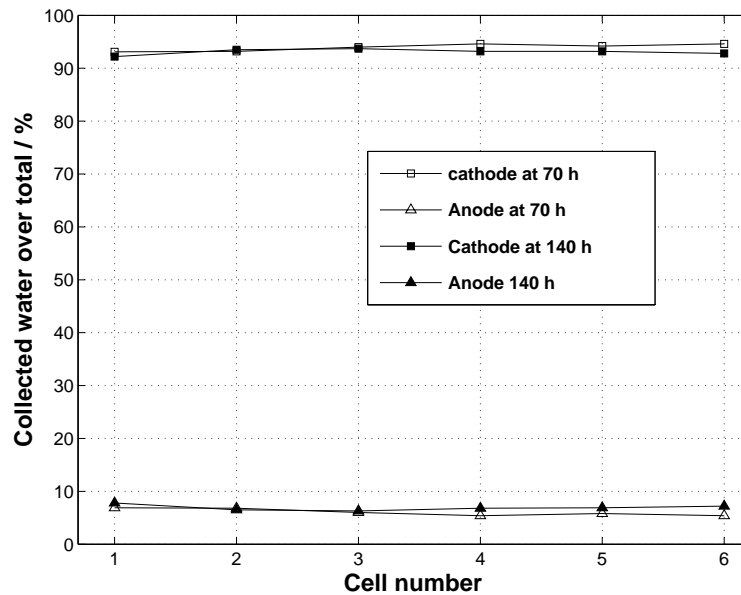
Figure 7.11: Water collected at anode and cathode outlets as fraction of total.

timated and compared. The aim of this comparison was to detect a possible limitation in the gas diffusion process related to the presence of the Catalyst Layer (CL). Actually, the diffusivity of the CL may be much smaller than the diffusivity of the GDL backing material. If this happens, the influence of the GDL may be neglected and the gas mass transport would depend only on the catalyst coating, which becomes the limiting element. The diffusivity of four non coated GDL backing materials was measured using the experimental system and the method reported in [63]. This system was originally implemented to study the water transport and the flooding in gas diffusion layers for low temperature PEMFCs. The same system was here used to measure the water vapor effective diffusivity (as defined in [63]) at 140°C and 160°C, which are the typical operating temperatures for HT-PEMFCs. In this condition the water condensation does not occur and the mass transport process happens in gas phase. For this reason the water vapor diffusivity was taken as indicator of the gas transport process. The obtained values are reported in table 7.3.   On the other side, a direct measurement of the water vapor diffusivity across the coated GDLs according to [63] could not be performed. Actually, the integrity of the

Table 7.3: Measured water vapor diffusivity across the bare GDL materials.

temperature [°C]	H2315 CX190 $[cm^2\,s^{-1}]$	H2315 CX165 $[cm^2\,s^{-1}]$	H2315 $[cm^2\,s^{-1}]$	TGP H 60 $[cm^2\,s^{-1}]$
140	0.062-0.064	0.066-0.067	0.078-0.079	0.078-0.08
160	0.066-0.07	0.068-0.072	0.084-0.087	0.086-0.088

sample could not be maintained during the diffusion process because the catalyst layer peeled off very easily. The effective diffusivity across the component was thus determined by means of a model available in literature [74]. The model was used to fit the polarization curves of the different fuel cells, also varying the oxygen diffusivity across the Gas Diffusion Layers and the Electrodes, more details about this process are reported in [88]. An estimation of this effective diffusivity was thus indirectly obtained. The estimated values are reported in table 7.4 together with the relative contribution of the electrode diffusive resistance to the global one. Over 80% of the diffusive resistance of the coated

Table 7.4: Estimated oxygen diffusivity across the coated Gas Diffusion Layers and contribution of the Electrode to the total diffusive resistance.

Parameter	H2315 CX190	H2315 CX165	H2315	TGP H 60
Diffusivity at 160°C $[cm^2\,s^{-1}]$	0.0123	0.0120	0.0140	0.0137
Contribution of Electrode to resistance [%]	81%	82%	83%	84%

Gas Diffusion Layers is due to the catalyst layer coating. This means that the importance of the electrode is fundamental for the mass transport process and in this specific case it becomes the limiting factor. The coated electrodes have a thickness around $100\mu m$ which is quite big if compared with the common

value of 10-20μm. Thinner electrodes with higher porosity may enhance gas diffusivity and consequently lower the mass transport limitations.

7.6   Remarks

The effect of six different gas diffusion layer materials on the performance of an HT-PEMFC has been studied by means of polarization curves, EIS spectra and product water collection. No remarkable difference between the assembled fuel cells could be observed in the investigated range of operating conditions. Slight differences between the fuel cell polarization curves could be observed with low cathode stoichiometry (λ_{Air}=1.2) and high current density (i=0.6 $A\,cm^{-2}$) only with the lowest permeability material (H2315 I3 CX190). In this case the fuel cell voltage consistently drops when approaching 0.6 $A\,cm^{-2}$ indicating the rise of mass transport limitations. The presence of the mass transport problems was confirmed by the EIS spectra in which the second circle, which represents the mass transport resistance, consistently increases. Even though such behavior is of interest to the study of mass transport limitations, it covers poor value for the application because it happens at voltage lower than 0,35 V where the fuel cell efficiency is low. Further analysis on the mass transport properties of the employed Gas Diffusion Layers pointed out the great importance of the coating which resulted responsible for mass transport limitations due to its thickness. The thickness of the coating must be reduced and its structure must be optimized in order to minimize the mass transport limitations.

Conclusions

In this work an extensive experimental characterization of a commercial type of HT-PEMFC (BASF Celtec-P2100®) has been reported. The performed experimental analyses allowed to characterize the performance, the internal mass transport, the effect of humidification and the degradation of this type of fuel cell. The measurements were conducted following a reliable experimental methodology and using an in-house assembled test station. The experimental setup was progressively adapted to meet the needs of the different sections of the experimental activity, thanks to the modularity of the measurement system. New electrochemical measurements (EIS, CV and LSV) were implemented and set up to investigate the single components of the fuel cell and gain insight in the internal phenomena. Particular attention was dedicated to the measurements uncertainty which was always quantified and controlled through the use of calibrated instruments. Literature was widely consulted and referred to support the observed experimental behaviours. These arrangements allowed to gain insight in the unclear points announced in Chapter 1. The main outcomes are here listed:

- The performance of the fuel cell was in agreement with the data published in the literature and demonstrated to be sensitive to the fuel cell temperature, to the air stoichiometry, but was not influenced by the hydrogen stoichiometry in the investigated range. The Ohmic resistance of the mem-

brane was also monitored throughout the investigation by means of an AC milliOhmeter. The measured values slightly decrease when the polymer is well hydrated confirming for a behavior which is also supported by the available literature.

- The presence of an anomalous air crossover rate was detected in one of the tested fuel cells thanks to the mass balance analysis of the exhausts. Such phenomenon is generally known as crossover leakage and represents a typical failure mode. Its effect on the fuel cell performance was estimated and a methodology for in-situ detection of gas crossover was developed. In the specific case, the fuel cell voltage was not affected by this internal gas leakage, but a sensible increase in hydrogen consumption that compromises the energy recovery was measured.

- An important water transport across the MEA was detected and quantified, water moves due to different concentration, pointing out a diffusive mechanism. With dry reactants water migrates from the cathode, where it is produced, to the anode across the polymer electrolyte. Conversely, when hydrogen is intensively humidified, as would be in a syngas-fed fuel cell, water transport can be reversed and water moves from anode to cathode. In every tested condition the water concentration at anode outlet is higher than the one at cathode outlet and shows increasing trends that underline a non linearity in water transport.

- The influence of humidification on the fuel cell performance was studied in detail analyzing its effect on the single fuel cell components by means of EIS and CV. The acid was found to play a fundamental role, actually when humidified reactants are fed, the phosphoric acid in the MEA shifts its equilibrium to the more conductive orthophosphoric form. As a consequence the number of proton conducting molecules in the membrane and in the electrodes increases. For this reason the conductivity of the membrane and of the electrodes becomes higher. At the same time the three phase zone in the electrodes grows contacting more catalyst particles and enlarging the catalyst active area. Therefore both the Ohmic resistance of the MEA and the kinetic resistance of the electrodes positively decrease.

Nevertheless, the partial pressure of the reactants becomes lower and off-
sets these positive effects, causing a global drop in the fuel cell voltage.

- The degradation of the fuel cell under reference operating conditions was mea-
  sured and confirmed on two different fuel cell samples. A faster degrada-
  tion rate was measured when the temperature was increased from 160°C
  to 180°C. The degradation of the single components was investigated by
  means of EIS and CV and the main reason of fuel cell performance drop
  was individuated in the decrease of the catalyst active area. Hysteresis
  was detected when changing the operative condition and its reason was at-
  tributed to slow internal equilibration mechanisms related to hydration,
  but further study is needed to clarify this point. The mass transport
  properties of the GDLs, the Ohmic resistance of the membrane and its
  crossover rate did not show noticeable variations during this activity and
  seem to be minor issues.

- Different cathode configurations have been experimentally studied in order
  to investigate their impact on the fuel cell. The investigated Gas Diffu-
  sion Layers resulted in the same fuel cell behavior due to the important
  thickness of the catalyst coating. This parameter resulted extremely im-
  portant, therefore the optimization of electrodes thickness and porosity is
  essential for a proper fuel cell operation.

Bibliography

[1] R.He, Q.Li, A.Bach, J.O.Jensen, and N.J.Bjerrum. Physicochemical properties of phosphoric acid doped polybenzimidazole membranes for fuel cells. *Journal of Membrane Science*, 277(1-2):38–45, 2006.

[2] Q.Li, R.He, J.O.Jensen, and N.J.Bjerrum. Approaches and recent development of polymer electrolyte membranes for fuel cells operating above 100°C. *Chemistry of Materials*, 15(26):4896–4915, 2003.

[3] J.Zhang, Y.Tang, C.Song, and J.Zhang. Polybenzimidazole-membrane based PEM fuel cell in the temperature range of 120-200°C. *Journal of Power Sources*, 172(1):163–171, 2007.

[4] J.S.Wainright, J.T.Wang, D.Weng, R.F.Savinell, and Litt M. Acid doped polybenzimidazoles: a new polymer electrolyte. *Journal of the Electrochemical Society*, 142(7):L121–3, 1995.

[5] Q.Li, R.He, J.O.Jensen, and N.J.Bjerrum. PBI-based polymer membranes for high temperature fuel cells - Preparation, characterization and fuel cell demonstration. *Fuel Cells*, 4(3):147–159, 2004.

[6] Q.Li, J.O.Jensen, R.F.Savinell, and N.J.Bjerrum. High temperature proton exchange membranes based on polybenzimidazole for fuel cells. *Progress in Polymer Science*, 34(5):449–477, 2009.

[7] Q.Li, H.A.Juhler, and N.J.Bjerrum. Phosphoric acid doped polybenzimidazole membranes: physiochemical characterization and fuel cell applications. *Journal of Applied Electrochemistry*, 31(7):773–779, 2001.

[8] H.Pu, W.H.Meyer, and G.Wegner. Proton transport in polybenzimidazole blended with H_3PO_4 or H_2SO_4. *Journal of Polymer Science*, 40:663–9, 2002.

[9] Q.Li, R.He, R.W.Berg, H.A.Hjuler, and N.J.Bjerrum. Water uptake and acid doping of polybenzimidazoles as electrolyte membranes for fuel cells. *Solid State Ionics*, 168(1-2):177–185, 2004.

[10] T.J.Schmidt and J.Baurmeister. Properties of high-temperature PEFC Celtec-P1000 MEAs in start/stop operation mode. *Journal of Power Sources*, 176(2):428–434, 2008.

[11] R.Bouchet and E.Siebert. Proton conduction in acid doped polybenzimidazole. *Solid States Ionics*, 118(3-4):287–299, 1999.

[12] Y.L.Ma, J.S.Wainright, M.H.Litt, and R.F.Savinell. Conductivity of PBI membranes for high-temperature polymer electrolyte fuel cells. *Journal of the Electrochemical Society*, 151(1):A8–A16, 2004.

[13] X.Ren, W.Henderson, and S.Gottesfeld. Electro-osmotic drag of water in ionomeric membranes. *Journal of the Electrochemical Society*, 144(9), 1997.

[14] T.A.Zawodzinski Jr., C.Derouin, S.Radzinski, R.J.Sherman, et al. Water uptake by and transport through Nafion 117 membranes. *Journal of the Electrochemical Society*, 140(4), 1993.

[15] A.Schechter, R.F.Savinell, J.S.Wainright, and D.Ray. ^{1}H and ^{31}P NMR study of phosphoric acid-doped polybenzimidazole under controlled water activity. *Journal of the Electrochemical Society*, 156(2):B283–B290, 2008.

[16] M.K.Daletou, J.K.Kallitsis, G.Voyatsis, and S.G.Neophytides. The interaction of water vapours with H_3PO_4 imbibed electrolyte based on PBI/polysulfone copolymer blends. *Journal of Membrane Science*, 326:76–83, 2009.

[17] Z.Liu, J.S.Wainright, M.H.Litt, and R.F.Savinell. Study of the oxygen reduction reaction (ORR) at Pt interfaced with phosphoric acid doped poly-

benzimidazole at elevated temperature and low relative humidity. *Electrochimica Acta*, 51(19):3914–3923, 2006.

[18] K.Wippermann, C.Wannek, H.F.Oetjen, J.Mergel, and W.Lehnert. Cell resistances of poly(2,5-benzimidazole)-based high temperature polymer membrane fuel cell membrane electrode assemblies: time dependence and influence of operating parameters. *Journal of Power Sources*, 195:2806–9, 2010.

[19] S.Slade, A.Campbell, T.R.Ralph, and F.C.Walsh. Ionic conductivity of an extruded nafion 1100 EW series of membranes. *Journal of the Electrochemical Society*, 149(12):A1556–1564, 2002.

[20] D.Weng, J.S.Wainright, U.Landau, and R.F.Savinell. Electro-osmotic drag coefficient of water and methanol in polymer electrolytes at elevated temperatures. *Journal of the Electrochemical Society*, 143(4):1260–1263, April 1996.

[21] C.Wannek, B.Kohnen, H.F.Oetjen, H.Lippert, and J.Mergel. Durability of ABPBI-based MEAs for high temperature PEMFCs at different operating conditions. *Fuel Cells*, 8(2):87–95, 2008.

[22] S.Yu, L.Xiao, and B.C.Benicewicz. Durability studies of PBI-based high temperature PEMFCs. *Fuel Cells*, 8(3-4):165–174, 2008.

[23] M.Boaventura and A.Mendes. Activation procedures characterization of MEA based on phosphoric acid doped PBI membranes. *International Journal of Hydrogen Energy*, 35:11649–60, 2010.

[24] N.H.Jalani, M.Ramani, K.Ohlsson, S.Buelte, et al. Performance analysis and impedance spectral signatures of high temperature PBI-phosphoric acid gel membrane fuel cells. *Journal of Power Sources*, 160(2):1096 – 1103, 2006.

[25] T.Suzuki, H.Murata, T.Hatanaka, and Y.Morimoto. Analysis of the catalyst layer of polymer electrolyte fuel cells. *R&D Review of Toyota CRDL*, 39(3), 2004.

[26] Y.Oono, A.Sounai, and M.Hori. Influence of the phosphoric acid-doping level in a polybenzimidazole membrane on the cell performance of high-temperature proton exchange membrane fuel cells. *Journal of Power Sources*, 189(2):943–949, 2009.

[27] K.Kwon, J.O.Park, D.Y.Yoo, and J.S.Yi. Phosphoric acid distribution in the membrane electrode assembly of high temperature proton exchange membrane fuel cells. *Electrochimica Acta*, 54:6570–5, 2009.

[28] F.A.deBruijn, V.A.T.Dam, and G.J.M.Janssen. Durability and degradation issues of PEM fuel cell components. *Fuel Cells*, 8(1):3–22, 2008.

[29] J.Hu, H.Zhang, Y.Zhai, G.Liu, and B.Yi. 500h continuous aging life test on PBI/H_3PO_4 high-temperature pemfc. *International Journal of Hydrogen Energy*, 31:1855–62, 2006.

[30] S.D.Knights, K.M.Colbow, J.St-Pierre, and D.P.Wilkinson. Aging mechanisms and lifetime of PEFC and DMFC. *Journal of Power Sources*, 127:127–134, 2004.

[31] D.A.Stevens and J.R.Dahn. Thermal degradation of the support in carbon - supported platinum electrocatalysts for PEM fuel cells. *Carbon*, 43(1):179 – 188, 2005.

[32] J.Lobato, P.Canizares, M.A.Rodrigo, and J.J.Linares. PBI-based polymer electrolyte membranes fuel cells: temperature effects on cell performance and catalyst stabilty. *Electrochimica Acta*, 52(12):3910–3920, 2007.

[33] Y.Oono, T.Fukuda, A.Sounai, and M.Hori. Influence of operating temperature on cell performance and endurance of high temperature proton exchange membrane fuel cells. *Journal of Power Sources*, 195(4):1007–1014, 2010.

[34] Q.Li, R.He, J.A.Gao, J.O.Jensen, and N.J.Bjerrum. The CO poisoning effect in PEMFC's operation at temperatures up to 200℃. *Journal of the Electrochemical Society*, 150(12):A1599–A1605, 2003.

[35] BASF Fuel Cells Gmbh. Cell assembling and start-up procedure for Celtec-P1000 MEA. Technical report, March 2009.

[36] BASF Fuel Cells Gmbh. Celtec-P1000 Membrane electrode assembly: technical information brochure. Technical report, June 2007.

[37] A.Baricci. Master's thesis, Politecnico di Milano, 2010.

[38] J.Lobato, P.Canizares, M.A.Rodrigo, J.J.Linares, D.Ubeda, and F.J.Pinar. Study of the catalytic layer in polybenzimidazole based high temperature PEMFC effect of platinum content on the carbon support. *Fuel Cells*, 10(2):312–319, 2010.

[39] R.He, Q.Li, G.Xiao, and N.J.Bjerrum. Proton conductivity of phosphoric acid doped polybenzimidazole and its composites with inorganic proton conductors. *Journal of Membrane Science*, 226(1-2):169–184, 2003.

[40] J.Zhang, Z.Xie, J.Zhang, Y.Yang, et al. High temperature PEM fuel cells. *Journal of Power Sources*, 160(2):872–891, 2006.

[41] J.Wu, X.Z.Yuan, J.J.Martin, H.Wang, J.Zhang, J.Shen, S.Wu, and W.Merida. A review of PEM fuel cell durability: degradation mechanisms and mitigation strategies. *Journal of Power Sources*, 184(1):104–119, 2008.

[42] Z.Wang, S.Lutz, and K.D.Inglehart. *United States Patent 6874352*.

[43] A.Husar, M.Serra, and C.Kunusch. Description of gasket failure in a 7 cell pemfc stack. *Journal of Power Sources*, 169:85–91, 2007.

[44] M.Inaba, T.Kinumoto, M.Kiriake, R.Umebayashi, A.Tasaka, and Z.Ogumi. Gas crossover and membrane degradation in polymer electrolyte fuel cells. *Electrochimica Acta*, 51:5746–53, 2006.

[45] M.Aoki, H.Uchida, and M.Watanabe. Novel evaluation method for degradation rate of polymer electrolytes in fuel cells. *Electrochemistry Communications*, 7:1434–38, 2005.

[46] G.Meuleman. *United States Patent 4424708*.

[47] S.Fanciullo. *United States Patent 5235846.*

[48] G.J.Lamont and D.P.Wilkinson. *United States Patent 5763765.*

[49] S.J.Pratt. *United States Patent 6662633.*

[50] S.D.Knights, D.P.Wilkinson, R.Nebelsiek, and J.Stumper. *United States Patent 6492043.*

[51] S.V.Kanuri and T.W.Patterson. *United States Patent Application 20110117469.*

[52] G.Tian, S.Wasterlain, I.Endichi, D.Candusso, F.Harel, X.Francois, et al. Diagnosis methods dedicated to the localisation of failed cells within PEMFC stacks. *Journal of Power Sources*, 182:449–461, 2008.

[53] G.Tian, S.Wasterlain, D.Candusso, F.Harel, D.Hissel, and X.Francois. Identification of failed cells inside PEMFC stacks in two cases: anode/cathode crossover and anode/cooling compartment leak. *International Journal of Hydrogen Energy*, 35:2772–76, 2010.

[54] S.Galbiati, A.Baricci, A.Casalegno, and R.Marchesi. Experimental study of water transport in a polybenzimidazole-based high temperature PEMFC. *International Journal of hydrogen Energy*, 37:2462–2469, 2012.

[55] International organization for standardization. *19 ISO Guide to expression of uncertainty in measurement*, 1993. Env. 13005:1999, corrected and reprinted 1995.

[56] A.D.Modestov, M.R.Tarasevich, V.Ya.Filimonov, and N.M.Zagudaeva. Degradation of high temperature MEA with PBI-H_3PO_4 membrane in a life test. *Electrochimica Acta*, 54(27):7123–7127, 2009.

[57] K.C.Neyerlin, A.Singh, and D.Chu. Kinetic characterization of a PtNi/C catalyst with a phosphoric acid doped PBI membrane in a proton exchange membrane fuel cell. *Journal of Power Sources*, 176:112–117, 2008.

[58] G.Liu, H.Zhang, J.Hu, Y.Zhai, D.Xu, and Z.Shao. Studies of performance degradation of a high temperature PEMFC based on H_3PO_4-doped PBI. *Journal of Power Sources*, 162:547–552, 2006.

[59] A.Arsalis, M.P.Nielsen, and S.K.Kaer. Modeling and parametric study of a $1kW_e$ HT-PEMFC-based residential micro-CHP system. *Journal of Power Sources*, 36:5010–20, 2011.

[60] J.O.Jensen, Q.Li, C.Pan, A.P.Vestbo, K.Mortensen, H.N.Petersen, et al. High temperature PEMFC and the possible utilization of the excess heat for fuel processing. *International Journal of Hydrogen Energy*, 32:1567–71, 2007.

[61] P.Mocoteguy, B.Ludwig, J.Scholta, Y.Nedellec, D.J.Jones, and J.Roziere. Long-term testing in dynamic mode of HT-PEMFC H_3PO_4/PBI Celtec-P based membrane electrode assemblies for micro-CHP applications. *Fuel cells*, 10(2):299–311, 2010.

[62] S.Giddey, F.T.Ciacchi, and S.P.S.Badwal. Fuel quality and operational issues for polymer electrolyte membrane PEM fuel cells. *Ionics*, 11, 2005.

[63] A.Casalegno, L.Colombo, S.Galbiati, and R.Marchesi. Quantitative characterization of water transport and flooding in the diffusion layers of polymer electrolyte fuel cells. *Journal of Power Sources*, 195(13):4143–8, 2010.

[64] Ecochemie B.V. *AUTOLAB PGSTAT User's Guide*, 2002.

[65] Edited by H.Wang, X.Yuan, and H.Li. *PEM fuel cell diagnostic tools*. Number 13:978-1-4398-3920-1. CRC Press.

[66] X.Yuan, H.Wang, J.C. Sun, and J. Zhang. AC impedance technique in PEM fuel cell diagnosis-a review. *International Journal of Hydrogen Energy*, 32(17):4365–4380, 2007.

[67] K.R.Cooper, V.Ramani, J.M.Fenton, and H.R.Russell Kunz. *Experimental methods and data analyses for polymer electrolyte fuel cells*. Scribner Associates, 2005.

[68] Gamry Instruments Inc. Basics of electrochemical impedance spectroscopy. Technical report, 2010.

[69] F.Barbir. *PEM fuel cells: theory and practice.* Elsevier Academic Press, 2005.

[70] R.O'Hayre, S-W.Cha, W.Colella, and F.B.Prinz. *Fuel Cell Fundamentals.* John Wiley and Sons, 2006.

[71] J.L.Jespersen, E.Schalz, and S.K.Kaer. Electrochemical characterization of a polybenzimidazole-based high temperature proton exchange membrane unit cell. *Journal of Power Sources*, 191:289–96, 2009.

[72] N.Wagner. Characterization of membrane electrode assemblies in polymer electrolyte fuel cells using a.c. impedance spectroscopy. *Journal of Appleid Electrochemistry*, 32:859–863, 2002.

[73] M.S. Kondratenko, M.O. Gallyamov, and A.R.Khokholov. Performance of high temperature fuel cells with different types of PBI membranes as analysed by imepdance spectroscopy. *International Journal of Hydrogen Energy*, 2011.

[74] S.K.Roy, M.E.Orazem, and B.Tribollet. Interpretation of low frequency inductive loops in PEM fuel cells. *Journal of the Electrochemical Society*, 154(12):B1378–B1388, 2007.

[75] T.E.Springer, T.A.Zawodzinski, M.S.Wilson, and S.Gottesfeld. Characterization of polymer electrolyte fuel cells using AC impedance spectroscopy. *Journal of the Electrochemical Society*, 143(2):587–599, 1996.

[76] D.Zhan, J.Velmurugan, and M.V.Mirkin. Adsorption/desorption of hydrogen on Pt nanoelectrodes: evidence of surface diffusion and spillover. *Journal of the American Chemical Society*, 2009.

[77] M.Mamlouk and K.Scott. Analysis of high temperature polymer electrolyte membrane fuel cell electrodes using electrochemical impedance spectroscopy. *Electrochimica Acta*, 56:5493–5512, 2011.

[78] C.Y. Chen and W.H. Lai. Effects of temperature and humidity on the cell performance and resistance of a phosphoric acid doped polybenzimidazole fuel cell. *Journal of Power Sources*, 195 (2010):7152–7159, 2010.

[79] J.Wu, X.Z.Yuan, J.J.Martin, H.Wang, J.Zhang, et al. A review of PEM fuel cell durability: Degradation mechanisms and mitigation strategies. *Journal of Power Sources*, 184:104–119, 2008.

[80] S.Zhang, X.Youan, H.Wang, W.Merida, H.Zhu, et al. A review of accelerated stress tests of MEA durability in PEM fuel cells. *International Journal of Hydrogen Energy*, 34:288–404, 2009.

[81] J.Yu, T.Matsuura, Y.Yoshikawa, Md. N. Islam, and M.Hori. Lifetime behavior of a PEM fuel cell with low humidificationof feed stream. *Physical Chemistry Chemical Physics*, 7:373–378, 2005.

[82] S.Galbiati, A.Baricci, A.Casalegno, and R.Marchesi. Gas crossover leakage in high temperature polymer electrolyte fuel cells: in situ quantification and effect on performance. *Journal of Power Sources*, 2012.

[83] G. Carcassola. Master's thesis, Politecnico di Milano, 2012.

[84] S.S. Kocha, J.D. Yang, and J.S. Yi. Characterization of gas crossover and its implications in PEM fuel cells. *American Institute of Chemical Engineers Journal*, 52:1916–1925, 2006.

[85] J.Lobato, P.Canizares, M.A.Rodrigo, C.Ruiz Lopez, and J.J.Linares. Influence of the teflon loading in the gas duffusion layer of PBI based pem fuel cells. *Journal of Appled Electrochemistry*, 38:793–802, 2008.

[86] J.Lobato, P.Canizares, M.A.Rodrigo, D.Ubeda, F.J.Pinar, and J.J.Linares. Optimisation of the microporous layer for a polybenzimidazole-based high temperature PEMFC: effect of carbon content. *Fuel Cells*, 10(5):770–777, 2010.

[87] J. Lobato, M.A. Rodrigo, J.J. Linares, and K. Scott. Effect of the catalytic ink preparation method on the performance of high temperature polymer

electrolyte membrane fuel cells. *Journal of Power Sources*, 157(1):284–292, 2006.

[88] S.Perego. Master's thesis, Politecnico di Milano, 2012.